Journal of Atmospheric and Solar–Terrestrial Physics 220 (2021) 105599

Contents lists available at ScienceDirect

Journal of Atmospheric and Solar–Terrestrial Physics

journal homepage: www.elsevier.com/locate/jastp

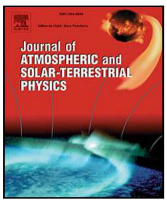

The impact of cold electrons and cold ions in magnetospheric physics

Gian Luca Delzanno [a,*], Joseph E. Borovsky [b], Michael G. Henderson [c], Pedro Alberto Resendiz Lira [a], Vadim Roytershteyn [b], Daniel T. Welling [d]

[a] T-5 Applied Mathematics and Plasma Physics, Los Alamos National Laboratory, Los Alamos, NM 87545, USA
[b] Space Science Institute, Boulder, CO 80301, USA
[c] ISR-1 Space Science and Applications, Los Alamos National Laboratory, Los Alamos, NM 87545, USA
[d] Physics Department, University of Texas, Arlington, TX 76019, USA

ARTICLE INFO

Keywords:
Cold-particle populations
Solar wind/magnetosphere coupling
Magnetosphere–ionosphere coupling
Magnetotail reconnection
Wave–particle interactions
Aurora structuring
Spacecraft charging

ABSTRACT

A review of the impact of the cold-ion and cold-electron populations in the Earth's magnetosphere is presented. The cold populations are defined by total energy less than approximately 100 eV, i.e. in the energy range which is strongly affected by spacecraft charging and that often dominates the total plasma density. We also include the warm plasma cloak in the review, since it overlaps partially with the cold energy range and is a population that is still not well understood.

The known impacts of cold ions and cold electrons that are discussed are: the source of hot magnetospheric plasma, solar-wind/magnetosphere coupling, magnetotail reconnection and substorms, Kelvin–Helmholtz instabilities on the magnetopause, chorus, hiss, electromagnetic-ion-cyclotron and ultra-low-frequency wave–particle interactions, aurora structuring and spacecraft charging. Other possible impacts are associated with refilling on open-drift trajectories, the remnant layer and plasmapause disruption. A discussion of the difficulty of cold-plasma measurements and the need for new measurement techniques that measure the full cold-ion and cold-electron distribution functions is also presented.

There remain a lot of unknowns about the cold-ion and cold-electron populations, associated with their origin, properties, drivers and impacts. These populations will need to be fully understood before the magnetosphere–ionosphere system can be fully understood.

1. Introduction

The Earth's magnetosphere contains multiple cold-ion and cold-electron particle populations that are not well characterized and whose impacts on the magnetospheric system have not been fully assessed. This overview discusses many of these particle populations and the potential impacts that they may have on the critical processes of the magnetosphere.

The magnetospheric environment comprises particle populations with a broad range of energies, from the sub-eV and eV particles of the ionosphere and plasmasphere all the way to the ultra-relativistic energies of the radiation belts. These diverse particle populations co-exist and interact by means of a variety of plasma waves. For the purpose of discussion in this paper, we classify particle populations in the following way: 'cold' is defined for total energies approximately less than 100 eV, 'warm' for total energies approximately between 100 eV and 1 keV, and 'hot' for total energies above 1 keV. Note that cold corresponds to the energy range which is strongly affected by spacecraft charging and that often dominates the total plasma density.

The particle populations of the Earth's magnetosphere originate from either the solar wind, the ionosphere, or the hydrogen geocorona. Most of the magnetosphere's cold populations come from the ionosphere, where cold outflows are commonly seen. It may be possible that some cold-electron populations come from the solar wind, particularly (1) under low-Mach-number conditions when the solar wind is only mildly heated in crossing the bow shock or (2) if the lower-energy core of the magnetosheath thermal population is captured into the magnetosphere.

There is growing evidence that the cold-particle populations of the magnetosphere play critical roles in several important processes that drive the dynamics of the magnetosphere. The primary goal of this overview is to survey the known and probable impacts of the cold-particle populations in magnetospheric physics. We will also include in this review the warm plasma cloak, which is composed of particles with energy from a few eV to a few hundred eV, since part of its energy range is cold and it remains a particle population which is not well understood.

* Corresponding author.
E-mail address: delzanno@lanl.gov (G.L. Delzanno).

https://doi.org/10.1016/j.jastp.2021.105599
Received 12 October 2020; Received in revised form 20 February 2021; Accepted 24 February 2021
Available online 17 March 2021
1364-6826/

A summary of the known and probable impacts of the cold-ion and cold-electron magnetospheric populations appears in Table 1 and these impacts will be discussed in the rest of the paper. The cold populations involved are plasmaspheric (and plume) ions, plasmaspheric (and plume) electrons, cloak ions (including the oxygen torus), cloak electrons, charge-exchange-byproduct protons from the hydrogen geocorona, structured cold electrons in the post-midnight dipolar regions, ion outflows, and electron outflows. Cold-electron outflows from the ionosphere are anticipated for the maintenance of charge neutrality in the magnetosphere: in addition to cold-electron outflow in the polar wind, two places where they should occur are (a) in the post-midnight to dawn region where the hot electron plasma sheet precipitates away to make diffuse aurora and (b) at the inner edge of the electron plasma sheet where (owing to gradient-curvature drift effects) the ion plasma sheet flows radially Earthward while the electron-plasma-sheet flow turns eastward. Cold-electron outflows into the magnetosphere are also expected in regions where there are downward field-aligned currents. There are also plasmaspheric-refilling cold-ion and cold-electron outflows into open-drift-trajectory flux tubes on the dayside.

Note that the magnetospheric cold-plasma literature discusses an ion population called the "oxygen torus", which is a cold-to-warm population of O^+ and O^{++} ions observed inside and outside of the plasmapause of the plasmasphere (Chappell, 1982a; Horwitz et al., 1984; Grew et al., 2007; Nosé et al., 2015; Nosé et al., 2020; Jahn et al., 2017). In this review, the oxygen torus will be considered to be the inner portion of the oxygen-rich warm plasma cloak since the morphology and locations of the two are nearly identical (Nosé et al., 2015). It is an important topic for future research to discern whether the oxygen torus is a separate population (with separate origin and separate evolution) from the warm plasma cloak.

Relative to other particle populations with higher energies, the cold populations are the least studied. In general, this is because issues associated with spacecraft charging and secondary-electron contamination make reliable measurements of the cold populations and their interpretation difficult. For ions, spacecraft-charging issues often prevent cold ions from reaching spacecraft instruments. For cold electrons, in addition to spacecraft-charging issues, spacecraft-produced photoelectrons and secondary electrons can overwhelm the fluxes of ambient magnetospheric low-energy electrons. This implies the need to develop new instruments that can make robust measurements of the cold plasma populations throughout the magnetosphere, including areas where the densities are low. Ion instruments that are negatively biased [e.g. Chappell (1982a), Fields et al. (1982)] and perhaps mounted on booms are needed; entire spacecraft that are negatively charged [e.g. Thomsen et al. (2013)] would also suffice. Electron instruments that avoid photoelectrons, or that are on spacecraft wherein photoelectron emission is suppressed, need to be developed and flown.

In general, the cold particle populations have not been thoroughly surveyed, their origins are often not understood, and their controlling factors (e.g. the geomagnetic-activity time history) are often unknown. Besides the known impacts that they have in magnetospheric dynamics, it is plausible that there could be impacts that are not yet known. We also wish to emphasize that the majority of work on the cold particle populations has focused on cold ions: a lot less is known about the cold electrons. Until the cold ions and cold electrons are understood, along with their controlling factors and their impacts, the magnetosphere–ionosphere system will not be fully understood.

This paper is organized as follows. In Section 2 the sources of cold plasma are discussed. Section 3 discusses that the cold ionospheric plasma can become a major source of hot plasma in the magnetosphere. Section 4 discusses the impact of the cold ions (including the warm plasma cloak) on magnetic reconnection, both on dayside and in the magnetotail. The impact of cold ions on the Kelvin–Helmholtz instability on the magnetopause is discussed in Section 5. The impact of the cold-particle populations on wave–particle interactions (cold electrons for chorus and hiss waves and cold ions for electromagnetic-ion-cyclotron (EMIC) and ultra-low-frequency (ULF) waves) is discussed in Section 6, while the impact of cold electrons on aurora structuring is presented in Section 7. Probable impacts associated with plasmaspheric refilling on open-drift trajectories and the remnant layer are presented in Section 8. The impact of cold electrons and cold ions on spacecraft charging is discussed in Section 9, while the problems associated with cold-electron and cold-ion measurements are discussed in Section 10. Conclusions are drawn in Section 11.

2. Sources of cold plasma

Broadly speaking, the source of cold plasma in the Earth's magnetosphere can be placed into three categories: the low latitude ionosphere, the high latitude ionosphere, and the solar wind. Exhaustive reviews of plasma sources at Earth, both cold and otherwise, are given by Hultqvist et al. (1999) and Welling et al. (2015a). The efficacy of each source depends on many factors, including solar extreme ultraviolet (EUV) flux, solar wind and interplanetary magnetic field conditions, and ionospheric conditions. These factors are responsible for controlling the originating reservoir for each source, acceleration or entry into the magnetosphere, and transport to regions of interest. All these factors must be considered when evaluating the potential and realized impact of cold plasma on the magnetosphere.

At low and medium latitudes, ionospheric ions upwell along closed field lines to produce the plasmasphere (Carpenter, 1962; Lemaire et al., 1998; Kotova, 2007). This is cold (< 1 eV) plasma consisting primarily of protons and electrons that, once in the magnetosphere, follows the local $\mathbf{E} \times \mathbf{B}$ drift velocity. Other species contribute moderately; He^+ accounts for $5-10\%$ of the total number density, reaching higher fractions as a function of geomagnetic activity (Darrouzet et al., 2009). Heavier ion abundance within the plasmasphere is around $\sim 3\%$ with few exceptions (Dandouras et al., 2013; Grew et al., 2007). While normally relegated to altitudes at or below geosynchronous, cold plasmasphere material may be transported to other areas of interest. This is achieved primarily via plasmaspheric plumes (Grebowsky, 1970; Spasojević et al., 2003; Sandel et al., 2003; Goldstein and Sandel, 2013; Goldstein, 2007), which can deliver as much as 2×10^{26} ions per second to the dayside magnetopause (Borovsky and Denton, 2008). Other processes for transporting cold plasma out of the plasmasphere and to higher L-shells may exist. One candidate process is the plasmaspheric wind, or radial expansion of the plasmasphere (Lemaire and Schunk, 1992; André and Lemaire, 2006; Pierrard et al., 2009). While some indirect evidence for this transport exists [e.g., Dandouras et al. (2013)], its existence remains controversial. Following the erosion of the plasmasphere after a severe geomagnetic storm, the plasma refilling time at $L > 3$ can be 4 days or even as long as 8 days (Park, 1970; Banks et al., 1971; Kotova, 2007; Obana et al., 2010). Note also that atmospheric photoelectrons are observed in the magnetosphere [e.g. Mantas et al. (1978), Coates et al. (1985), Peterson et al. (2009, 2013)]: it is known that they are important for plasmaspheric-refilling processes (Bailey et al., 1997; Varney et al., 2012).

At higher latitudes, i.e., auroral regions and open field line regions, cold ions originate from the topside ionosphere, outflowing along field lines and into the magnetosphere. This source of plasma is critical for understanding geospace dynamics; at times, it can become the dominant source of plasma in the magnetosphere (Chappell et al., 1987). Unlike lower latitude outflows, the composition includes non-trace amounts of H^+, He^+, O^+, and N^+ [e.g., Hoffman (1967), Chappell et al. (1982b), Chandler et al. (1991), Yau et al. (1991) and many more]. It can be decomposed into bulk ionospheric outflow [the "classical polar wind" (Axford, 1968; Banks and Holzer, 1968)] where ambipolar electric fields modify Jean's escape parameters, and suprathermal outflows, where different acceleration processes (including wave–particle interactions, centrifugal acceleration, and effects of hot electron populations) (Cladis, 1986; Horwitz et al., 1994; Khazanov et al., 1997; Schunk and Sojka, 1997; Moore et al., 1999a; Chaston et al., 2004, 2007; Moore and Khazanov, 2010) raise parallel velocities significantly

Table 1
Cold plasma populations of the Earth's magnetosphere and their known or probable effects on the magnetosphere–ionosphere system.

Cold population	Impact on the magnetosphere
Plasmasphere ions	Alter ULF frequency and radial diffusion of energetic electrons and ions Alter EMIC scattering of electron radiation belt
Plasmasphere electrons	Alter hiss decay of radiation-belt electrons Create whistler ducts
Plasmapause	Hiss-chorus boundary Site of enhanced ULF activity Site of shear-flow instabilities leading to giant undulations
Plasmaspheric plume ions	Reduce the dayside reconnection rate Alter Hall microphysics of dayside reconnection Alter EMIC scattering of outer electron radiation belt
Cloak ions (and oxygen torus)	Alter ULF frequency and radial diffusion of energetic electrons and ions Reduce the dayside reconnection rate Alter Hall microphysics of dayside reconnection Alter EMIC scattering of electron radiation belt Reduce electron-plasma-sheet-driven spacecraft charging Reduce threshold for Kelvin–Helmholtz on magnetopause
Cloak electrons	Alter chorus and affect electron-radiation-belt energization
Structured dawnside cold electrons	Produce spatial structure of (a) chorus-wave amplitudes and (b) the pulsating aurora
Charge-exchange-byproduct protons	Alter Hall-microphysics of dayside reconnection May increase early-time plasmaspheric refilling rate Alter EMIC scattering of electron radiation belt
Ionospheric ion outflows	Provide a major source of magnetospheric plasma
Ionospheric ion outflows in magnetotail	Alter Hall microphysics of magnetotail reconnection Mass loading of magnetotail reconnection; altering magnetotail tearing instability
Ionospheric electron outflows	Alter chorus properties

over background values. The bulk polar wind is characterized by velocities of the order of 1–10 km/s at altitudes around 10,000 km (Yau and André, 1997), corresponding to a drift energy of 1–10 eV. The thermal energy is at most a few eV (Abe et al., 1996). It yields fluxes of $1–20\times10^7$ cm^{-2} s^{-1} for H^+; O^+ fluxes tend to be around a factor of two lower. Note that these ionospheric outflows can also include molecular ions, e.g. NO^+, N_2^+ and O_2^+. For instance, the Dynamics Explorer 1 mission measured fluxes up to 2×10^6 cm^{-2} s^{-1} of molecular ions at geocentric distances up to 3 Earth radii over the polar cap during a large geomagnetic storm (Craven et al., 1985). Similar fluxes were also observed at lunar distances by the Acceleration, Reconnection, Turbulence, and Electrodynamics of the Moon's Interaction with the Sun (ARTEMIS) mission during geomagnetically active times (Poppe et al., 2016). The polar wind also contains outflowing photoelectrons from the sunlit atmosphere (Kitamura et al., 2012) that are important components of the driving of the polar wind (Khazanov et al., 1997; Su et al., 1998; Glocer et al., 2017). Outflow fluxes and composition vary considerably and are strongly correlated with solar and magnetospheric activity, including solar EUV radiation, interplanetary magnetic fields, solar wind pressure, geomagnetic indices, and, more directly, precipitating electron fluxes and Poynting fluxes into the ionosphere (Yau et al., 1985; Tam et al., 1998; Barghouthi et al., 1998; Barakat and Schunk, 2001; Moore et al., 1999b; Cully et al., 2003a; Strangeway et al., 2005; Kitamura et al., 2011).

Understanding the fate of these outflows as they are transported through the magnetosphere is critical to understanding their eventual impacts on the system. In the lobes, the coldest populations can be significant, but incredibly difficult to observe (Engwall et al., 2006; Engwall et al., 2009a; André and Cully, 2012; Haaland et al., 2015). The energy spectra of faster outflowing populations provide hints as to their source. For example, "beams" indicate ionospheric ions originating from the cusp or dayside polar cap (Candidi et al., 1982; Seki et al., 1998, 2000; Kistler et al., 2010; Liao et al., 2010, 2015), velocity filtered and segregated by composition via the well-known geomagnetic mass spectrometer effect during their journey across the lobes to the tail (Horwitz, 1986; Chappell et al., 1987; Delcourt et al., 1992). Conversely, dispersed patterns indicate contributions from the nightside auroral oval that can directly feed the plasma sheet (Sauvaud et al., 2004; Kistler et al., 2010). Upon arrival to the plasma sheet, these populations change the temperature, density, and mass profiles of the local plasma. Under southward interplanetary magnetic field (IMF) conditions, they advect daywards, are heated, and contribute significantly to the ring current — no longer a true "cold plasma" [e.g., Sharp et al. (1985), Daglis et al. (1999), Kozyra et al. (2002), Welling et al. (2011), Kronberg et al. (2012, 2014)]. A portion forms the "warm plasma cloak", a portion circulating through and around the inner magnetosphere without substantial heating (Chappell et al., 2008). This population (which might be synonymous with the oxygen torus) may affect dayside dynamics (Zhang et al., 2016).

The final source of cold plasma is the solar wind, which is not traditionally considered a cold plasma population. The solar wind consists primarily of electrons and protons with temperature of the order of 10 eV flowing at around 400 km/s. For ions, the flow kinetic energy is ~1 keV and dominates over the thermal energy. Crossing the bow shock, the solar wind temperature in the magnetosheath rises to ~20-60 eV for electrons and ~100 eV-1 keV for ions on the dayside (Wang et al., 2012), with a flow velocity which is about half of the upstream solar wind velocity [see Fig. 4 of Dimmock and Nykyri (2013)]. The magnetosheath plasma cools off to ~10-30 eV for electrons and ~30-300 eV for ions as it moves to the nightside, while its drift velocity returns to values comparable to the upstream solar wind (Wang et al., 2012; Dimmock and Nykyri, 2013). Thus, the total energy of the magnetosheath is ~1 keV for ions while magnetosheath electrons can remain cold. Historically, the most important entry mechanism for the solar wind is thought to be dayside reconnection under southward IMF conditions [Dungey (1961); see reviews by Fuselier and Lewis (2011); Paschmann et al. (2013)]. Plasma entering at or near the reconnection region can be heated and is not typically thought of as being "cold". Entry through reconnection regions only accounts for a fraction of solar wind entry, however, and other mechanisms allow entry without significant heating. Plasma captured along newly reconnected flux tubes can allow entry through the mantle without heating. Under northward IMF conditions, high latitude reconnection will draw magnetosheath plasma into the low-latitude boundary layer (LLBL). The LLBL can be further populated by a myriad of other processes, including Kelvin–Helmholtz waves along the flanks. From

the LLBL, magnetosheath plasma makes its way to the central plasma sheet [see, e.g., Wing et al. (2014)]. However, the exact mechanism for its inward flow is unclear [see Welling et al. (2015a) for an in-depth discussion]. Inward diffusion of this plasma, interchange instabilities, Kelvin–Helmholtz vortices, and other processes have been investigated but the dominant mechanism remains unclear.

Under periods of extended quiet times, the magnetosheath source of plasma builds into the 'cold, dense plasma sheet' (CDPS)- a nightside population whose characteristics (> 1 cm^{-3}, < 1 keV) are colder and denser than the typical hot and tenuous plasma sheet [e.g., Lennartsson (1992), Terasawa et al. (1997), Fujimoto et al. (1998), Phan et al. (2000), Huang et al. (2002), Øieroset et al. (2005)]. The role of this population is that of a reservoir for active periods. Under southward IMF conditions, the CDPS advects daywards and the overall density drops precipitously. The entry mechanisms described above are most efficacious under quiet conditions, so the CDPS does not reappear until stably quiet conditions return. For these reasons, this population is only likely to affect the magnetosphere during prolonged quiet times and during the early phases of geomagnetic storms [e.g., Thomsen et al. (2003), Lavraud et al. (2006)].

Many open questions remain concerning sources of cold ion and cold-electron populations to the magnetosphere. Fundamentally, how the solar wind and ionospheric sources of plasma balance each other, and how this balance changes with solar and terrestrial activity, remains only poorly understood. The amount and rate of new plasma provided by these sources is only roughly quantified. Many sub-questions about entry and acceleration mechanisms are also unanswered. What acceleration mechanisms are most important for delivering light and heavy ions from the ionosphere to the magnetosphere? What processes are most important for transporting LLBL plasma to the central plasma sheet? While ionospheric outflow rates are affected by magnetospheric dynamics and processes, the outflowing populations then, in turn, affect magnetospheric dynamics. Several studies have made this connection, identifying mass–energy feedback loops between the two domains (Brambles et al., 2011; Moore et al., 2014; Welling et al., 2015a). Open questions persist concerning the existence of such feedback loops and their importance in the near-Earth space system (Welling and Liemohn, 2016). Further, questions about heavy-ion composition remain poorly explored. Notably, the ionosphere is capable of providing large amounts of nitrogen ions to the magnetosphere, which has different properties than the widely-studied oxygen populations. The existence of nitrogen in the magnetosphere has been confirmed, but its role largely neglected (Ilie and Liemohn, 2016). These questions are only a selection of a greater set of unknowns concerning cold ion sources in the magnetosphere.

3. Cold-plasma source of hot magnetospheric plasma

One of the most important impacts of the cold plasma is that it can become the dominant source of hot magnetospheric plasma. Early on in the space age, the solar wind was considered the main source of plasma throughout the magnetosphere. The discovery of energetic O^+ ions in the inner magnetosphere (Shelley et al., 1972), clearly of ionospheric origin, began to change this prevailing point of view. Earlier missions were limited in the lowest ion energy that could be measured but the development of more sophisticated instrumentation, culminating with the retarding ion mass spectrometer (RIMS) instrument on the Dynamics Explorer 1 mission that measured cold ions with energies from the spacecraft potential to ~50 eV (Chappell et al., 1981), allowed a much better characterization of the ionospheric sources of cold plasma as well as their transport and energization mechanisms in the magnetosphere [see Chappell et al. (1987) and references therein]. Aided by available data on ionospheric outflow, Chappell et al. (1987) estimated the ion density in the plasmasphere, plasma through, plasma sheet and magnetotail lobes and concluded that the observed magnetospheric densities could be fully obtained by an ionospheric source, without any contribution from the solar wind.

Subsequent numerical studies have confirmed that the ionosphere can be the dominant source of magnetospheric plasma. Huddleston et al. (2005) used test particle simulations to study the dynamics of ionospheric ion outflow, whose initial properties were obtained from the Polar mission. These simulations indicate that cold ionospheric ions can be accelerated to plasma sheet (1 – 10 keV) or even ring current (1 – 100 keV) energies as they cross the neutral sheet far (tens of Earth radii) downtail and then move Earthward through the cross-tail potential. More recently, multi-fluid simulations have been used to study the impact of ionospheric outflow on the dynamics of the magnetosphere and to separate the contributions of the ionospheric and solar wind sources (Winglee, 2000; Glocer et al., 2009; Welling and Ridley, 2010; Brambles et al., 2010). Welling and Ridley (2010) showed that during southward IMF the dominant source of magnetospheric plasma comes from ionospheric plasma entering deep down tail through reconnecting field lines. During northward IMF, the dominant source is solar wind entering from the flanks of the magnetosphere. Spacecraft surveys have shown that the relative contribution of the ionosphere relative to the solar wind (1) increases with increasing geomagnetic activity (Young et al., 1982; Lennartsson and Shelley, 1986; Maggiolo and Kistler, 2014) and (2) increases with increasing solar F10.7 (Lennartsson, 1989; Kistler and Mouikis, 2016).

In general, it is important to emphasize that these multi-fluid numerical studies show that the outflow is not just a source of plasma, but can strongly affect the dynamics of the magnetosphere: examples of this impact include the reduction of the cross cap potential during geomagnetic storms (Winglee et al., 2002; Glocer et al., 2009), the increase of the strength of the ring current (Brambles et al., 2010; Welling et al., 2015b), which in turn can feed back on the strength of the outflow (Welling et al., 2015b), altering the dynamics of the magnetotail and increasing substorm activity (Wiltberger et al., 2010), and controlling the magnetospheric sawtooth cycle (Brambles et al., 2011; Ouellette et al., 2013).

4. Magnetic reconnection

In this section, we discuss the impact of cold ions (including those of the warm plasma cloak) on magnetic reconnection.

4.1. Dayside

Dayside reconnection magnetically connects the Earth's magnetosphere with the moving solar-wind plasma. This drives magnetospheric convection, ionospheric convection, and geomagnetic activity. Whatever controls the dayside reconnection rate controls solar-wind/magnetosphere coupling, convection, and geomagnetic activity. The entry of solar-wind plasma into the magnetosphere also depends, in part, on the dayside reconnection rate. In collisionless plasmas the local reconnection rate is controlled by the Alfvén speed $v_A = \frac{B}{\sqrt{\mu_0 \rho}}$ in the plasma at the site of the reconnection, where B is the magnetic-field strength and ρ is the mass–density of the plasma. A rule of thumb for classic collisionless reconnection is that the reconnection rate R is $R = 0.1 B v_A$ [e.g. Petschek (1964), Parker (1973), Birn and Hesse (2001)], with the plasma on both sides flowing into the reconnection site at $0.1 v_A$ carrying a field B. For asymmetric reconnection (Borovsky and Hesse, 2007; Cassak and Shay, 2007; Birn et al., 2008) where the two plasmas on either side of the reconnection site have differing B and/or ρ values, the local reconnection rate is governed by a hybrid Alfvén speed. This local reconnection rate R is described by the Cassak–Shay equation [cf. Eq. (1) of Borovsky (2008)]

$$R = 2K \frac{B_m^{3/2} B_s^{3/2}}{\sqrt{B_m \rho_s + B_s \rho_m} \sqrt{B_s + B_m}} \quad (1)$$

where $K \approx 0.1$ is a coefficient representing the geometry of the inflow and outflow through the reconnection site. In expression (1) the subscripts "m" represents the magnetospheric side of the dayside reconnection site and "s" represents the magnetosheath side. There are four variables affecting the dayside reconnection rate: B_s, B_m, ρ_s, and ρ_m. The values of the three variables B_s, B_m, and ρ_s are controlled by the solar wind [cf. Borovsky (2008), Borovsky and Birn (2014)], but ρ_m is not. This gives the Earth some control over solar-wind/magnetosphere coupling (Borovsky, 2014): at times the magnetospheric plasma can "mass load" the reconnection site and reduce the reconnection rate. From the mass–density denominator of expression (1) a dimensionless parameter M can be written which gauges the effect of ρ_m on the dayside reconnection rate:

$$M = \frac{1}{\sqrt{1 + \frac{\rho_m B_s}{\rho_s B_m}}}. \tag{2}$$

For typical solar-wind values upstream of the bow shock ($n_{sw} = 6.3$ cm^{-3}, $B_{sw} = 5.8$ nT, and $v_{sw} = 430$ km/s) the values of B_s, B_m, and ρ_s at the nose of the magnetosphere are $B_s \approx 44$ nT, $B_m \approx 70$ nT, and $\rho_s \approx 25$ amu/cm^3. Using those values in expression (2), the quantity $\rho_m B_s/\rho_s B_m$ is greater than 1 if $\rho_m > \rho_s B_m/B_s \approx 40$ amu/cm^3. Under typical geomagnetic conditions, the mass–density in the dayside magnetosphere near the magnetopause is lower than this value, and so the mass–density of the magnetosphere does not strongly affect the dayside reconnection rate. During geomagnetic storms, the case is different.

There are three magnetospheric particle populations that come into play for dayside reconnection: (1) the plasmaspheric drainage plume, (2) O^+ in the warm plasma cloak, and (3) O^+ in the ion plasma sheet.

The magnetospheric mass loading of dayside reconnection was first suggested for the plasmaspheric drainage plume (Borovsky and Steinberg, 2006; Borovsky and Denton, 2006), where the mass loading was known as the "plasmasphere effect". At the dayside magnetosphere the plasmaspheric drainage plume can have a number density $\rho_m \sim 200$ cm^{-3} [cf. Fig. 4 of Borovsky et al. (1997) and Fig. 4 of Walsh et al. (2013)]. If the plume plasma were 100% protons, the mass–density would be $\rho_m \sim 200$ amu/cm^3, large enough to be important in expressions (1) and (2), even against the stormtime magnetosheath conditions (Borovsky et al., 2013). During geomagnetic storms the dayside reconnection rate can be strongly suppressed where the plasmaspheric drainage plume flows into the magnetopause, a region that is many hours of local time wide early in a storm and then narrows to a couple of hours of local time for the duration of the storm. An assessment of this mass loading can be found in Borovsky et al. (2013). The mass loading of the dayside local reconnection rate by the plasmasphere has been confirmed via global-MHD computer simulations (Borovsky et al., 2008; Ouellette et al., 2016) and via coordinated radar and in-situ magnetospheric measurements (Walsh et al., 2014).

The warm plasma cloak flows Sunward through the dipolar magnetosphere and into the dayside magnetopause. The cloak is more dense when geomagnetic activity is higher, when the solar UV flux (as proxied by F10.7) is higher, and on the dawn side of the dipole more than on the dusk side [cf. the properties of the oxygen torus (Nosé et al., 2015; Nosé et al., 2020)]. Unlike the plasmaspheric drainage plume, which can be narrow, the cloak flows into the dayside reconnection line across most of the dayside magnetopause. The mass–density of the cloak ions near the magnetopause is not well known. In-situ spacecraft surveys (Jahn et al., 2017; Gkioulidou et al., 2019) indicate that the O^+ number density is ~1 cm^{-3} in the outer dayside magnetosphere, yielding total mass–densities (with He^+ and H^+) of $\rho_m \sim 20$ amu/cm^3. Ultra-low-frequency (ULF) sounding from equatorial spacecraft (Takahashi et al., 2010, 2014; Denton et al., 2011, 2014) indicates considerable variability of the dayside mass–density. Borovsky et al. (2013) analyzing ULF sounding results came up with the rule of thumb for the 8 - 12 local time region that if the solar F10.7 index is low, mass–densities $\rho_{geo} \sim 3$–15 amu/cm^3 are found, and if F10.7 is high, mass–densities $\rho_{geo} \sim 15$–100 amu/cm^3 are found. At the upper end of these mass–density values, the cloak ions certainly could globally reduce the dayside reconnection rate. A detailed assessment of the effect appears in Borovsky et al. (2013). Fuselier et al. (2017) conducted a survey of the impact of magnetospheric (plume and cloak) ions at the magnetopause, using over five months of data (from September 2015 to March 2016) collected by the Magnetospheric Multiscale (MMS) mission. They concluded that reductions of the reconnection rate by more than 20% occur infrequently (a few percent of the time) during weak geomagnetic activity. A follow-up study (Fuselier et al., 2019) focusing on the warm plasma cloak during geomagnetically active times concluded that the reconnection rate was reduced by more than 20% in about 25% of the magnetopause encounters. This study, however, also acknowledges the difficulty of capturing the full extent of the reconnection-rate reduction during storms due to the fact that MMS might not have observed the peak of the oxygen density and that these events occurred during the declining phase of a weak solar cycle. Note that earlier assessments argued that the substantial reduction of the dayside reconnection rate by the magnetospheric plasma would only occur during geomagnetic storms [e.g. Borovsky and Steinberg (2006), Borovsky et al. (2013)].

The third population that is important for magnetospheric control of the dayside reconnection rate is O^+ in the ion plasma sheet, which is also important during geomagnetic storms (Borovsky et al., 2013). Since this is an overview of cold plasma effects, and the ion-plasma-sheet oxygen is hot (multiple keV), this third population will not be discussed.

An open controversy that particularly applies to the case of dayside-reconnection mass loading by the plasmaspheric drainage plume is whether reconnection increases outside of the plume region to maintain the total reconnection rate on the dayside magnetosphere (Lopez, 2016; Ouellette et al., 2016; Zhang et al., 2016, 2017). The change in the magnetosheath flow pattern caused by the localized reduction in reconnection could result in changes in the magnetosheath mass–density and field strength along other regions of the reconnection line, resulting in changes in the localized reconnection rates.

In addition to mass loading, cold ions can also modify the microscopic physics of magnetic reconnection via modification of the Hall physics. In essence, cold ions introduce an intermediate scale (the cold ion gyroradius) in the diffusion region where hot ions are demagnetized but cold ions and electrons are not. This results in a reduction of the Hall current carried by the electrons (Toledo-Redondo et al., 2015; André et al., 2016; Toledo-Redondo et al., 2018). Simulations have shown that this effect occurs along the whole separatrix region (Dargent et al., 2017). In general, the reduction of the Hall current can lead to changes in the ions drift speed and affect local drift instabilities (Toledo-Redondo et al., 2018), such as the ion–ion drift instabilities associated with the formation of lower-hybrid drift waves in the separatrix region (Graham et al., 2017). The peak Hall electric field is also reduced, however Toledo-Redondo et al. (2018) showed with kinetic simulations that this reduction is not accompanied by significant changes in the potential drop across the Hall electric field region. Finally, cold ions can be heated by waves and electric-field gradients in the in-flow region as they cross the magnetospheric separatrix. Cold ion heating is significant and has been estimated in at least 10–25% of the total energy converted into ion heating by reconnection (Toledo-Redondo et al., 2017). In terms of impact on the local reconnection rate, recent kinetic simulations have shown that cold ions affect the reconnection rate predominantly via mass loading and not via kinetic effects (Dargent et al., 2017, 2020).

An outstanding issue about cold plasma and the dayside reconnection rate involves the lack of understanding of the mass–density of the warm plasma cloak in the dayside magnetosphere and what controls it. A quality survey of the ion composition and density of the cloak as functions of local time and distance from the Earth in the dayside

magnetosphere is needed, along with an understanding of the roles of the time histories of the solar wind, geomagnetic activity, and solar UV flux. Until such knowledge is gained, accurate predictions of the strength of solar-wind/magnetosphere coupling cannot be made.

4.2. Magnetotail

Similarly to reconnection on the dayside magnetopause, reconnection in the magnetotail can be affected by mass loading. However, there are several factors that differentiate reconnection processes in the tail from those on the dayside: (i) the reconnection layer is nearly symmetric; (ii) the equilibrium configuration, including plasma composition, is determined by global magnetospheric dynamics and may depend on the history of the system; (iii) the question of how and when magnetic reconnection is initiated (the onset problem) is of considerable practical significance; (iv) the question of how near-Earth reconnection turns off once it has commenced is an outstanding issue.

Observations demonstrate that the composition of the plasma sheet in the Earth's magnetotail depends on both solar EUV radiation and geomagnetic conditions. The ionospheric contribution to the plasma sheet may originate from several regions, such as the "cleft ion fountain" or from the nightside aurora. These contributions may contain significant fluxes of O^+, especially during geomagnetically active times [e.g. Nosé et al. (2009), Mouikis et al. (2010), Maggiolo and Kistler (2014)]. Typical values for the O^+/H^+ ratio in the plasma sheet range from 0.01 to 0.5, but large deviations from these values are also possible (Kistler et al., 2005). Ionospheric ion outflows from the cusp and polar cap tend to be of lower energies: the polar wind is typically only a few eV (Chappell et al., 1987). Ion outflows from the auroral zone, on the other hand, can be in the keV energy range [e.g. Yau et al. (1985)].

One aspect of the problem concerns the impact of cold ions on substorm onset. Several authors have performed test particle simulations constrained by available observational data to determine the magnetospheric dynamics of ionospheric cold-ion sources (Cully et al., 2003b; Huddleston et al., 2005; Li et al., 2013a). Despite their limitations, mostly associated with the choice of a particular model of the magnetospheric electric and magnetic fields which could be inaccurate away from Earth, these studies have shown that the ionosphere could be the dominant source of charged particles of the magnetosphere and have identified the acceleration mechanisms of ionospheric particles drifting through the magnetosphere. Huddleston et al. (2005) indicate that cold ionospheric ions can be accelerated to plasma sheet or ring current energies depending on where they cross the neutral sheet. Particles with equatorial magnetotail crossings closer to the Earth experience less acceleration, as in the case of the particles that end up forming the warm plasma cloak (Chappell et al., 2008). Some ion outflows can also reach the plasma sheet experiencing relatively low acceleration, ~10-100 eV (Cully et al., 2003b; Huddleston et al., 2005; Li et al., 2013a). Observations have indeed confirmed the presence of low-energy cold/warm ions coexisting with the traditional plasma sheet populations (Seki et al., 2003; Thomsen et al., 2003). Seki et al. (2003), for instance, show a Geotail event in eclipse, at $X_{GSM} \sim -9\,R_E$ (in geocentric solar magnetic coordinates, with R_E the Earth's radius), characterized by few-hundred eV ions with density ~ 0.2 cm^{-3} comparable with the density of ions in the $1-20$ keV range. In principle, these cold/warm ion populations could mass load near-Earth tail reconnection, particularly for those rare events that occur closer to geosynchronous orbit (Angelopoulos et al., 2020). However, whether there is sufficiently high cold-ion density at distances that are relevant to typical near-Earth tail reconnection ($\sim 15\,R_E$) remains an open question. Similarly, colder ions could in principle also affect the Hall microphysics of near-Earth tail reconnection but whether this effect could really be important remains unclear.

On the other hand, significant attention has been paid to the possible influence of (mostly warm) heavy ions on substorm onset. Since the electron tearing mode is expected to be stable in a magnetotail configuration due to the presence of a magnetic field component normal to the current sheet, the ion tearing instability has long been considered as a possible mechanism of reconnection onset (Schindler, 1974). For a given thickness of the current sheet, the growth rate of the ion tearing mode increases with the ion gyroradius and, consequently, with the ion mass. Based on these considerations, Baker et al. (1982) proposed that the growth rate of the ion tearing mode is locally enhanced in those regions of the plasma sheet where the density of O^+ ions is enhanced and demonstrated that the statistical distribution of the dusk–dawn asymmetry of such enhancements is consistent with substorm observations [see also Frey (2004)]. However, a long-term study using 16 years of Geotail data reported by Nosé et al. (2009) found no correlation between plasma sheet ion composition and the substorm occurrence rate.

More recently, Liu et al. (2013b) used Cluster data to monitor how the maximum magnetotail pressure and its rate of change during substorms depend on the O^+ content of the plasma sheet. They demonstrated that both the pressure and the rate of pressure decrease are strongly correlated with the density of O^+. Based on these observations, Liu et al. (2013b) proposed that an increased O^+ content makes it more difficult to trigger the substorm onset. However, once triggered, the unloading rates appear to be positively correlated with the O^+ content [see also Kistler et al. (2006)].

These observations have proven difficult to reconcile with simulations. For example, Shay and Swisdak (2004) performed a three-fluid reconnection simulation and concluded, in general agreement with a symmetric form of Eq. (1), that the presence of O^+ reduces the reconnection rate and that the expansion phase of substorms will take longer to occur or will reconnect less lobe field in the same amount of time. Similar conclusions were reached by Karimabadi et al. (2011) based on the results of particle-in-cell simulations [see also Markidis et al. (2011)]. They also demonstrated that O^+ ions have an appreciable effect on the reconnection onset only if they carry a significant portion of the cross-tail current. One of the ways lobe O^+ could be assimilated into the current sheet is through the "flushing" mechanism — once reconnection begins, lobe O^+ ions are quickly assimilated into the current sheet (Karimabadi et al., 2011).

Taken together, existing observations and theoretical and numerical analysis paint a rather complicated picture of the influence of heavy ions, and in particular of O^+, on magnetic reconnection in the tail. [See also Brambles et al. (2011); Ouellette et al. (2013) and Kolstø et al. (2020).] The ion composition of the plasma sheet in the tail depends on several factors, including geomagnetic activity, EUV flux, and the history of the system. While the presence of O^+ decreases local reconnection rates, a delay in the onset of a substorm may allow for a larger accumulation of thermal and magnetic pressure in the tail, which may compensate for the decreasing Alfvén speed and result in a net *increase* of the unloading rate.

Another longstanding question of magnetospheric physics has been how near-Earth reconnection in the magnetotail ceases [cf. Sect. 2.2 of Borovsky et al. (2020)]. The ceasing of near-Earth reconnection marks the end of the substorm expansion phase (Hesse and Birn, 2004). One candidate mechanism to shut off near-Earth reconnection is the entry of mantle plasma into the near-Earth neutral line. Cusp ionospheric outflows plus magnetosheath plasma entering the cusp are both caught up in the advection of open magnetic-field lines from the dayside reconnection site, over the polar cap, and into the lobes in the magnetotail. Ions are free to move along the magnetic field lines so, even if the plasma is initially warm (such as the ~keV temperature of the magnetosheath), time-of-flight cooling of the plasma will occur in the parallel-to-**B** direction (Rosenbauer et al., 1975). In the lobes, the mantle ions appear as a cold, dense, field-aligned beam traveling downtail. As substorm near-Earth reconnection progresses, it reconnects all of the field lines in the plasma sheet and begins to reconnect lobe magnetic-field lines. Eventually, reconnection reaches the mantle

plasma in the lobes where the high-density plasma can reduce (mass load) the near-Earth reconnection rate and where the large downtail momentum of the mantle ions can push the near-Earth neutral line downtail.

In all, it is clear that further progress requires a global view of these problems, supported by a comprehensive set of observations, as well as by simulation tools capable of accurately describing global dynamics of the magnetotail, transport of cold ions from the ionosphere into the magnetotail, and their influence on the local reconnection process, including the kinetics of the reconnection onset.

5. Kelvin-Helmholtz instability on the magnetopause

It is well known that Kelvin–Helmholtz waves occur on the Earth's magnetopause driven by the relative flow between the magnetosheath plasma and the magnetospheric plasma (Farrugia et al., 2000; Kavosi and Raeder, 2015). The Kelvin–Helmholz waves are capable of transporting mass and momentum from the magnetosheath into the magnetosphere. For decades the Kelvin–Helmholtz instability has been thought to be an important mechanism for the viscous interaction between the solar wind and the Earth's magnetosphere (Axford and Hines, 2013), accounting for a residual level of magnetospheric convection and geomagnetic activity when dayside reconnection should not be operating (Tsurutani and Gonzalez, 1995). The Kelvin–Helmholtz instability on the magnetopause is probably important for mass entry of solar-wind plasma into the magnetosphere, wherein large-scale Kelvin–Helmholtz waves on the magnetopause are believed to exchange plasma parcels and that may lead to reconnection in the LLBL (Nykyri and Otto, 2001; Cowee et al., 2010; Hasegawa et al., 2004; Masson and Nykyri, 2018; Nakamura et al., 2017). Kelvin–Helmholtz waves on the magnetopause are also suspected for producing ULF oscillations in the interior of the magnetosphere (Claudepierre et al., 2008; Kozyreva and Kleimenova, 2010).

The magnetospheric mass–density affects the onset conditions and the growth rate for the Kelvin–Helmholtz instability on the magnetopause (Walsh et al., 2015). Otto and Fairfield (2000) give the onset condition of the instability to be

$$\left[\mathbf{k}\cdot\left(\mathbf{v}_s-\mathbf{v}_m\right)\right]^2 > \frac{\left[\left(\mathbf{k}\cdot\mathbf{B}_s\right)^2+\left(\mathbf{k}\cdot\mathbf{B}_m\right)^2\right]\left(\rho_s+\rho_m\right)}{4\pi\rho_s\rho_m}, \tag{3}$$

where $\mathbf{k}$ is the wavevector, $\mathbf{v}$ is the flow velocity, $\mathbf{B}$ is the magnetic-field vector, ρ is the plasma mass–density, and again the subscripts 's' indicate the magnetosheath and 'm' indicate the magnetosphere. This instability threshold contains the ratio

$$\bar{R} = \frac{\rho_s+\rho_m}{\rho_s\rho_m}. \tag{4}$$

The warm plasma cloak can substantially change the mass–density ρ_m of the magnetosphere. Take $\rho_s = 20$ amu/cm^3. If the magnetosphere does not have a warm plasma cloak, then $\rho_m \sim 1$ amu/cm^3 and $\bar{R} \sim 1$ cm^3/amu. If the magnetosphere does have a cloak, then $\rho_m \sim 10$ amu/cm^3 and $\bar{R} \sim 0.15$ cm^3/amu. For the same values of $\mathbf{k}$, $\mathbf{v}$, and $\mathbf{B}$, the presence of the cloak plasma in the magnetosphere lowers the threshold for the Kelvin–Helmholtz instability on the magnetopause by a factor of about 7. Changing the threshold condition controls when and where the Kelvin–Helmholtz waves are active on the magnetopause, altering the strength of the viscous interaction and impacting the transport of solar-wind plasma into the magnetosphere. We also note that finite compressibility effects tend to be stabilizing for Kelvin–Helmholtz modes. For simple limiting cases previously considered in the literature, this imposes an upper bound on the magnitude of the velocity jump between the two sides of the interface in Eq. (3) that depends on the sound speed [e.g. Miura and Pritchett (1982)]. Mass loading the interface with cold plasma may significantly affect the sound speed, thus significantly affecting the range of the unstable modes.

6. Wave–particle interactions

In this section, we discuss the impact of cold electrons and cold ions on wave–particle interactions.

6.1. Whistler waves

Whistler waves are right-hand polarized, electromagnetic emissions with frequency between the lower hybrid frequency and the electron–cyclotron frequency, i.e. 100 Hz to 30 kHz for conditions relevant to the Earth's magnetosphere. They are ubiquitous and play a major role in determining the dynamics of the near-Earth environment through wave–particle interaction physics (Thorne, 2010). They are typically classified as chorus and hiss waves because of their somewhat different properties (leading to a different sound when converted to audio), and these two types of whistlers will be discussed separately in the next two subsections.

6.1.1. Whistler-mode chorus waves

Whistler-mode chorus waves are discrete emissions often occurring in two distinct bands, above and below half of the local electron cyclotron frequency (Burtis and Helliwell, 1969; Tsurutani and Smith, 1974; Santolík et al., 2009; Li et al., 2013b). Chorus waves are excited predominantly near the magnetic equator outside the plasmasphere and in the nightside-to-morning sectors (Hayosh et al., 2010). They come in a variety of forms, including rising and (less frequently) falling tones (Santolík et al., 2004; Macúšová et al., 2010). They are responsible for local acceleration (Summers et al., 1998; Meredith et al., 2002, 2003b) and electron precipitation in the form of diffuse (Ni et al., 2014) and pulsating aurora (Nishimura et al., 2010; Kasahara et al., 2018) or microbursts (Oliven and Gurnett, 1968; Breneman et al., 2017).

Chorus waves are believed to be generated by an electromagnetic instability driven by temperature anisotropy (i.e. perpendicular temperature larger than parallel temperature, where parallel and perpendicular are relative to the local magnetic field) (Kennel and Petschek, 1966; Gary, 2005), which will be referred to as the cyclotron instability in the following. On the nightside, they are associated with the injection of hot (~keV) electrons from the plasma sheet during substorms.

Chorus waves are strongly affected by the presence of a cold electron population (Cuperman and Landau, 1974; Gary et al., 2012b; Wu et al., 2013; Cuperman et al., 1973), i.e. electrons whose thermal speed is much lower than the phase speed of the whistler waves. This can be easily understood by analyzing the role played by cold electrons on the cyclotron instability that generates the waves. We specialize the calculation to the case of an isotropic Maxwellian distribution function of cold electrons (with density n_c and temperature $T_e^c \longrightarrow 0$) and a bi-Maxwellian distribution function for the energetic electrons (with density n_h, parallel temperature $T_{e\|}^h$ and perpendicular temperature $T_{e\perp}^h$). The background magnetic field B_0 is along the z axis in a Cartesian (x, y, z) reference frame. Starting from the classic dispersion relation of kinetic plasma theory, neglecting the ion response and assuming that the wave-vector $\mathbf{k}$ is aligned to the local magnetic field, $\mathbf{k} = k\mathbf{e}_z$ (with $\mathbf{e}_z$ the unit vector along z), we obtain (Cuperman and Landau, 1974)

$$\omega^2-(ck)^2-\frac{\omega_{pe,c}^2\omega}{\omega-\omega_{ce}}+\frac{\omega_{pe,h}^2\omega}{\omega-\omega_{ce}}\zeta Z(\zeta)+A\omega_{pe,h}^2\left[1+\zeta Z(\zeta)\right]=0. \tag{5}$$

In Eq. (5), $\omega = \omega_r + i\omega_i$ is the frequency of the waves (with ω_r and ω_i real and imaginary parts), c is the speed of light, $\omega_{pe,c}$ ($\omega_{pe,h}$) is the electron plasma frequency calculated with the cold (hot) density, ω_{ce} is the positive electron cyclotron frequency evaluated with the background magnetic field, $\zeta = \frac{\omega-\omega_{ce}}{kv_{t\|}^h}$, $v_{t\|}^h = \sqrt{2T_{e\|}^h/m_e}$ is the parallel thermal velocity of the hot electrons (m_e is the electron mass), Z is the plasma dispersion function (Fried and Conte, 1961), $A = \frac{T_{e\perp}^h}{T_{e\|}^h} - 1$ is the hot

temperature anisotropy, and we are considering the case where $\omega_i > 0$ (i.e. the system is unstable) and $\omega_r, k > 0$.

We consider Eq. (5) in the limit where the index of refraction $n = ck/\omega \gg 1$ and $|\zeta| \gg 1$. This allows us to neglect the first term of Eq. (5) and to use the large-argument expansion of the plasma dispersion function $Z(\zeta)$ [see Fitzpatrick (2014)]. With an ordering where $kd_e^t < 1$ ($d_e^t = c/\omega_{pe,t}$ is the electron inertial length evaluated with the total electron density $n_t = n_c + n_h$), $(kd_e^t)^2 \ll 1$ and $\omega_r \ll \omega_{ce}$, these two conditions become an inequality for kd_e^t, $kd_e^t \ll \min\left(\frac{\omega_{pe,t}}{\omega_{ce}}, \frac{1}{\frac{\omega_{pe,t}}{\omega_{ce}}\frac{v_{t\parallel}^h}{c}}\right)$. Note that for typical conditions relevant to chorus waves, $\omega_{pe,t}/\omega_{ce} > 1$ while $T_{e\parallel}^h$ is in the keV range so that $\frac{v_{t\parallel}^h}{c} \ll 1$. In the limit $\omega_i/\omega_r \ll 1$, we obtain

$$\omega_r = \omega_{ce}\frac{\left(kd_e^t\right)^2}{1+\left(kd_e^t\right)^2} \simeq \omega_{ce}\left(kd_e^t\right)^2, \tag{6}$$

$$\omega_i = \sqrt{\pi}\frac{n_h}{n_t}\omega_{ce}\left(1-\frac{\omega_r}{\omega_{ce}}\right)^2\left(A-\frac{1}{\frac{\omega_{ce}}{\omega_r}-1}\right)\exp\left[-\left(\frac{V_R}{v_{t\parallel}^h}\right)^2\right]\left|\frac{V_R}{v_{t\parallel}^h}\right| \tag{7}$$

to first order in ω_i and valid for $\omega_i/\omega_r < \left(\frac{\omega_{pe,t}}{\omega_{ce}}\frac{v_{t\parallel}^h}{c}\right)^2$. In Eq. (7) we have introduced the resonant velocity

$$V_R = \frac{\omega_r - \omega_{ce}}{k}, \tag{8}$$

i.e. the velocity at which electrons are in resonance with the waves. When $n_c = 0$ ($n_h = n_t$), the growth rate (7) recovers the expression derived in Kennel and Petschek (1966) and one can see that a sufficiently large temperature anisotropy drives the instability, $A > 1/\left(\frac{\omega_{ce}}{\omega_r} - 1\right)$. Eq. (6) is the classic dispersion relation for whistler waves.

The role of the cold electrons becomes evident by looking at Eqs. (6) and (7). The cold electrons often dominate the total density in the system. Adding a cold electron component leads to a larger plasma frequency $\omega_{pe,t}$ and a smaller electron inertial length d_e^t. It follows that:

1. The cold electron density controls the properties of the waves, Eq. (6): if we hold the wave frequency fixed, the wave-vector k increases with the cold electron density. Hence, the phase velocity and, most important, the group velocity of the waves change. Fig. 1 shows the wave-vector (top left) of whistler waves obtained by solving the full dispersion relation (5) for a case where $n_h = 1\ \mathrm{cm}^{-3}$, $T_{e\parallel}^h = 2$ keV, $A = 4$, $B_0 = 150$ nT and the cold density is varied parametrically between 0.01 and 100 cm^{-3}. Five values of the wave frequency ω_r are shown in Fig. 1 (top left), confirming the considerations just made.
2. A corollary to the previous point is that the cold electrons lower the minimum resonant energy: if the wave frequency is fixed, the magnitude of the resonant velocity (hence the resonant energy) decreases with the cold electron density. Note that this is a very well known and important result (Kennel and Petschek, 1966; Brice and Lucas, 1971) since the resonant energy is linked to the energy of the electrons that could precipitate due to the interaction with the waves.
3. The cold electrons affect the growth rate of the waves, Eq. (7). The growth rate is decreased by the ratio n_h/n_t. If we hold the wave frequency fixed, the decrease in the resonant velocity can lead to both a decrease (through the term $|V_R/v_{t\parallel}^h|$) or an increase (through the exponential term) of the growth rate, so that whether the growth rate decreases or increases depends on the specific case. Fig. 1 (top right) shows the growth rate versus cold electron density for the parameters discussed above and for the values of the real frequency considered in Fig. 1 (top left). For instance, for $\omega_r/\omega_{ce} = 0.7$ the effect of the cold electrons is primarily to reduce the growth rate, while for $\omega_r/\omega_{ce} = 0.4$ the growth rate peaks at $n_c \sim 10\ \mathrm{cm}^{-3}$ with $\omega_i/\omega_{ce} \sim 0.047$ (while for $n_c = 0$ the mode is practically stable). Fig. 1 (bottom left) shows the growth rate versus cold electron density and wave-vector kd_e^t, from which we can further appreciate that the cold electrons control the range of wave-vectors that are unstable. The maximum growth rate versus cold electron density is shown in Fig. 1 (bottom right). For this particular set of parameters, the maximum growth rate peaks at about $n_c \sim 1\ \mathrm{cm}^{-3}$ with a $\sim 10\%$ increases over its value for $n_c = 0$. Larger values of the cold electron density decrease the growth rate and a sizeable reduction is obtained for $n_c \gtrsim 20\ \mathrm{cm}^{-3}$ (corresponding to 95% of the total density being carried by the cold electrons).
4. A corollary to the previous point is that the cold electron density lowers the stability threshold of the cyclotron instability (Cuperman and Landau, 1974). The value of hot temperature anisotropy corresponding to marginal stability has been parametrized with a power law dependence on the hot parallel electron beta, whose coefficients depend on the cold electron density (Gary et al., 2012b). Note that the temperature anisotropy marginal stability limit has indeed been observed for whistler waves in the Earth's magnetosheath (Gary et al., 2005), at geosynchronous orbit (MacDonald et al., 2008) and outside the plasmasphere where chorus waves typically reside (Yue et al., 2016). To further illustrate this point, Fig. 2 shows the growth rate of the whistler instability versus kd_e^t and n_c and for different values of the hot temperature anisotropy A. The parameters are the same as those in Fig. 1, except that we have changed $T_{e\perp}^h$ to match the desired level of anisotropy. While for the parameters of Fig. 1 (A=4) the system is strongly unstable with $n_c = 0$ and the cold electron density leads only to a small increase of the growth rate for $n_c \sim 1\ \mathrm{cm}^{-3}$ before providing strong stabilization, the situation is quite different for lower values of A. For instance, for A=1 the system is practically stable for $n_c = 0$ (which, for the purpose of this discussion, we define as having a growth rate less than $10^{-4}\omega_{ce}$) and it becomes unstable for $n_c \sim$ 10–50 cm^{-3}, with $\omega_i^{max}/\omega_{ce} \sim 6\cdot 10^{-3}$. Taken together with the decrease of the minimum resonant energy induced by the cold plasma, these results form the basis for active space experiments aimed at releasing a cold plasma to enable particle precipitation and substorm triggering. These ideas were suggested in the seventies (Brice, 1970) and attempted in the following decades (Krimigis et al., 1982; Bernhardt, 1992; Haerendel, 2019; Borovsky and Delzanno, 2019).
5. By changing the growth rate, the cold electrons change the saturation amplitude of the waves. Recent modeling works have parametrized the saturation amplitude of the chorus waves, δB, generated by the cyclotron instability but without including a cold-electron population (Tao et al., 2017; An et al., 2017). In particular, Tao et al. (2017) used quasi-linear theory to show the scaling of wave amplitude with the maximum linear growth rate, γ_{0m}, obtaining $(\delta B/B_0)^2 \sim \gamma_{0m}^{0.76}$. We have performed Particle-In-Cell (PIC) simulations of the cyclotron instability in order to investigate the effect of a cold electron population on the saturation properties of the waves. In this case, the anisotropic hot electron population is defined by the bi-Maxwellian–Jüttner distribution with $T_{e\parallel}^h = 6$ keV, $A = 1$, and $n_h = 1\,\mathrm{cm}^{-3}$. When present, the cold electrons are characterized by an isotropic Maxwellian distribution with $n_c = 20\,\mathrm{cm}^{-3}$ and $T_e^c = 30$ eV. An isotropic Maxwellian distribution of protons with $n_p = n_h + n_c$ and $T_p = 30$ eV is also included to maintain charge neutrality. The runs were one-dimensional with the background magnetic field B_0 aligned with the computational domain. Fig. 3 shows the time-dependent magnetic field fluctuation amplitude δB obtained by two PIC runs, with and without cold electrons. One can see that for these parameters the presence of cold electrons significantly increases the growth rate and the saturation amplitude of the waves.

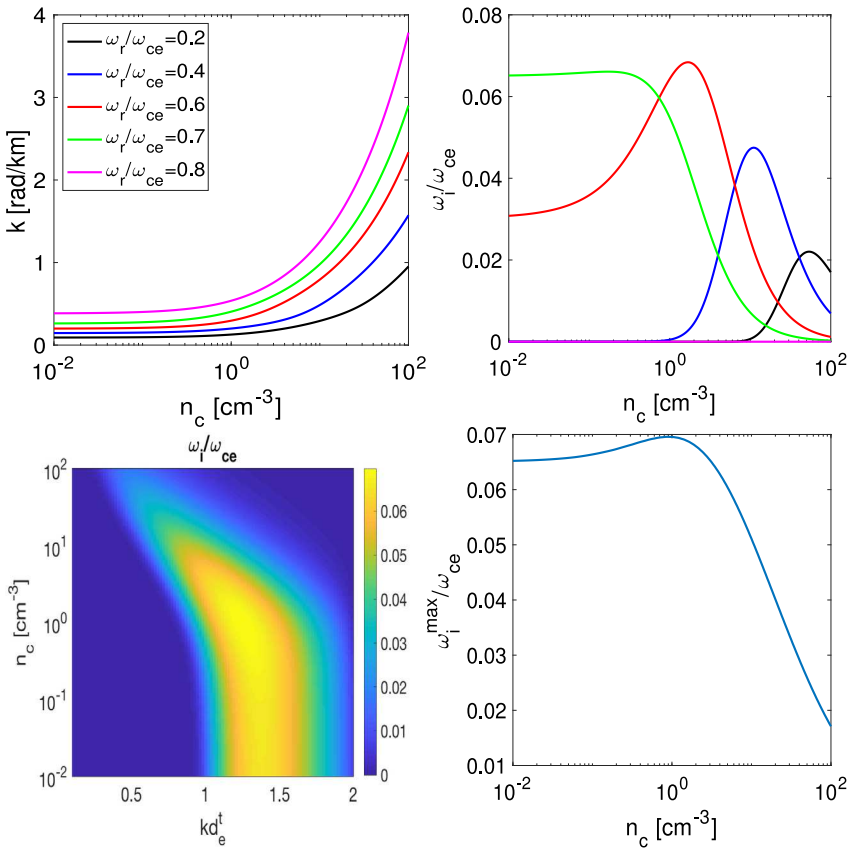

Fig. 1. (Top left) k wave-vector versus cold electron density for selected wave frequencies; (top right) growth rate versus cold electron density for the same wave frequencies of top left; (bottom left) growth rate versus cold electron density and wave-vector kd_e^t; (bottom right) maximum growth rate versus cold electron density, for whistler waves created by the cyclotron instability. Other parameters are $n_h = 1$ cm^{-3}, $T_{e\|}^h = 2$ keV, A=4 and $B_0 = 150$ nT.

In summary, while the free energy for the generation of chorus waves is provided by the keV electron population, the cold electrons control all the properties of the generated waves: frequency, growth rate and saturation amplitude.

While so far we have focused the discussion on the generation of the chorus waves, the same arguments made above for Eq. (6) imply that the cold electrons control the propagation of the waves in regions where they dominate the total density. Once again, as the waves propagate away from their generation region with constant frequency, the wave-vector changes in response to changes in the local plasma density and this changes the group velocity of the waves and their propagation trajectories. In order to make these arguments more concrete, let us first note that the equations of geometric optics (i.e. ray-tracing) (Bernstein, 1975; Swanson, 2003; Tracy et al., 2014) are often used to study the propagation of wave packets in the inhomogeneous magnetospheric plasma (Horne, 1989):

$$\frac{d\mathbf{x}}{dt} = -\frac{\frac{\partial D}{\partial \mathbf{k}}}{\frac{\partial D}{\partial \omega}}, \tag{9}$$

$$\frac{d\mathbf{k}}{dt} = \frac{\frac{\partial D}{\partial \mathbf{x}}}{\frac{\partial D}{\partial \omega}}, \tag{10}$$

where t is time, $\mathbf{x}$ is the position of the wave packet (or ray), $\mathbf{k}$ is the wave-vector and D is the dispersion relation for a given plasma model. The right-hand-side of Eq. (9) is the group velocity. For oblique whistler waves, a form of the dispersion relation is given by

$$D(k_\perp, k_\|, \omega) = \omega - \frac{c^2 \omega_{ce}}{\omega_{pe,t}^2} k_\| \sqrt{k_\perp^2 + k_\|^2} = 0, \tag{11}$$

which is the generalization of Eq. (6) [but still valid in the limit of $\left(\sqrt{k_\perp^2 + k_\|^2} d_e^t\right)^2 \ll 1$]. Here subscripts $\perp$ and $\|$ refer to perpendicular and parallel to the background magnetic field, which is still oriented along the z axis. For illustration purposes, let us consider a simple model with a constant magnetic field and an inhomogeneous background density along the field, $n_t = n_0 g(z)$ with $g(0) = 1$. From Eq. (10), since there is no dependence of the dispersion relation on x and y, it is easy to see that a given ray propagates with constant $k_\perp$. The dispersion relation (11) then trivially gives

$$k_\| \sqrt{k_\perp^2 + k_\|^2} = C_0 g(z) \tag{12}$$

with C_0 a constant [one can also verify that this is the solution of Eqs. (9) and (10)]. Eq. (12) shows how density gradients affect wave propagation: since $k_\perp$ is constant, a wave packet moving towards a positive (negative) density gradient becomes more (less) field aligned. From the nature of the dispersion relation (11), one can also infer that a positive magnetic field gradient would make the wave packets more oblique. In addition, density (and magnetic field) gradients can focus/defocus the waves, changing the wave amplitudes. Damping effects are also very important in determining wave amplitudes. Warmer electrons (with energy above 100 eV) are typically responsible for Landau damping of the chorus waves (Bortnik et al., 2007; Chen et al., 2013), with thermal effects associated with cold electrons or ions becoming important only near resonances (Maxworth and Golkowski, 2017). [Note, however, that recent work suggests the possibility for new couplings between cold electrons and whistler waves where thermal effects are very important (Roytershteyn and Delzanno, 2021)]. In general, ray-tracing is commonly used in magnetospheric modeling [see for instance Starks et al. (2008), Bortnik et al. (2008), Kulkarni et al. (2008), Bortnik et al. (2009), Chen et al. (2012), Crabtree et al. (2012), Maxworth and Golkowski (2017), Starks et al. (2020), Colpitts et al. (2020) for some applications to whistler waves] and the importance of the background density model is well established.

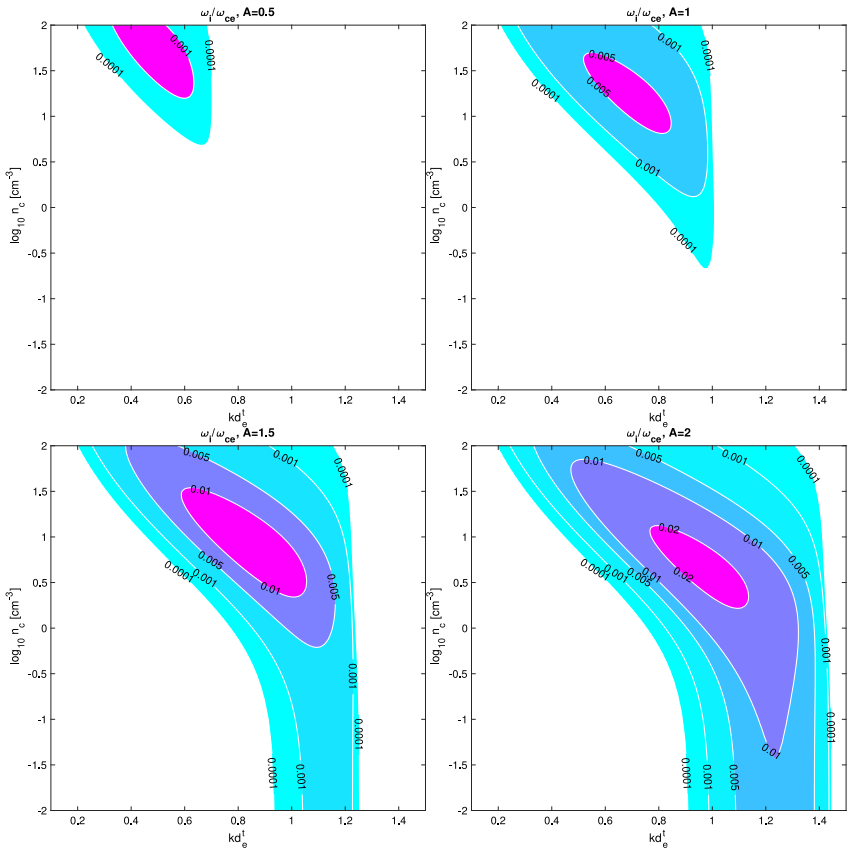

Fig. 2. Growth rate versus cold electron density and wave-vector kd_e^t, for different values of the hot electron anisotropy A. Other parameters are $n_h = 1$ cm^{-3}, $T_{e\|}^h = 2$ keV, and $B_0 = 150$ nT.

It is important to emphasize that the wave properties, including amplitude, control the wave–particle scattering and energization rates. For instance, recall that in quasi-linear theory the resonant diffusion coefficients scale as $\left(\delta B/B_0\right)^2$ (Walt, 1994). Hence, either at the level of wave generation or through wave propagation, the cold electrons control the most important properties of the whistler waves, with strong implications on the dynamics of the plasma sheet, ring current, and radiation belts.

6.1.2. *Whistler-mode hiss waves*

Whistler-mode hiss waves are incoherent, broadband emissions mostly found in the plasmasphere (Dunckel and Helliwell, 1969; Russell et al., 1969; Thorne et al., 1973; Hartley et al., 2018) and in plasmaspheric plumes (Chan and Holzer, 1976). They can be generated by different mechanisms such as lightning (Sonwalkar and Inan, 1989) or by chorus waves entering the plasmasphere after reflection at high latitudes (Bortnik et al., 2008, 2009; Chen et al., 2012). Some fraction of hiss waves might also be generated by the cyclotron instability (Laakso et al., 2015). In general, however, the origin of hiss waves remains an open question [see for instance the discussion in Ripoll et al. (2020)]. Hiss waves are mainly associated with the decay of the radiation belts and particularly with the formation of the slot region via pitch-angle scattering (Lyons et al., 1972).

For the hiss waves associated with the cyclotron instability (either directly or indirectly through chorus), the same considerations made in Section 6.1.1 for chorus waves still apply. In all cases, including hiss generated by lightning or very-low-frequency (VLF) whistler waves generated by powerful ground-based transmitters, the cold electron density (including density ducts discussed in Section 6.5) is critical for the propagation of the waves and their trapping in the plasmasphere. For instance, Chen et al. (2012) used ray-tracing simulations to investigate parametrically the effect of the cold plasma density on the formation of hiss waves from the evolution of chorus waves, showing the key role played by the trough density distribution in regulating the peak hiss intensity. Agapitov et al. (2020) used Van Allen Probes

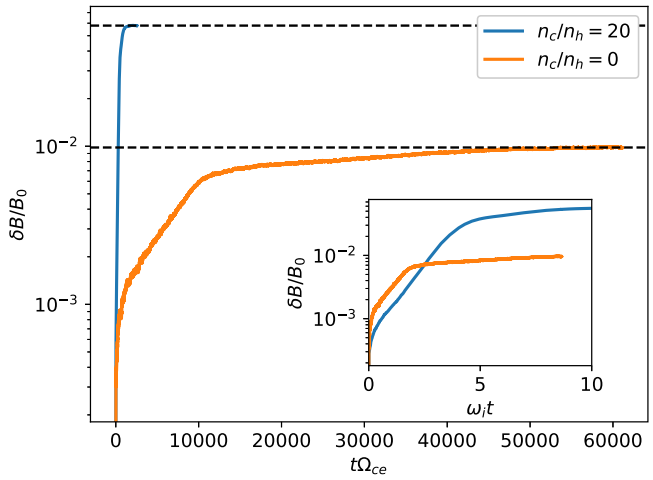

Fig. 3. Amplitude of magnetic fluctuations δB in PIC simulations of the time-dependent whistler wave amplitude. The simulations include an anisotropic hot electron population with bi-Maxwellian–Jüttner distribution with $T_{e\|}^h = 6$ keV, $A = 1$, and $n_h = 1\,\mathrm{cm}^{-3}$. For the simulation with cold electrons, the cold electron population is Maxwellian with temperature $T_e^c = 30$ eV and density $n_c = 20\,\mathrm{cm}^{-3}$ and an isotropic Maxwellian population of protons with $T_p = 30$ eV and $n_p = 21\,\mathrm{cm}^{-3}$ was also included to maintain charge neutrality. The insert shows the same figure, but with time normalized to the respective growth rate ω_i observed in each simulation. The simulations were one-dimensional, with the background magnetic field B_0 aligned with the computational domain.

data to show how the spatio-temporal variations of the electron plasma frequency to cyclotron frequency ratio are one of the factors that controls MeV-electron scattering rates from plasmaspheric hiss.

6.2. EMIC waves

EMIC waves are discrete electromagnetic emissions occurring in three distinct bands below the local cyclotron frequencies of H^+, He^+ and O^+. EMIC waves are predominantly left-hand polarized and their frequency is between 0.1 and 5 Hz in the Earth's magnetosphere. They occur primarily in the afternoon sector (often with prevalence of the He^+ band, which can also have more power relative to the other bands) and on the dayside (with prevalence of the H^+ band), although the O^+ band occurrence peaks in the morning sector and some differences exist in EMIC statistics between the inner and outer magnetosphere (Min et al., 2012; Usanova et al., 2012; Keika et al., 2013; Saikin et al., 2015). EMIC waves lead to pitch-angle scattering and precipitation of ring current ions (Jordanova et al., 2007) and radiation belt electrons (Meredith et al., 2003c). A recent review that discusses EMIC waves in the context of radiation belt losses is given by Blum and Breneman (2020).

EMIC waves are also believed to be generated by the cyclotron instability driven primarily by keV proton populations (Cornwall, 1965; Kennel and Petschek, 1966). On the dayside, this is associated with solar wind compression (Usanova et al., 2012; Keika et al., 2013). On the dusk side in the inner magnetosphere, this is associated with injection of plasma sheet ion populations overlapping with the plasmaspheric densities (Halford et al., 2010). Therefore, the same considerations made for chorus waves are also applicable for EMIC waves, with cold ions playing a critical role in the generation of EMIC waves. The effect of cold ions on the cyclotron instability has been studied with linear theory (Gary et al., 1994; Chen et al., 2011; Gary et al., 2012a; Lee and Angelopoulos, 2014a) and linear-theory results have been used as a proxy of EMIC activity with geosynchronous orbit data (Blum et al., 2009). Lee and Angelopoulos (2014a) have used linear theory to interpret EMIC wave events at various local times, highlighting the role of cold ions in lowering the threshold for instability and of warm cloak ions in producing damping. An association between the cold oxygen torus and EMIC waves has also been recently made using spacecraft observations (Nosé et al., 2020).

Similar considerations to what has been discussed for whistler waves also apply to wave propagation, with a number of ray tracing studies showing the importance of the cold plasma in determining the properties of EMIC waves. This includes highlighting the role of density gradients to enhance wave growth (Thorne and Horne, 1992; Horne and Thorne, 1994; Chen et al., 2009) and showing, consistent with observations (Anderson et al., 1992; Min et al., 2012), that EMIC waves can become linearly polarized as they propagate at higher latitudes in the inhomogeneous magnetospheric plasma (Horne and Thorne, 1994).

However, when compared with whistler waves, there are some important differences with regard to the role played by cold ions for EMIC waves that need to be emphasized. First of all, the ion composition is critical to determine the properties of the EMIC waves and, in turn, the resonant energy for strong interaction between the waves and the local particle populations. In general, the cold magnetospheric plasma with multiple ion species features stop bands at the local gyrofrequencies of He^+ and O^+. Hot plasma effects can, however, eliminate the He^+ stop band, as shown by Chen et al. (2011). Furthermore, the presence of an isotropic population of cold and dense He^+ ions can lead to instability of both H^+ and He^+ bands (Chen et al., 2011; Gary et al., 2012a) and, in general, composition and hot plasma effects, particularly near the He^+ gyrofrequency, profoundly affect the conditions for instability and the property of the unstable modes (Chen et al., 2011). Second, observations have shown strong perpendicular heating of He^+ ions, from cold/thermal (~eV) to warm/suprathermal (hundreds of eV) energies, associated with the presence of EMIC waves (Young et al., 1981; Roux et al., 1982). Some works used linear theory to make a qualitative association of cold-ion heating with strong cyclotron damping of the EMIC waves (Chen et al., 2011). Simulation studies with both hybrid and test-particle approaches have allowed a more in-depth analysis of the processes involved in cold-ion heating, showing that cold ions are scattered non-resonantly and experience strong phase bunching (Omidi et al., 2010; Bortnik et al., 2010; Omidi et al., 2013).

Note that EMIC waves can also interact very efficiently with cold electrons, leading to cold-electron heating (Zhou et al., 2013; Yuan et al., 2014). The interaction between oblique EMIC waves and cold plasmaspheric electrons is one of the mechanisms that can lead to ionospheric heating and the formation of stable auroral red arcs during geomagnetic storms (Cornwall et al., 1971; Thorne and Horne, 1992).

6.3. Additional considerations on the coupling between whistler waves and cold electrons and EMIC waves and cold ions

From the discussion so far, it is clear (and well recognized) that the cold plasma *density* plays a crucial role in determining the properties of whistler and EMIC waves, both for their generation and propagation. We will refer to this as the 'density coupling'. Several cold plasma density empirical models based on in-situ and ground-based observations exist for the inner magnetosphere [see the discussion by Reinisch et al. (2009)]. These models are however limited in their ability to represent accurately the plasmasphere (Ozhogin et al., 2014), particularly the off-equator density, and might not be adequate for specific events. Thus, there remains a strong need for better cold-plasma density models.

A very important open problem is associated with cold-plasma heating and we wish to emphasize its implications for magnetospheric dynamics. If the waves give energy to the cold plasma, they can damp and lower their amplitude. This takes away energy that would otherwise be available to energize or scatter ring-current particles or radiation belt electrons. Moreover, the cold plasma and the higher-energy particle populations can now become efficiently coupled by the waves. We will refer to this as 'energy coupling'. The local properties of the cold/warm plasma (i.e. its distribution function) strongly affect the energy coupling and must therefore be properly characterized, both with measurements and in models. This also implies that magnetospheric models need to include the cold plasma dynamically, through both the mass–density and the energy distribution. This is something that is not currently done: for instance, ring-current or radiation-belt models include only the cold-plasma density (Jordanova et al., 2007, 2016). While, as we have discussed above, cold-plasma heating by EMIC waves has been demonstrated with observations and modeling, a similar association between cold-electron heating and whistler waves appears to have not yet been made conclusively. In this regard, however, we note that recent work suggests that whistler waves can excite secondary, kinetic instabilities in the cold electrons that lead to cold-electron heating and damping of the primary whistler waves (Roytershteyn and Delzanno, 2021). In summary, the non-linear energy couplings that involve the cold plasma and the waves have not been fully explored and might impose new, more stringent limits (relative to those set by the density coupling alone) on the maximum wave amplitudes attainable in the environment. In addition, they create new couplings with other particle populations that are not yet accounted for in any existing space-weather model. Given the importance of wave–particle interactions in the dynamics of the near-Earth environment, accounting for the full density and energy couplings of the various higher-energy particle populations with the cold plasma appears a crucial next step towards predictive modeling.

6.4. ULF waves

ULF waves in the Earth's magnetosphere are few-minute-period standing magnetohydrodynamics (MHD) waves (Walker, 1998,

McPherron, 2005; Hartinger et al., 2013a), both shear and compressional, associated with eigenfrequencies (resonances) of the mass loaded dipole magnetic field lines. They are detected within the magnetosphere by spacecraft magnetic-field measurements (Kazue and McPherron, 1984) or plasma flow measurements (Su et al., 1980; Borovsky and Denton, 2016), and they can be detected from the ground by magnetometer measurements (Kessel, 2008; Pahud et al., 2009) or radar measurements (Wright and Yeoman, 1999). ULF waves can also be detected optically from the ground via the "field-line-resonance" auroral arcs that they produce (Baddeley et al., 2017; Gillies et al., 2018). Long-term hourly indices of magnetospheric ULF intensities are available (Kozyreva et al., 2007; Romanova et al., 2007).

ULF wave intensity in the magnetosphere is greatly elevated during geomagnetic storms (Kozyreva and Kleimenova, 2009, 2010; Borovsky and Denton, 2016). The intensity of ULF waves in the magnetosphere is well correlated with a number of solar-wind parameters [cf. Table 1 of Borovsky and Denton (2014)], in particular with the solar-wind speed (Singer et al., 1977; Mathie and Mann, 2001), temporal variations in the solar-wind speed (Vassiliadis et al., 2007), and temporal variations in the solar-wind dynamic pressure (Liu et al., 2010). Magnetospheric ULF waves can be driven by buffeting of the magnetosphere by dynamic-pressure variations of the solar wind (Eriksson et al., 2006; Shen et al., 2015), by Kelvin–Helmholz waves driven by magnetosheath flow along the magnetopause (Mann et al., 1999; Claudepierre et al., 2008), by the occurrence of hot flow anomalies and other foreshock instabilities (Eastwood et al., 2011; Hartinger et al., 2013b), by kinetic instabilities in the hot-ion population of the magnetosphere (Hughes et al., 1978; Ozeke and Mann, 2008; Mager et al., 2013), and by substorm injections (Zolotukhina et al., 2008; Yeoman et al., 2010). Periodic density structures in the solar wind near the heliospheric current sheet are particularly effective in producing magnetospheric ULF oscillations (Viall et al., 2009; Kepko and Viall, 2019).

ULF waves play many roles in the solar-wind-driven magnetosphere–ionosphere system. Of particular interest is the known connection between the amplitude of magnetospheric ULF oscillations and the energization of the electron radiation belt (Rostoker et al., 1998; Mathie and Mann, 2000; Elkington et al., 2003; Borovsky and Valdivia, 2018). A major role is the production of radial diffusion for radiation-belt particles (Fälthammar, 1965; Ozeke et al., 2012), which redistributes the radiation belts (Shprits et al., 2008) and the ring current (Murphy et al., 2014) and which can energize particles in the diffusion process (Degeling et al., 2011).

Enhanced ULF radial diffusion during magnetopause shadowing events is thought to be critical for the sudden loss of outer-radiation-belt electrons in the early phases of storms (Degeling et al., 2013). Radiation-belt particles can be energized by drift-resonant interaction with ULF waves (Elkington et al., 1999, 2003; Sauvaud et al., 2013). Ring-current ions can also be resonantly energized by ULF waves (Ozeke and Mann, 2008). There is evidence for the modulation of electron–cyclotron waves (Liang et al., 2010) and chorus waves (Li et al., 2011b; Jaynes et al., 2015) by compressional ULF waves to produce pulsating aurora. It has been argued that compressional ULF oscillations can produce EMIC waves (Fraser et al., 1992; Loto'aniu et al., 2010), but also see Usanova et al. (2010). Other forms of magnetospheric particle precipitation and ionospheric modification are associated with magnetospheric ULF waves (Baddeley et al., 2017; Gillies et al., 2018; Wang et al., 2020). Magnetospheric ULF waves also produce perturbations in the ionosphere (Yizengaw et al., 2013; Pilipenko et al., 2014; Vorontsova et al., 2016) and result in ionospheric Joule heating (Rae et al., 2007; Hartinger et al., 2015).

Cold ions in the magnetosphere affect the mass–density ρ of the magnetospheric plasma, which changes Alfvén speeds $v_A = \frac{B}{\sqrt{\mu_0 \rho}}$ and the MHD eigenfrequencies of the dipole magnetic-field lines of the magnetosphere. Changes in the cold-ion populations change the frequencies of ULF oscillations (Takahashi et al., 2010, 2014; Denton et al., 2011, 2014). The two magnetospheric populations of most relevance are the plasmasphere and the cloak (oxygen torus), with their highly variable mass–densities in the dipolar magnetosphere. Changing the mass–density changes the locations where ULF waves can exist and be driven (Poulter et al., 1988; Fraser et al., 2005; Claudepierre et al., 2016). An example of this is the enhanced ULF activity at the plasmapause and the refilling outer plasmasphere (Lanzerotti and Surkan, 1974; Liu et al., 2013a), their amplitudes, and consequently how ULF waves interact with the energetic-particle populations of the magnetosphere. Cold-ion alteration of ULF waves impacts the evolution of the radiation belts and the ring current.

Presently lacking is (a) knowledge of the cold-ion mass–density of the magnetosphere, (b) knowledge of what controls that mass–density, and (c) an ability to predict the mass–density.

6.5. Density ducts in the plasmasphere

In the plasmasphere, it is well known that field-aligned (electron) number-density enhancements or depletions will duct whistler waves along the magnetic field (Adachi, 1966; Carpenter, 1968; Angerami, 1970; Karpman and Kaufman, 1987). The field-aligned nature of the electron-density ducts has been demonstrated using radio interferometry (Jacobson et al., 1995, 1996; Hoogeveen and Jacobson, 1997), and using total electron content Loi et al. (2015) visualized the plasmaspheric network of underdense and overdense flux tubes aligned with the geomagnetic field. Spacecraft measurements find typical duct diameters of 100s to 1000s of km (Darrouzet et al., 2004), while formation and decay lifetimes of whistler ducts inside of the plasmasphere may be ~1 hr (Thomson, 1978; Singh et al., 2013). Spacecraft observations have shown localized enhancements in the intensity of whistler-mode hiss associated with localized enhancements in the electron number density (Chan et al., 1974; Koons, 1989; Kozyra et al., 1994) and spacecraft observations have shown localized enhancements in the intensity of whistler-mode chorus associated with both localized enhancements and localized depletions in the electron number density (Li et al., 2011a; Haque et al., 2011). The density ducts not only guide the whistler waves, they also alter the convective growth properties (Carpenter, 1968; Li et al., 2011b). Further, ducted versus non-ducted whistler waves pitch-angle scatter radiation-belt electrons to different degrees (Rodger et al., 2010).

Field-aligned ion density perturbations in the plasmasphere affect the propagation and growth of EMIC waves (Chen et al., 2009; Mann et al., 2014; Usanova et al., 2016). The number density of the plasmaspheric drainage plume is particularly structured (Borovsky and Denton, 2008; Matsui et al., 2012; Borovsky et al., 2014b) and there is evidence for EMIC wave scattering in plumes (Spasojević et al., 2004; Fraser et al., 2013; Yahnin and Yahnina, 2007; Borovsky et al., 2014a) and in situ observations of EMIC waves in plumes or plume locations (Usanova et al., 2013; Yuan et al., 2014; Halford et al., 2015; Grison et al., 2018).

Magnetosonic waves (ion-Bernstein waves) have been associated with localized ion density depletions in the plasmasphere (Yuan et al., 2017, 2018), not so much by ducting but rather by having instability growth rates that depend on plasma densities.

A longstanding issue in magnetospheric plasma physics is the origin of the density ducts in the plasmaspheric plasma. The formation of ducts seems to be associated with convection: as soon as magnetospheric convection increases, the plasmasphere is observed to suddenly become structured (Borovsky and Denton, 2008) and density ducts have been observed to form when traveling ionospheric disturbances pass (Loi et al., 2016). Ideas about the causes of the density ducts include (1) interchange instabilities (Cole, 1971; Jacobson et al., 1996; Pierrard and Lemaire, 2004; Buzulukova et al., 2008), (2) thunderstorm electric fields (Park and Helliwell, 1971; Rodger et al., 1998), (3) ionospheric feedback (Park and Banks, 1974), and (4) ULF waves (Adrian et al., 2004). For density structures near the plasmapause, the drift-wave instability (Hasegawa, 1971) and the pressure-gradient instability (Richmond, 1973) have been considered. The lack of understanding of the formation mechanisms and controlling factors for plasmaspheric ducts contributes to our incomplete understanding of the evolution of the electron radiation belt.

7. Aurora structuring

7.1. Pulsating aurora

Pulsating aurora are slowly drifting irregularly shaped patches of atmospheric airglow that blink on and off on timescales of 2 - 20 s (Creswell, 1972; Johnstone, 1978; Lessard, 2013; Partamies et al., 2017b; Nishimura et al., 2020). The various patches have asynchronous blink periods (Scourfield et al., 1972; Nishiyama et al., 2012) and there are higher-frequency modulations to the airglow (Kataoka et al., 2012). Pulsating aurora occur most frequently in the midnight-to-dawn local-time sector after the occurrence of a substorm (Royrvik and Davis, 1977). An interval of pulsating aurora can last for hours (Jones et al., 2011) with the individual patches slowing evolving (Partamies et al., 2019). Pulsating aurora is an example of an emergent phenomenon in the complex system of the magnetosphere and ionosphere (Borovsky and Valdivia, 2018), something that would not be predicted from an understanding of the individual parts of the system alone.

The blinking airglow of pulsating aurora is caused by temporal variations in the flux of electrons precipitating from the magnetosphere (McEwen et al., 1981). The energies of the precipitating electrons are typically in the range of keV to 10s of keV (Sato et al., 2004; Miyoshi et al., 2015), but the precipitating energy can also be lower than these values (Liang et al., 2016) or higher than these values into the relativistic energy range (Østgaard et al., 1998; Miyoshi et al., 2015). The backscattering of precipitating energetic electrons off of the atmosphere and the production of low-energy secondary electrons from the atmosphere, and the bouncing of those backscattered and secondary electrons between the northern and southern hemispheres, is also thought to play a role in pulsating structured aurora [e.g. Samara et al. (2017)].

Pulsating aurora have been correlated with temporal variations in the intensity of whistler-chorus waves in the magnetosphere (Nishimura et al., 2010; Ozaki et al., 2015) and with temporal variations in the intensity of electrostatic electron–cyclotron waves in the magnetosphere (Liang et al., 2010; Fukizawa et al., 2018), those two types of waves acting to pitch-angle scatter magnetospheric electrons into the atmospheric loss cone. Pulsating aurora have also been connected to electrical time-domain electric-field structures in the magnetosphere (Mozer et al., 2017a), which can also pitch-angle scatter electrons. It is important to understand pulsating aurora and the temporally varying waves that cause it: these are the same waves that energize the radiation-belt electrons (Meredith et al., 2003a), that pitch-angle scatter the radiation belt electrons (Glauert and Horne, 2005), and that produce microbursts (Thorne et al., 2005; Saito et al., 2012) that can affect atmospheric chemistry (Clilverd et al., 2009; Turunen et al., 2016) and atmospheric electricity (Rodger et al., 2007; Borovsky, 2017).

An individual evolving pulsating patch has a lifetime of 10 min or so (Humberset et al., 2016; Partamies et al., 2019). The patches of pulsating aurora drift at approximately the $\mathbf{E}\times\mathbf{B}$ drift velocity (Scourfield et al., 1983), eastward in the post-midnight region of local time and westward in the premidnight region of local time (Yang et al., 2017) as expected for magnetospheric convection from nightside to the dayside. Because of the drifting at approximately the $\mathbf{E}\times\mathbf{B}$ drift speed, the spatial structuring of pulsating aurora has been inferred to be related to a structuring of cold electrons in the magnetosphere (Oguti, 1976; Scourfield et al., 1983; Nemzek et al., 1995). If one could spatially structure the hot plasma in the dipolar regions of the magnetosphere, the variations in gradient-and-curvature drift speeds in the velocity distribution function would lead to a smearing out of the spatial structure as the particles drift. It is well known that whistler waves can be ducted by field-aligned electron-density structures (Haque et al., 2011; Li et al., 2011a). Theories of the pulsating aurora typically are based on a high-frequency plasma wave living in the cold plasma driven by hot electrons drifting through the cold-plasma structure (Johnstone, 1978; Davidson, 1990; Demekhov and Trakhtengerts, 1994). Detailed observations of ionospheric-electron heating in pulsating aurora have led to evidence for a cold plasma population in the magnetosphere associated with the pulsating aurora (Liang et al., 2017, 2018).

Attempts to measure the cold-electron population in the magnetosphere when a spacecraft is magnetically connected to pulsating aurora are generally hindered by the overwhelming population of spacecraft-generated photoelectrons and secondary electrons [e.g. Suszcynsky et al. (1997)]. Nishimura et al. (2015) have seen modulations of the equatorial cold-ion number density (< 100 eV, a proxy for the cold-electron number density) in locations in the nightside plasma sheet that were magnetically connected to observed pulsating aurora in the atmosphere. The cold-ion densities observed were on the order of 0.1 cm^{-3}, considerably lower than the ambient hot-ion and hot-electron densities of the plasma sheet.

The origins of the magnetospheric cold electrons, the cause of the spatial structure of those electrons, and what controls both are not understood. One possibility is a feedback between auroral electron precipitation and ionospheric plasma outflow that could produce spatially-structured outflows (Liang et al., 2015). However, without direct observations of these cold electrons, progress on understanding their origins and control will be uncertain. This also means a hindrance to understanding pulsating aurora. Further, without understanding the control of these cold electrons, the control of chorus and electrostatic electron–cyclotron waves are not understood and so there is an incomplete understanding of the evolution of the electron radiation belt.

7.2. Structured dayside aurora

Several types of structured aurora are found in the dayside region of local time (Frey et al., 2019; Nishimura et al., 2020). These dayside structured aurora have been much less studied than nightside aurora have and less is known about dayside structuring.

Diffuse patches of aurora in the dayside are known to be associated with magnetospheric spatial variations in the cold/warm plasma density and spatial variations in the chorus-wave intensity [cf. Nishimura et al. (2013) for an example with $\delta n \sim 1$ cm^{-3} density variations on a $n \sim 1$ cm^{-3} baseline number density]. Localized density enhancements with correlated chorus-wave-intensity enhancements are seen throughout the dayside magnetosphere (Li et al., 2011b).

"Stripy aurora" are seen in the noon region of local time. These stripy aurora are thought to be associated with spatially structured cold plasma in the dayside magnetosphere [e.g. Han et al. (2015, 2017)]. The flux tubes of the stripy aurora correspond to regions of the magnetosphere where the cloak plasma is expected to exist.

Another dayside auroral feature hypothesized to connect with magnetospheric cold plasma is the quasi-stationary auroral patch observed in the upper atmosphere at the South geographic pole. Ebihara et al. (2007) hypothesize that a mini plasmasphere of cold plasma can form in the dayside magnetosphere on magnetic-field lines connected to the southern geographic pole, scattering hot magnetospheric electrons into the atmospheric loss cone to produce the very-long-lived auroral patch at the South Pole.

7.3. Giant undulations at the plasmapause

The low-latitude edge of the diffuse aurora in the atmosphere corresponds to the inner edge of the electron plasma sheet in the nightside magnetosphere (Lassen, 1974; Gussenhoven et al., 1983) and the inner edge of the electron plasma sheet is often co-located with the plasmapause (Horwitz et al., 1982; Fairfield and Vinãs, 1984; Elphic et al., 1999), the outer boundary of the cold, dense plasmasphere. (When they are not co-located, the spatial gap between the plasmapause and the Earthward edge of the electron plasma sheet is known as the "remnant layer" [cf. Galperin and Feldstein (1996)].) The equatorward edge of

the aurora is nominally smooth and relatively unstructured, however during times of high geomagnetic activity wave-like undulations on the low-latitude boundary of the aurora can develop in the pre-midnight to afternoon sector. The undulations have wavelengths of ~ 200–900 km and amplitudes of ~ 40–400 km (Lui et al., 1982; Providakes et al., 1989; Mendillo et al., 1989; Murphree and Johnson, 1996; Baishev et al., 2000; Henderson et al., 2010; Baishev et al., 2012). When the amplitudes of these undulations are similar to their wavelength, they are called "giant undulations". These structures were first discovered by Lui et al. (1982) using auroral imagery from the DMSP spacecraft. By examining sequential orbital passes, Lui et al. (1982) were able to determine that giant undulations can persist over timescales of 0.5–3 hours. Subsequent studies have also established that the optical undulations tend to propagate Sunward along the equatorward auroral boundary with phase speeds of ~ 540–700 km/s (Nishitani et al., 1994; Baishev et al., 2000; Henderson et al., 2010). Ground magnetic perturbations in the Pc5 range have also been detected in response to the passage of giant undulations overhead (Baishev et al., 2000; Henderson et al., 2010).

An example of giant undulations is shown in Fig. 4. The full-Earth image was taken on 9 November, 1998 at 10:09:35 UT by the VIS/Earth Camera instrument on board the NASA POLAR spacecraft. In the figure North is up and the direction to the Sun is off to the upper left as indicated by the dayglow visible on the Earth. The black-and-white image overlayed on top of the POLAR image is from a DMSP/OLS imager at low Earth orbit taken at approximately the same time. The spatial resolution of the DMSP image is quite high and clearly reveals a series of very well-developed giant undulations on the duskside of the equatorward boundary of the optical aurora. Note that giant undulations are different from omega bands (Henderson, 2013; Partamies et al., 2017a), which are typically located farther poleward in the region where auroral streamers and auroral torch structures form.

The generation mechanism for giant undulations is thought to result from a shear-flow interaction between hot plasma sheet flows and the cold-dense plasmasphere (Kelley, 1986; Viñas and Madden, 1986). At the duskside plasmapause cold plasmaspheric plasma corotates with the Earth and is flowing tailward while hot plasma-sheet ions flow Sunward from the magnetotail under the combined $\mathbf{E}\times\mathbf{B}$ and gradient-and-curvature drifts. Thus, at the dusk-side plasmapause the warm ion plasma sheet flow opposes the flow of the cold plasmasphere. This is a classical shear-flow geometry that can potentially excite Kelvin–Helmholtz-type surface waves. Although this ion flow geometry persists in the inner magnetosphere, auroral undulations are not seen all the time on the plasmapause because the strength of the shear is typically not large enough (Kelley, 1986; Viñas and Madden, 1986). The fact that hot plasma-sheet ions penetrate closer to the Earth on the dusk-side than do the hot plasma-sheet electrons results in a complex feedback between the ionosphere and magnetosphere whereby a strong localized charge-separation electric field produces a Sunward $\mathbf{E}\times\mathbf{B}$ enhancement of the ion flow. This process is illustrated in Fig. 5. Ions penetrating Earthward of the electrons cause a field-aligned current to flow downward (along magnetic field lines) into the ionosphere where it is diverted northward through the resistive ionosphere towards the auroral region and then back out to the magnetosphere as an upward field-aligned current. The ionospheric part of this current loop, in the sub-auroral region, passes through a region where the ionospheric conductivity is low due to lack of precipitating auroral electrons. To maintain current continuity, a northward ionospheric electric field strengthens in this region. This strong ionospheric electric field maps out along magnetic-field lines and drives very strong and localized $\mathbf{E}\times\mathbf{B}$ ion flow channels in the magnetosphere called sub auroral polarization streams (SAPS) (Foster and Burke, 2002). These "SAPS flows" produce much stronger shears between hot and cold populations than the nominal Sunward plasma sheet flows do — especially during geomagnetically active time periods. Thus, SAPS are a fundamentally important aspect of the dynamics of the plasmapause and its magnetosphere–ionosphere feedback. As discussed by Kelley (1986), enhanced SAPS flows are far more likely to produce Kelvin–Helmholtz-type waves on the plasmapause boundary that can then lead to giant undulations of the auroral boundary. The intermittent presence of SAPS would also explain why giant undulations are not always observed. The association of strong SAPS flows with the formation of giant undulations was confirmed by Henderson et al. (2010), who studied a giant-undulation event from start to finish using global auroral imaging from the POLAR and IMAGE spacecraft together with in-situ SAPS observations from the DMSP spacecraft. A theory of giant undulation formation was presented by Viñas and Madden (1986) in terms of a combined shear-flow ballooning instability analysis. However, the theory suffers from a number of over-simplifications and sufficient observational constraints were not well established at the time. Other theoretical studies have been performed since [e.g. Lakhina et al. (1990), Satyanarayana et al. (1987), Wang and Pritchett (1989)], but to date, none have provided a robust analytical theory that takes into account all of the important physics.

It is also possible that the intermixed dynamics of the cold and hot plasma at the plasmapause might be related to other supposedly-unrelated phenomena such as STEVE emissions (MacDonald et al., 2018; Gallardo-Lacourt et al., 2018) and long-lived drainage plumes (Borovsky et al., 2014b) and we present some discussion of these ideas in the next paragraph.

Recent studies have shown that interesting airglow structures called STEVE emissions can develop in the pre-midnight sub-auroral region (MacDonald et al., 2018; Gallardo-Lacourt et al., 2018). It has been demonstrated that: (1) giant undulations are driven by SAPS (Henderson et al., 2010); (2) the region where auroral giant undulations form can become rapidly disrupted (Henderson et al., 2018); (3) some giant undulations can lead to the formation of detached emission regions equatorward of the main auroras (Henderson et al., 2018); (4) the development of STEVE emissions is closely related to strong SAPS flows (Nishimura et al., 2019); and (5) long-lived plasmaspheric drainage plumes occur during sustained geomagnetic disturbances (Borovsky et al., 2014b). Plasmaspheric drainage plumes are associated with enhanced SAPS flows [e.g. Goldstein et al. (2003)]. These observations taken together suggest a common physical mechanism. One hypothesis is that an actual disruption of the plasmapause can occur, instead of just waves forming there. The disruption of the plasmapause surface would lead to cold dense plasma from the plasmasphere moving radially outward to become entrained into the open drift regions feeding the drainage plume, while hot plasma sheet plasma formerly outside of the plasmapause would become entrained in the plasmasphere. The main driver of SAPS flows are substorm injections of hot plasma from the tail and these occur every few hours during active times; hence it is possible that repeating abrupt disruptions of the plasmapause may occur for days to feed quasi-periodic bursts of cold plasma into the drainage plume structures. This radial transport of cold plasmaspheric plasma via giant undulations might explain the observations of "long-lived" drainage plumes, which are plumes that persist for times much longer than could be explained by $\mathbf{E}\times\mathbf{B}$-drift drainage of the outer plasmasphere (Borovsky et al., 2014b).

8. Additional probable impacts of cold electrons and ions

In this section we discuss some additional probable impacts of cold electrons and cold ions that have not yet received much attention.

8.1. Refilling-process ions and electrons in the outer dipole

It is well known that the outer plasmasphere refills from the ionosphere when geomagnetic activity decreases after being strong [e.g. Chappell et al. (1970), Park (1970)]. The refilling process occurs into flux tubes that were on open $\mathbf{E}\times\mathbf{B}$ drift trajectories (going from

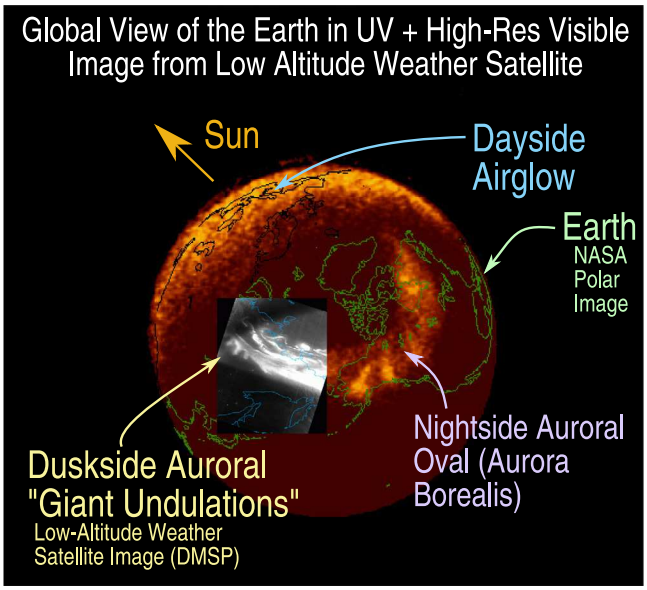

Fig. 4. A combined image showing DMSP/OLS and POLAR/VIS Earth Camera images together.

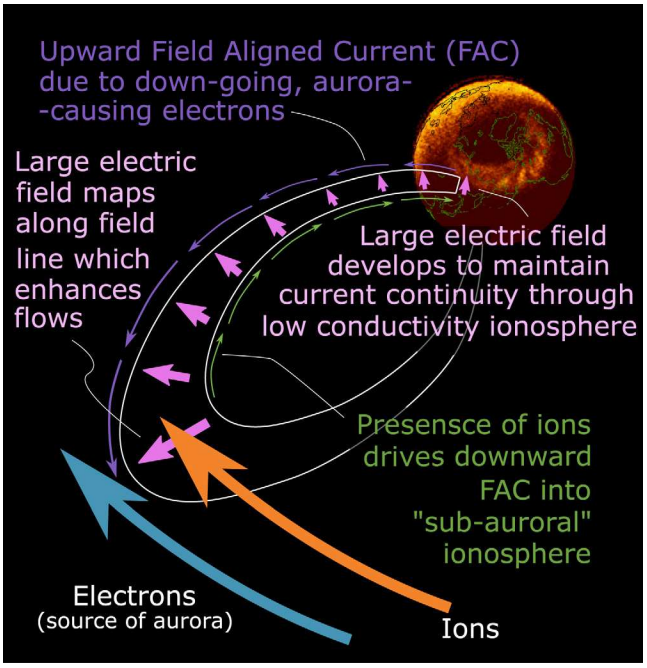

Fig. 5. SAPS formation mechanism.

the magnetotail to the dayside magnetopause) that became closed. The closed nature of the drift trajectories allows the refilling plasma from the ionosphere to build up in density (over the timescale of days) to become the high-density outer plasmasphere. The ion temperature of the plasmasphere is about 1 eV or less (Kotova, 2007). The electron temperature of the plasmasphere is similarly about 1 eV (Décréau et al., 1982). Since there is no reasonable mechanism to cool the plasmaspheric ions and electrons down to ~1 eV, it can be assumed that the temperatures of the outflowing ions and electrons are both about 1 eV.

Note that the plasmasphere refills into flux tubes that already contained the oxygen-rich plasma cloak, resulting in oxygen ions in the composition of the outer plasmasphere.

Less appreciated, the refilling process should be occurring on flux tubes beyond the plasmapause that are on open drift trajectories. With shorter lifetimes before they are opened by reconnection at the dayside magnetopause, these open-drift-trajectory flux tubes will not exhibit cold-plasma densities in the range of plasmaspheric densities: nevertheless the refilling-process ions and electrons flow into them for a fraction of a day and could easily compete in density with the hot ion-plasma-sheet and electron-plasma-sheet populations in the dipolar regions of the magnetosphere. When they are at low number densities, the refilling-process ions should be field aligned at the equator.

The outflows of the plasmaspheric-refilling process are chiefly from the sunlit ionosphere into the dayside magnetosphere, so refilling protons, He^+ ions, and electrons should be found Sunward of the dawn–dusk terminator. At $L = 6.6$ in the dipole, the distance along the magnetic field from the ionosphere to the equatorial magnetosphere is about 8.1 R_E. A 1-eV proton has a speed of about 14 km/s and a 1-eV He^+ ion has a speed of about 3.5 km/s. Hence it takes ionospheric-outflow refilling protons about 1 h to reach the equator and it takes refilling He^+ ions about 4 h to reach the equator. It is more likely that refilling protons will be seen in the open-drift regions of the dayside magnetosphere. Denton et al. (2014) argue [see also Chappell (1974) and Sojka and Wrenn (1985)] that proton refilling rates at L = 6.6 can be as high as 2 cm^{-3}/hr; at larger L values the rate will be lower.

The impact of refilling-process ions and electrons in the open-drift-trajectory regions of the dayside magnetosphere has not been assessed.

8.2. Impact of the remnant layer

The Earthward edge of the electron plasma sheet is often co-located with the plasmapause (Horwitz et al., 1982; Fairfield and Vinãs, 1984; Elphic et al., 1999). This is the case when magnetospheric convection has been steady or when it is increasing. When geomagnetic activity (and magnetospheric convection) temporally decreases, the zero-energy open-closed **E**×**B** drift trajectory in the equatorial plane moves outward from the Earth. At such a time, two things should be noted. (1) Eventually, the plasmasphere will refill out to the new location of the open-closed boundary, but initially the plasmapause is closer to the Earth than the open-closed boundary. (2) Fresh hot plasma-sheet electrons will have their inner edge at the open-closed boundary away from the plasmapause as they advect from the magnetotail into the dipole.

This spatial gap between the plasmapause and the Earthward edge of the fresh electron plasma sheet is known as the "remnant layer" [cf. Feldstein and Galperin (1985), Galperin and Feldstein (1996)]. Particle-population-wise, the remnant layer contains (1) decaying hot populations and (2) growing cold populations. (1) Old electron-plasma-sheet electrons that are now on closed drift trajectories decay in intensity owing to precipitation to the atmosphere. Energetic ions and electrons previously injected into this region by prior substorms also decay with time. These are "remnant" hot populations. Electrons of the outer electron radiation belt are found in the remnant layer, as they are in the plasmasphere and in the inner portions of the electron plasma sheet. (2) The plasmaspheric-refilling process is ongoing in the remnant layer depositing ~ 1-eV protons and electrons with a density increasing with a timescale of days.

The remnant layer has been poorly studied. Two questions for the future are (1) What is the plasma-wave activity in the remnant layer? and (2) How does the remnant layer affect the evolution of the electron radiation belt?

For models wherein the whistler-mode hiss inside of the plasmasphere originates from whistler-mode chorus outside of the plasmasphere [e.g. Bortnik et al. (2008), Santolík and Chum (2009)], the role of the remnant layer (and its waves) between the region of strong chorus generation (the electron plasma sheet) and the plasmapause should be considered.

9. Spacecraft charging

Despite the fact that spacecraft charging interferes with cold-plasma measurements (see Section 10), it is interesting to point out that the presence of the cold plasma is actually beneficial from the perspective of the potential damage that spacecraft can incur from spacecraft charging.

Spacecraft charging is a major application of research on space weather since charging can lead to spacecraft anomalies (Baker, 2000, 2002; Choi et al., 2011; Ferguson et al., 2015; Thomsen et al., 2013). The latter can range from inconsequential (single event upsets, memory bit flipping) to catastrophic (damage to sensitive electronics and total loss of the spacecraft). In essence, spacecraft charging is the balance of currents on spacecraft surfaces. It involves the collection of ambient electrons and ions and emission of electrons via secondary emission due to electron/ion impact or photo-emission on surfaces exposed to sunlight (Hastings and Garrett, 2004; Lai, 2011). Cold to hot plasma particles deposit their charge on spacecraft surfaces and give rise to surface charging, while relativistic electrons can penetrate satellite shielding and reach internal components causing deep-dielectric charging (Hastings and Garrett, 2004; Lai, 2011). Surface charging can be non-uniform on the spacecraft, causing potential differences across adjacent surfaces (i.e. differential charging).

In order to illustrate the impact of the cold plasma on spacecraft charging, we may use the expressions for the currents obtained by an approximated charging theory known as the orbital-motion-limited (OML) theory (Mott-Smith and Langmuir, 1926). We will consider a conducting, spherical spacecraft since we are only interested in charging estimates. The OML electron collected current is given by

$$I_e = -e4\pi r_{sc}^2 n_e \sqrt{\frac{T_e}{2\pi m_e}} \exp\left(\frac{e\phi_{sc}}{T_e}\right), \quad \phi_{sc} < 0, \tag{13}$$

and

$$I_e = -e4\pi r_{sc}^2 n_e \sqrt{\frac{T_e}{2\pi m_e}} \left(1 + \frac{e\phi_{sc}}{T_e}\right), \quad \phi_{sc} \geq 0, \tag{14}$$

where n_e (T_e) is the ambient unperturbed electron density (temperature), obtained with the assumption that the ambient electrons are Maxwellian. In Eqs. (13) and (14), e is the positive elementary charge, r_{sc} is the spacecraft radius and ϕ_{sc} is the spacecraft potential (relative to the plasma potential). If multiple electron populations with different energy are present at the same time, the current collected from each population is still described by Eqs. (13)–(14) with appropriate values for n_e and T_e. Assuming Maxwellian, singly-charged ions, the ion collected current is given by

$$I_i = e4\pi r_{sc}^2 n_i \sqrt{\frac{T_i}{2\pi m_i}} \left(1 - \frac{e\phi_{sc}}{T_i}\right), \quad \phi_{sc} \leq 0, \tag{15}$$

and

$$I_i = e4\pi r_{sc}^2 n_i \sqrt{\frac{T_i}{2\pi m_i}} \exp\left(-\frac{e\phi_{sc}}{T_i}\right), \quad \phi_{sc} > 0, \tag{16}$$

with m_i the ion mass and n_i (T_i) the unperturbed ion density (temperature). Current balance is expressed by the net current on the spacecraft being equal to zero and, given plasma and spacecraft material parameters, this translates into an equation for the spacecraft potential known as the floating condition.

In sunlight, the current collected from the ambient electrons is typically balanced by photoemission. The photoemission current density exiting the sunlit surfaces of typical spacecraft materials is ~1 nA/cm^2 (Whipple, 1981). In the magnetosphere, this photoelectron current normally overwhelms the flux of ambient electrons to the spacecraft and so the spacecraft charges positively with respect to infinity to pull back and recollect most of the photoelectrons. As a result, the spacecraft potential ranges between few Volts and several tens of Volts positive, depending on the density of ambient electrons.

Strong negative charging events can occur in eclipse conditions, where photoemission is absent. If secondary electron emission can also be neglected, the spacecraft potential is now determined by the balance of electron and ion collection [i.e. Eqs. (13) and (15)]. Under these conditions, the spacecraft potential becomes negative, proportional to the electron temperature, to repel some of the ambient electrons away from the spacecraft. Thus kV potentials are possible if the electron temperature is in the keV range. On the other hand, if the cold plasma populations dominate charging, the spacecraft potential only charges to a few Volts negative. This is indeed the case for ionospheric conditions (Samir and Willmore, 1966; Knudsen et al., 2017; Diego et al., 2019).

To be more concrete, let us consider an environment at geosynchronous orbit characterized by hot plasma sheet properties (for electrons and protons) typical of geomagnetically active times, with $n_h = n_{eh} = n_{ph} = 1$ cm^{-3}, T_{eh}=1 keV and $T_{ph} = 10$ keV. Solving the OML floating condition equation for a spacecraft in eclipse, i.e. $I_e(\phi_{sc}) + I_i(\phi_{sc}) = 0$ with I_e and I_i given by Eqs. (13) and (15), yields a spacecraft potential of −2.4 kV. Let us now add a cold ion and a cold electron population each with density parametrized by

$$n_c = 20\left(\frac{3.5}{L}\right)^4 \text{cm}^{-3} \tag{17}$$

with L the drift shell. Eq. (17) comes from fitting Fig. 5 of Gallagher et al. (1995) and was obtained at midnight for $K_p = 5$ levels of geomagnetic activity. For L=6.6, this gives $n_c = n_{ec} = n_{pc} = 1.6$ cm^{-3} and we will assume a temperature of $T_{ec} = T_{pc} = 5$ eV. In this case, the spacecraft potential decreases to −744 V. If we use cold plasma parameters typical of geomagnetically quite conditions, given by

$$n_c = 10^{-0.3145L+3.9043} \text{ cm}^{-3}, \tag{18}$$

(Gallagher et al., 1995), we obtain $n_c = n_{ec} = n_{pc} = 67$ cm^{-3} and the spacecraft potential drops to −35 V.

Note also that cloak ions help reducing strong negative spacecraft charging. Assuming nominal cloak parameters with oxygen ions and $n_{e,cloak} = n_{O,cloak} = 1$ cm^{-3} with $T_e = T_O = 100$ eV together with the plasma sheet properties used above ($n_h = n_{eh} = n_{ph} = 1$ cm^{-3}, $T_{eh} = 1$ keV and $T_{ph} = 10$ keV) yields a spacecraft potential of −2 kV.

10. The difficulty of cold-ion and cold-electron measurements

Reliable measurements of the cold-ion and cold electron populations and their interpretation are notoriously difficult. The primary reason is the charging of the spacecraft by the local space environment and by electron emission from the spacecraft surfaces.

For the sake of the discussion, let us consider a particle detector measuring down to eV energies and mounted on the surface of a spacecraft. In sunlight, the spacecraft typically floats a few Volts to several tens of Volts positive. Cold ions are therefore repelled by the spacecraft potential. If the spacecraft potential is much higher than the mean cold-ion energy, this typically means that there is no hope to measure the cold-ion particle distribution without using some additional technique. If the spacecraft potential is higher but of the order of the mean cold-ion energy, the spacecraft can collect a small fraction of cold ions from the tail of the distribution able to overcome the spacecraft potential. In this case, one could use techniques that extrapolate the cold-ion tail measurements to learn some of the properties of the cold ions (Genestreti et al., 2017). Note, however, that errors from the extrapolation become larger as the spacecraft potential increases. A notable exception to the problems just described occurs in times of strong convection, when the ion drift velocity becomes sufficiently large to overcome the spacecraft potential (Lee and Angelopoulos, 2014b). When the spacecraft is negatively charged (such as in eclipse conditions), cold ions are attracted by the spacecraft and in principle one has access to the full cold-ion particle distribution after correcting for the acceleration and sheath focusing induced by the spacecraft

potential. In practice, this is true only if the energy resolution of the particle detector is not much larger than the cold-ion temperature. If not, the information on the cold-ion energy distribution is lost but one can obtain an estimate of the cold-ion density.

For cold electrons, similar spacecraft-charging issues apply with an additional complication arising from the fact that spacecraft also emit ∼eV electrons due to photoemission and secondary emission. It is possible to distinguish these emitted electrons from ambient cold electrons due to their different energy spectra, and so techniques to filter out the emitted electrons from cold-electron measurements exist (Mozer et al., 2017b; Gershman et al., 2017). These techniques, however, become inaccurate when the cold-electron signal is overwhelmed by the photoelectron signal. When a spacecraft is negatively charged, cold electrons are repelled and so, if particle measurements are available, one could in principle once again extrapolate from the tail of the cold-electron distribution. However, spacecraft can charge to large negative potentials (i.e. well below -100 V) [e.g. Li and Whipple (1988), Thomsen et al. (2013)], in which case there is no hope to recover any information on cold electrons. When the spacecraft is positively charged, ambient electrons are attracted to the spacecraft and accelerated by the spacecraft potential. Spacecraft-generated electrons are attracted back to the spacecraft. In general, one can then have access to the cold-electron distribution, provided that photoelectrons and secondary electrons can be filtered out. Note, however, that often missions equipped with particle instruments do not measure electrons with energy below ∼10 eV (arguably to stay away from energies that can be contaminated by the emitted electrons). For instance, the lowest electron energy resolution on the Van Allen Probes spacecraft was 15 eV (1 eV for ions) and on the Magnestospheric MultiScale spacecraft is 10 eV. Thus, if the spacecraft is only charged to a few Volts positive, one is again forced to extrapolate from the tail of the cold-electron distribution. If the spacecraft potential is ∼10 V or higher, the full cold-electron energy distribution is measured.

Several techniques have been developed in the past to overcome the issues with cold-plasma measurements. Perhaps the most obvious is to take the measurements in the unperturbed plasma outside the spacecraft sheath, using booms of size longer than the local Debye length. Langmuir probes measurements of the electron density and temperature and ion density on a boom have indeed been performed many times before, particularly in the ionosphere where the plasma is dense and cold and booms of ∼ 1 m length are sufficient (Brace, 2013). Active wave experiments based on the mutual impedance of a double probe have also been successful to determine the cold electron density and temperature (Décréau et al., 1979; Décréau et al., 1982), while techniques based on measurements of characteristic frequencies of the ambient plasma can also be used to determine the total electron density. This is the case on the Van Allen Probes spacecraft which uses the upper-hybrid frequency (Kurth et al., 2015). A method based on the electric field measurements of the spacecraft wake has also been successfully developed, yielding the cold-ion density and flow velocity (Engwall et al., 2009a; Engwall et al., 2009b). All these techniques have known limitations, often exposed by low plasma densities, and, most important, do not yield the full energy distribution.

The measurement of the cold ion distribution below the spacecraft potential has been achieved with a retarding ion mass spectrometer on the Dynamics Explorer 1 mission, where a negative electrostatic bias (up to −8 V relative to the spacecraft potential) was applied to the sensor apertures to collect cold ions that would have been otherwise repelled by the spacecraft potential (Chappell et al., 1981). An alternative but very popular technique is active spacecraft potential control (Lai, 2003). For example an ion emitter can be used to balance photoemission and reduce the positive spacecraft potential in sunlight. This technique has been used extensively in the past, on missions such as Geotail (Schmidt et al., 1995), Cluster (Torkar et al., 2001) and MMS (Torkar et al., 2016). Note that the spacecraft potential from these missions was not exactly zero with active control but maintained moderate positive values (Torkar et al., 2001). This implies that some fraction of the cold ion distribution was still not collected by the spacecraft. Active control with a neutral plasma source (i.e. a plasma contactor) was also performed on POLAR (Moore et al., 1995; Comfort et al., 1998). Note that the emission of a plasma can interfere with other spacecraft measurements, notably waves and electric fields.

Measurements of the cold electron energy distribution with good resolution have been lacking in the magnetosphere. One notable exception comes from the Time History of Events and Macroscale Interactions during Substorms (THEMIS) mission, which in 2016 operated for two hundred days in a special mode where the first 15 electron energy channels were lowered to cover the energy range 0–30 eV (Mozer et al., 2017b). In this case, THEMIS-D was in the dayside magnetosphere, the spacecraft potential was in the range +5–9 V and photoelectron contamination did not appear to be a problem. In general, however, measurements of the cold electron energy distribution can be strongly complicated by photoelectrons or secondary electrons since those electron fluxes can completely obscure the signal coming from the ambient cold electrons. Given the importance of cold electrons in magnetospheric dynamics, new methods that can reliably suppress photoemission or that can robustly distinguish photoelectrons from the cold-electron fluxes need to be developed and flown.

In summary, cold-plasma measurements are difficult and this has so far prevented a systematic and comprehensive study of cold-plasma properties throughout the magnetosphere, including those regions where the plasma density is low. Techniques to enable measurements of the cold-ion energy distributions have been developed and quite successfully flown in space. We may therefore conclude that cold-ion measurements are sufficiently mature. Measurements of the cold-electron energy distribution, on the other hand, can be strongly affected by photoemission and secondary-electron emission and methods that suppress the secondary electrons robustly need to be further developed.

11. Conclusions

We have presented a review of the known and probable impacts of the cold-electron and cold-ion populations in the Earth's magnetosphere (summarized in Table 1), motivated by the growing evidence that these populations play a major role in the dynamics of the system. Specifically,

1. The cold ionospheric plasma is a major source of plasma for the magnetosphere, at times dominating the contribution from the solar wind. Polar wind ions can be accelerated to plasma sheet or ring current energies as they drift in the cross-tail potential.
2. Cold-ions (in plumes and in the warm plasma cloak) are important for solar wind/magnetosphere coupling during geomagnetically-active times, since they can increase the total mass–density and reduce the reconnection rate. They can also affect reconnection at a microscopic level, acting on the Hall currents. Similar effects are expected to play a role in the magnetotail during substorms, although whether sufficient cold-ion density exists at distances relevant to near-Earth tail reconnection is still an open question.
3. Cold ions (specifically the warm plasma cloak) also affect the magnetopause stability to Kelvin–Helmholtz waves, altering the resulting viscous interaction and hence the transport of solar wind into the magnetosphere.
4. Cold electrons and cold ions (including ion composition) play a major role in controlling wave–particle interactions in the inner magnetosphere. Cold electrons (ions) control the generation of whistler (EMIC) waves by the cyclotron instability, reducing the threshold for the instability and affecting the main properties of the generated waves: frequency, growth rate and saturation amplitude. Cold electrons (ions) also control the propagation

of whistler (EMIC) waves in the environment, determining the waves' properties (including amplitude) and area of influence. Cold ions also affect the frequencies and amplitudes of the ULF waves. In this way, the cold electrons and cold ions control the scattering and energization rates of the higher-energy populations, impacting the dynamics of the plasma sheet, ring current and radiation belts.

5. Because of their effect on wave–particle interactions, cold electrons are believed to be responsible for the structuring of the pulsating aurora. Shear-flow instabilities between cold plasmaspheric and hot plasma-sheet plasmas at the plasmapause are believed to be the generation mechanisms for giant undulations and associated Pc5 pulsations (and might possibly be related to STEVE emissions and long-lived drainage plumes). Other areas where the cold populations should play a role include refilling in the open-drift trajectories and the remnant layer.
6. Cold electrons and cold ions also help reduce spacecraft charging.
7. Cold electrons and cold ions play roles in the properties of parallel electric fields in the magnetosphere: when the cold particles are either accelerated across the parallel-electric-field region or reflected away from the region, they will make a space-charge contribution to supporting the electric field.

It is important to emphasize that some of the impacts discussed above are associated primarily with the density of the cold populations, while some involve their energy distributions. Furthermore, a lot of work on the impact of cold populations has focused on cold ions, arguably because of their importance in determining the local mass–density. A lot less is known about the cold-electron populations, which however play a very important role for instance in the physics of outflow, whistler waves and pulsating aurora structuring. Thus, to fully understand the impact of the cold populations on the magnetosphere–ionosphere system, measurements of the cold-electron and cold-ion distribution functions are needed together with advances in spacecraft measurements techniques.

Innovations are needed in the design of low-energy ion instruments (Fernandes and Lynch, 2016; Moore and Spann, 2017), including ion-composition measurements [e.g. Yau and Howarth (2016)]. Ion instruments with large geometric factors are needed [e.g. Moore et al. (1995)]. To overcome unfavorable positive spacecraft potentials, either (a) the use of a plasma contactor (Comfort et al., 1998) or (b) the use of ion detectors that are negatively biased and possibly mounted on a boom (Chappell et al., 1981) will be necessary.

Measurements of low-energy electrons (Pollock et al., 2013; Cohen et al., 2016) are hindered by the presence of spacecraft-generated photoelectrons and secondary electrons (Thomsen et al., 2013; Mozer et al., 2017b). Designs using shadowing of the electron instrument combined with differential biases to reduce the fluxes of photoelectrons and secondary electrons at the electron instrument may be feasible. Smart spacecraft material designs that suppress electron emission would be another valuable development. The emission of an electron beam from the spacecraft to drive its potential positive with respect to infinity [e.g. Delzanno et al. (2015)] would result in the acceleration of ambient cold electrons to energies above the spacecraft-generated photoelectrons and secondaries. Some information about the cold-electron populations can also be gained with the use of a mutual impedance probe (Décréau et al., 1979).

There remain many unknowns about the cold-ion and cold-electron populations of the Earth's magnetosphere since in general these populations are not yet well characterized and their origins and controlling factors are often not well understood. Besides their known impacts, they likely have impacts that are not yet known. The cold electrons and ions need to be fully understood before we can fully understand the magnetosphere–ionosphere system.

Acknowledgments

This work was performed in coordination with the activities of the GEM Focus Group 'The Impact of Cold Plasma in Magnetospheric Physics'. The authors thank Lauren Blum, Natalia Buzulukova, Pat Colestock, Rick Chappell, Mick Denton, Richard Denton, Reiner Friedel, Stephen Fuselier, Dennis Gallagher, Brian Gilchrist, Barbara Giles, Raluca Ilie, Lynn Kistler, Craig Kletzing, Alex Koshkarov, Jonathan Krall, Elena Kronberg, Omar Leon, Naomi Maruyama, Grant Miars, Thom Moore, Toshi Nishimura, Ruth Skoug, Michelle Thomsen, Maria Usanova, Roger Varney, Brian Walsh, Kateryna Yakymenko for helpful conversations. GLD wishes to thank Caterina Baravalle for her constant 'presence' and support. GLD and PARL were supported by the Laboratory Directed Research and Development program, USA at Los Alamos National Laboratory (LANL) under project 20200276ER. LANL is operated by Triad National Security, LLC, for the National Nuclear Security Administration of U.S. Department of Energy (DOE) (Contract No. 89233218CNA000001). JEB was supported by the National Science Foundation (NSF) GEM program, USA via awards AGS-2027569 and AGS-1502947, by NASA Heliophysics LWS TRT program, USA via grant NNX14AN90G, by the NASA Heliophysics Guest Investigator Program, USA via grant NNX17AB71G, and by the NSF SHINE program, USA via award AGS-1723416. VR was partially supported by NSF, USA awards 1602748 and 1707275.

References

Abe, T., Watanabe, S., Whalen, B.A., Yau, A.W., Sagawa, E., 1996. Observations of Polar Wind and Thermal Ion Outflow by Akebono/SMS. J. Geomagn. Geoelectr. 48 (3), 319–325. http://dx.doi.org/10.5636/jgg.48.319.

Adachi, S., 1966. Theory of Duct Propagation of Whistler Radio Waves. Radio Sci. 1 (6), 671–678. http://dx.doi.org/10.1002/rds196616671, https://agupubs.onlinelibrary.wiley.com/doi/pdf/10.1002/rds196616671, https://agupubs.onlinelibrary.wiley.com/doi/abs/10.1002/rds196616671.

Adrian, M.L., Gallagher, D.L., Avanov, L.A., 2004. IMAGE EUV observation of radially bifurcated plasmaspheric features: First observations of a possible standing ULF waveform in the inner magnetosphere. J. Geophys. Res.: Space Phys. 109 (A1), A01203. http://dx.doi.org/10.1029/2003JA009974, https://agupubs.onlinelibrary.wiley.com/doi/pdf/10.1029/2003JA009974, https://agupubs.onlinelibrary.wiley.com/doi/abs/10.1029/2003JA009974.

Agapitov, O., Mourenas, D., Artemyev, A., Claudepierre, S.G., Hospodarsky, G., Bonnell, J.W., 2020. Lifetimes of Relativistic Electrons as Determined From Plasmaspheric Hiss Scattering Rates Statistics: Effects of ω_{pe}/Ω_{ce} and Wave Frequency Dependence on Geomagnetic Activity. Geophys. Res. Lett. 47 (13), e2020GL088052. http://dx.doi.org/10.1029/2020GL088052, arXiv: https://agupubs.onlinelibrary.wiley.com/doi/pdf/10.1029/2020GL088052 https://agupubs.onlinelibrary.wiley.com/doi/abs/10.1029/2020GL088052 e2020GL088052 2020GL088052.

An, X., Yue, C., Bortnik, J., Decyk, V., Li, W., Thorne, R.M., 2017. On the parameter dependence of the whistler anisotropy instability. J. Geophys. Res.: Space Phys. 122 (2), 2001–2009. http://dx.doi.org/10.1002/2017JA023895, arXiv:https://agupubs.onlinelibrary.wiley.com/doi/pdf/10.1002/2017JA023895. https://agupubs.onlinelibrary.wiley.com/doi/abs/10.1002/2017JA023895.

Anderson, B.J., Erlandson, R.E., Zanetti, L.J., 1992. A statistical study of Pc 1-2 magnetic pulsations in the equatorial magnetosphere: 2. Wave properties. J. Geophys. Res.: Space Phys. 97 (A3), 3089–3101. http://dx.doi.org/10.1029/91JA02697, arXiv:https://agupubs.onlinelibrary.wiley.com/doi/pdf/10.1029/91JA02697. https://agupubs.onlinelibrary.wiley.com/doi/abs/10.1029/91JA02697.

André, M., Cully, C.M., 2012. Low-energy ions: A previously hidden solar system particle population. Geophys. Res. Lett. 39 (3), L03101. http://dx.doi.org/10.1029/2011GL050242, arXiv:https://agupubs.onlinelibrary.wiley.com/doi/pdf/10.1029/2011GL050242. https://agupubs.onlinelibrary.wiley.com/doi/abs/10.1029/2011GL050242.

André, N., Lemaire, J., 2006. Convective instabilities in the plasmasphere. J. Atmos. Sol.-Terr. Phys. 68 (2), 213–227. http://dx.doi.org/10.1016/j.jastp.2005.10.013, http://www.sciencedirect.com/science/article/pii/S1364682605002932.

André, M., Li, W., Toledo-Redondo, S., Khotyaintsev, Y.V., Vaivads, A., Graham, D.B., Norgren, C., Burch, J., Lindqvist, P.-A., Marklund, G., Ergun, R., Torbert, R., Magnes, W., Russell, C.T., Giles, B., Moore, T.E., Chandler, M.O., Pollock, C., Young, D.T., Avanov, L.A., Dorelli, J.C., Gershman, D.J., Paterson, W.R., Lavraud, B., Saito, Y., 2016. Magnetic reconnection and modification of the Hall physics due to cold ions at the magnetopause. Geophys. Res. Lett. 43 (13), 6705–6712. http://dx.doi.org/10.1002/2016GL069665, arXiv:https://agupubs.onlinelibrary.wiley.com/doi/pdf/10.1002/2016GL069665. https://agupubs.onlinelibrary.wiley.com/doi/abs/10.1002/2016GL069665.

Angelopoulos, V., Artemyev, A., Phan, T.D., Miyashita, Y., 2020. Near-Earth magnetotail reconnection powers space storms. Nat. Phys. 16 (3), 317–321, https://doi.org/10.1038/s41567-019-0749-4.

Angerami, J.J., 1970. Whistler duct properties deduced from VLF observations made with the Ogo 3 satellite near the magnetic equator. J. Geophys. Res. 75 (31), 6115–6135. http://dx.doi.org/10.1029/JA075i031p06115, arXiv:https://agupubs.onlinelibrary.wiley.com/doi/pdf/10.1029/JA075i031p06115. https://agupubs.onlinelibrary.wiley.com/doi/abs/10.1029/JA075i031p06115.

Axford, W.I., 1968. The polar wind and the terrestrial helium budget. J. Geophys. Res. 73 (21), 6855–6859. http://dx.doi.org/10.1029/JA073i021p06855, arXiv:https://agupubs.onlinelibrary.wiley.com/doi/pdf/10.1029/JA073i021p06855. https://agupubs.onlinelibrary.wiley.com/doi/abs/10.1029/JA073i021p06855.

Axford, W.I., Hines, C.O., 2013. A Unifying Theory of High-Latitude Geophysical Phenomena and Geomagnetic Storms. In: The Upper Atmosphere in Motion. American Geophysical Union (AGU), pp. 936–967. http://dx.doi.org/10.1029/GM018p0936, arXiv:https://agupubs.onlinelibrary.wiley.com/doi/pdf/10.1029/GM018p0936. https://agupubs.onlinelibrary.wiley.com/doi/abs/10.1029/GM018p0936.

Baddeley, L.J., Lorentzen, D.A., Partamies, N., Denig, M., Pilipenko, V.A., Oksavik, K., Chen, X., Zhang, Y., 2017. Equatorward propagating auroral arcs driven by ULF wave activity: Multipoint ground- and space-based observations in the dusk sector auroral oval. J. Geophys. Res.: Space Phys. 122 (5), 5591–5605. http://dx.doi.org/10.1002/2016JA023427, arXiv:https://agupubs.onlinelibrary.wiley.com/doi/pdf/10.1002/2016JA023427. https://agupubs.onlinelibrary.wiley.com/doi/abs/10.1002/2016JA023427.

Bailey, G., Balan, N., Su, Y., 1997. The Sheffield University plasmasphere ionosphere model - a review. J. Atmos. Sol.-Terr. Phys. 59 (13), 1541–1552. http://dx.doi.org/10.1016/S1364-6826(96)00155-1, http://www.sciencedirect.com/science/article/pii/S1364682696001551 The Ninth International Symposium on Equatorial Aeronomy.

Baishev, D.G., Barkova, E.S., Solovyev, S.I., Yumoto, K., Engebretson, M.J., Koustov, A.V., 2000. Formation of Large-Scale, 'Giant' Undulations at the Equatorial Boundary of Diffuse Aurora and Pc5 Magnetic Pulsations during the January 14, 1999 Magnetic Storm. In: Wilson, A. (Ed.), Fifth International Conference on Substorms. In: ESA Special Publication, 443, p. 427.

Baishev, D.G., Barkova, E.S., Yumoto, K., 2012. Optical observations of large-scale undulations in the 23rd cycle of solar activity. Geomagn. Aeronomy 52 (2), 197–203, https://doi.org/10.1134/S0016793212020028.

Baker, D., 2000. The occurrence of operational anomalies in spacecraft and their relationship to space weather. IEEE Trans. Plasma Sci. 28, 2007–2016.

Baker, D., 2002. How to Cope with Space Weather. Science 297, 1486–1487.

Baker, D.N., Hones, E.W., Young, D.T., Birn, J., 1982. The possible role of ionospheric oxygen in the initiation and development of plasma sheet instabilities. Geophys. Res. Lett. 9 (12), 1337–1340. http://dx.doi.org/10.1029/GL009i012p01337, http://doi.wiley.com/10.1029/GL009i012p01337.

Banks, P.M., Holzer, T.E., 1968. The polar wind. J. Geophys. Res. 73 (21), 6846–6854. http://dx.doi.org/10.1029/JA073i021p06846, arXiv:https://agupubs.onlinelibrary.wiley.com/doi/pdf/10.1029/JA073i021p06846. https://agupubs.onlinelibrary.wiley.com/doi/abs/10.1029/JA073i021p06846.

Banks, P., Nagy, A., Axford, W., 1971. Dynamical behavior of thermal protons in the mid-latitude ionosphere and magnetosphere. Planet. Space Sci. 19 (9), 1053–1067. http://dx.doi.org/10.1016/0032-0633(71)90104-8, http://www.sciencedirect.com/science/article/pii/0032063371901048.

Barakat, A., Schunk, R., 2001. Effects of wave-particle interactions on the dynamic behavior of the generalized polar wind. J. Atmos. Sol.-Terr. Phys. 63 (1), 75–83. http://dx.doi.org/10.1016/S1364-6826(00)00106-1, http://www.sciencedirect.com/science/article/pii/S1364682600001061.

Barghouthi, I.A., Barakat, A.R., Persoon, A.M., 1998. The Effects of Altitude-Dependent Wave Particle Interactions on the Polar Wind Plasma. Astrophys. Space Sci. 259 (2), 117–140, https://doi.org/10.1023/A:1001569207346.

Bernhardt, P.A., 1992. Probing the magnetosphere using chemical releases from the Combined Release and Radiation Effects Satellite. Phys. Fluids B: Plasma Phys. 4 (7), 2249–2256, https://doi.org/10.1063/1.860193.

Bernstein, I.B., 1975. Geometric optics in space- and time-varying plasmas. Phys. Fluids 18 (3), 320–324. http://dx.doi.org/10.1063/1.861140, arXiv:https://aip.scitation.org/doi/pdf/10.1063/1.861140.

Birn, J., Borovsky, J.E., Hesse, M., 2008. Properties of asymmetric magnetic reconnection. Phys. Plasmas 15 (3), 032101. http://dx.doi.org/10.1063/1.2888491, arXiv:https://doi.org/10.1063/1.2888491. URL: https://doi.org/10.1063/1.2888491.

Birn, J., Hesse, M., 2001. Geospace Environment Modeling (GEM) magnetic reconnection challenge: Resistive tearing, anisotropic pressure and Hall effects. J. Geophys. Res.: Space Phys. 106 (A3), 3737–3750. http://dx.doi.org/10.1029/1999JA001001, arXiv:https://agupubs.onlinelibrary.wiley.com/doi/pdf/10.1029/1999JA001001. https://agupubs.onlinelibrary.wiley.com/doi/abs/10.1029/1999JA001001.

Blum, L.W., Breneman, A.W., 2020. Chapter 3 - Observations of radiation belt losses due to cyclotron wave-particle interactions. In: Jaynes, A.N., Usanova, M.E. (Eds.), The Dynamic Loss of Earth's Radiation Belts. Elsevier, pp. 49–98. http://dx.doi.org/10.1016/B978-0-12-813371-2.00003-2, http://www.sciencedirect.com/science/article/pii/B9780128133712000032.

Blum, L.W., MacDonald, E.A., Gary, S.P., Thomsen, M.F., Spence, H.E., 2009. Ion observations from geosynchronous orbit as a proxy for ion cyclotron wave growth during storm times. J. Geophys. Res.: Space Phys. 114 (A10), A10214. http://dx.doi.org/10.1029/2009JA014396, arXiv:https://agupubs.onlinelibrary.wiley.com/doi/pdf/10.1029/2009JA014396. https://agupubs.onlinelibrary.wiley.com/doi/abs/10.1029/2009JA014396.

Borovsky, J.E., 2008. The rudiments of a theory of solar wind/magnetosphere coupling derived from first principles. J. Geophys. Res.: Space Phys. 113 (A8), A08228. http://dx.doi.org/10.1029/2007JA012646, arXiv:https://agupubs.onlinelibrary.wiley.com/doi/pdf/10.1029/2007JA012646. https://agupubs.onlinelibrary.wiley.com/doi/abs/10.1029/2007JA012646.

Borovsky, J.E., 2014. Feedback of the Magnetosphere. Science 343 (6175), 1086–1087. http://dx.doi.org/10.1126/science.1250590, arXiv:https://science.sciencemag.org/content/343/6175/1086.full.pdf. https://science.sciencemag.org/content/343/6175/1086.

Borovsky, J.E., 2017. Electrical conductivity channels in the atmosphere produced by relativistic-electron microbursts from the magnetosphere. J. Atmos. Sol.-Terr. Phys. 155, 22–26. http://dx.doi.org/10.1016/j.jastp.2017.01.004, http://www.sciencedirect.com/science/article/pii/S1364682616302140.

Borovsky, J.E., Birn, J., 2014. The solar wind electric field does not control the dayside reconnection rate. J. Geophys. Res.: Space Phys. 119 (2), 751–760. http://dx.doi.org/10.1002/2013JA019193, arXiv:https://agupubs.onlinelibrary.wiley.com/doi/pdf/10.1002/2013JA019193. https://agupubs.onlinelibrary.wiley.com/doi/abs/10.1002/2013JA019193.

Borovsky, J.E., Delzanno, G.L., 2019. Active Experiments in Space: The Future. Front. Astron. Space Sci. 6, 31. http://dx.doi.org/10.3389/fspas.2019.00031, https://www.frontiersin.org/article/10.3389/fspas.2019.00031.

Borovsky, J.E., Delzanno, G.L., Valdivia, J.A., Moya, P.S., Stepanova, M., Birn, J., Blum, L.W., Lotko, W., Hesse, M., 2020. Outstanding questions in magnetospheric plasma physics: The pollenzo view. J. Atmos. Sol.-Terr. Phys. 208, 105377. http://dx.doi.org/10.1016/j.jastp.2020.105377, http://www.sciencedirect.com/science/article/pii/S1364682620301887.

Borovsky, J.E., Denton, M.H., 2006. Effect of plasmaspheric drainage plumes on solar-wind/magnetosphere coupling. Geophys. Res. Lett. 33 (20), L20101. http://dx.doi.org/10.1029/2006GL026519, arXiv:https://agupubs.onlinelibrary.wiley.com/doi/pdf/10.1029/2006GL026519. https://agupubs.onlinelibrary.wiley.com/doi/abs/10.1029/2006GL026519.

Borovsky, J.E., Denton, M.H., 2008. A statistical look at plasmaspheric drainage plumes. J. Geophys. Res.: Space Phys. 113 (A9), A09221. http://dx.doi.org/10.1029/2007JA012994, arXiv:https://agupubs.onlinelibrary.wiley.com/doi/pdf/10.1029/2007JA012994. https://agupubs.onlinelibrary.wiley.com/doi/abs/10.1029/2007JA012994.

Borovsky, J.E., Denton, M.H., 2014. Exploring the cross correlations and auto-correlations of the ULF indices and incorporating the ULF indices into the systems science of the solar wind-driven magnetosphere. J. Geophys. Res.: Space Phys. 119 (6), 4307–4334. http://dx.doi.org/10.1002/2014JA019876, arXiv:https://agupubs.onlinelibrary.wiley.com/doi/pdf/10.1002/2014JA019876. https://agupubs.onlinelibrary.wiley.com/doi/abs/10.1002/2014JA019876.

Borovsky, J.E., Denton, M.H., 2016. Compressional perturbations of the dayside magnetosphere during high-speed-stream-driven geomagnetic storms. J. Geophys. Res.: Space Phys. 121 (5), 4569–4589. http://dx.doi.org/10.1002/2015JA022136, arXiv:https://agupubs.onlinelibrary.wiley.com/doi/pdf/10.1002/2015JA022136. https://agupubs.onlinelibrary.wiley.com/doi/abs/10.1002/2015JA022136.

Borovsky, J.E., Denton, M.H., Denton, R.E., Jordanova, V.K., Krall, J., 2013. Estimating the effects of ionospheric plasma on solar wind/magnetosphere coupling via mass loading of dayside reconnection: Ion-plasma-sheet oxygen, plasmaspheric drainage plumes, and the plasma cloak. J. Geophys. Res.: Space Phys. 118 (9), 5695–5719. http://dx.doi.org/10.1002/jgra.50527, arXiv:https://agupubs.onlinelibrary.wiley.com/doi/pdf/10.1002/jgra.50527. https://agupubs.onlinelibrary.wiley.com/doi/abs/10.1002/jgra.50527.

Borovsky, J.E., Friedel, R.H.W., Denton, M.H., 2014a. Statistically measuring the amount of pitch angle scattering that energetic electrons undergo as they drift across the plasmaspheric drainage plume at geosynchronous orbit. J. Geophys. Res.: Space Phys. 119 (3), 1814–1826. http://dx.doi.org/10.1002/2013JA019310, arXiv:https://agupubs.onlinelibrary.wiley.com/doi/pdf/10.1002/2013JA019310. https://agupubs.onlinelibrary.wiley.com/doi/abs/10.1002/2013JA019310.

Borovsky, J.E., Hesse, M., 2007. The reconnection of magnetic fields between plasmas with different densities: Scaling relations. Phys. Plasmas 14 (10), 102309, arXiv:https://doi.org/10.1063/1.2772619.

Borovsky, J.E., Hesse, M., Birn, J., Kuznetsova, M.M., 2008. What determines the reconnection rate at the dayside magnetosphere?. J. Geophys. Res.: Space Phys. 113 (A7), A07210. http://dx.doi.org/10.1029/2007JA012645, arXiv:https://agupubs.onlinelibrary.wiley.com/doi/pdf/10.1029/2007JA012645. https://agupubs.onlinelibrary.wiley.com/doi/abs/10.1029/2007JA012645.

Borovsky, J.E., Steinberg, J.T., 2006. The "calm before the storm" in CIR/magnetosphere interactions: Occurrence statistics, solar wind statistics, and magnetospheric preconditioning. J. Geophys. Res.: Space Phys. 111 (A7), A07S10. http://dx.doi.org/10.1029/2005JA011397, arXiv:https://agupubs.onlinelibrary.wiley.com/doi/pdf/10.1029/2005JA011397. https://agupubs.onlinelibrary.wiley.com/doi/abs/10.1029/2005JA011397.

Borovsky, J.E., Thomsen, M.F., McComas, D.J., 1997. The superdense plasma sheet: Plasmaspheric origin, solar wind origin, or ionospheric origin?. J. Geophys. Res.: Space Phys. 102 (A10), 22089–22097. http://dx.doi.org/10.1029/96JA02469, arXiv:https://agupubs.onlinelibrary.wiley.com/doi/pdf/10.1029/96JA02469. https://agupubs.onlinelibrary.wiley.com/doi/abs/10.1029/96JA02469.

Borovsky, J.E., Valdivia, J.A., 2018. The Earth's Magnetosphere: A Systems Science Overview and Assessment. Surv. Geophys. 39 (5), 817–859, https://doi.org/10.1007/s10712-018-9487-x.

Borovsky, J.E., Welling, D.T., Thomsen, M.F., Denton, M.H., 2014b. Long-lived plasmaspheric drainage plumes: Where does the plasma come from?. J. Geophys. Res.: Space Phys. 119 (8), 6496–6520. http://dx.doi.org/10.1002/2014JA020228, arXiv:https://agupubs.onlinelibrary.wiley.com/doi/pdf/10.1002/2014JA020228. https://agupubs.onlinelibrary.wiley.com/doi/abs/10.1002/2014JA020228.

Bortnik, J., Li, W., Thorne, R.M., Angelopoulos, V., Cully, C., Bonnell, J., Le Contel, O., Roux, A., 2009. An Observation Linking the Origin of Plasmaspheric Hiss to Discrete Chorus Emissions. Science 324 (5928), 775–778. http://dx.doi.org/10.1126/science.1171273, arXiv:https://science.sciencemag.org/content/324/5928/775.full.pdf. https://science.sciencemag.org/content/324/5928/775.

Bortnik, J., Thorne, R.M., Meredith, N.P., 2007. Modeling the propagation characteristics of chorus using CRRES suprathermal electron fluxes. J. Geophys. Res.: Space Phys. 112 (A8), A08204. http://dx.doi.org/10.1029/2006JA012237, arXiv:https://agupubs.onlinelibrary.wiley.com/doi/pdf/10.1029/2006JA012237. https://agupubs.onlinelibrary.wiley.com/doi/abs/10.1029/2006JA012237.

Bortnik, J., Thorne, R.M., Meredith, N.P., 2008. The unexpected origin of plasmaspheric hiss from discrete chorus emissions. Nature 452 (7183), 62–66. http://dx.doi.org/10.1038/nature06741.

Bortnik, J., Thorne, R.M., Omidi, N., 2010. Nonlinear evolution of EMIC waves in a uniform magnetic field: 2. Test-particle scattering. J. Geophys. Res.: Space Phys. 115 (A12), A12242. http://dx.doi.org/10.1029/2010JA015603, arXiv:https://agupubs.onlinelibrary.wiley.com/doi/pdf/10.1029/2010JA015603. https://agupubs.onlinelibrary.wiley.com/doi/abs/10.1029/2010JA015603.

Brace, L.H., 2013. Langmuir Probe Measurements in the Ionosphere. In: Measurement Techniques in Space Plasmas: Particles. American Geophysical Union (AGU), pp. 23–35. http://dx.doi.org/10.1029/GM102p0023, arXiv:https://agupubs.onlinelibrary.wiley.com/doi/pdf/10.1029/GM102p0023. https://agupubs.onlinelibrary.wiley.com/doi/abs/10.1029/GM102p0023.

Brambles, O.J., Lotko, W., Damiano, P.A., Zhang, B., Wiltberger, M., Lyon, J., 2010. Effects of causally driven cusp O+ outflow on the storm time magnetosphere-ionosphere system using a multifluid global simulation. J. Geophys. Res.: Space Phys. 115 (A9), A00J04. http://dx.doi.org/10.1029/2010JA015469, arXiv:https://agupubs.onlinelibrary.wiley.com/doi/pdf/10.1029/2010JA015469. https://agupubs.onlinelibrary.wiley.com/doi/abs/10.1029/2010JA015469.

Brambles, O., Lotko, W., Zhang, B., Wiltberger, M., Lyon, J., Strangeway, R.J., 2011. Magnetosphere Sawtooth Oscillations Induced by Ionospheric Outflow. Science 332 (6034), 1183–1186, http://www.jstor.org/stable/27977983.

Breneman, A.W., Crew, A., Sample, J., Klumpar, D., Johnson, A., Agapitov, O., Shumko, M., Turner, D.L., Santolík, O., Wygant, J.R., Cattell, C.A., Thaller, S., Blake, B., Spence, H., Kletzing, C.A., 2017. Observations Directly Linking Relativistic Electron Microbursts to Whistler Mode Chorus: Van Allen Probes and FIREBIRD II. Geophys. Res. Lett. 44 (22), 11,265–11,272. http://dx.doi.org/10.1002/2017GL075001, arXiv:https://agupubs.onlinelibrary.wiley.com/doi/pdf/10.1002/2017GL075001. https://agupubs.onlinelibrary.wiley.com/doi/abs/10.1002/2017GL075001.

Brice, N., 1970. Artificial enhancement of energetic particle precipitation through cold plasma injection: A technique for seeding substorms?. J. Geophys. Res. 75 (25), 4890–4892. http://dx.doi.org/10.1029/JA075i025p04890, arXiv:https://agupubs.onlinelibrary.wiley.com/doi/pdf/10.1029/JA075i025p04890. https://agupubs.onlinelibrary.wiley.com/doi/abs/10.1029/JA075i025p04890.

Brice, N., Lucas, C., 1971. Influence of magnetospheric convection and polar wind on loss of electrons from the outer radiation belt. J. Geophys. Res. 76 (4), 900–908. http://dx.doi.org/10.1029/JA076i004p00900, arXiv:https://agupubs.onlinelibrary.wiley.com/doi/pdf/10.1029/JA076i004p00900. https://agupubs.onlinelibrary.wiley.com/doi/abs/10.1029/JA076i004p00900.

Burtis, W.J., Helliwell, R.A., 1969. Banded chorus — A new type of VLF radiation observed in the magnetosphere by OGO 1 and OGO 3. J. Geophys. Res. 74 (11), 3002–3010. http://dx.doi.org/10.1029/JA074i011p03002, arXiv:https://agupubs.onlinelibrary.wiley.com/doi/pdf/10.1029/JA074i011p03002. https://agupubs.onlinelibrary.wiley.com/doi/abs/10.1029/JA074i011p03002.

Buzulukova, N., Fok, M.-C., Moore, T.E., Ober, D.M., 2008. Generation of plasmaspheric undulations. Geophys. Res. Lett. 35 (13), L13105. http://dx.doi.org/10.1029/2008GL034164, arXiv:https://agupubs.onlinelibrary.wiley.com/doi/pdf/10.1029/2008GL034164. https://agupubs.onlinelibrary.wiley.com/doi/abs/10.1029/2008GL034164.

Candidi, M., Orsini, S., Formisano, V., 1982. The properties of ionospheric O+ ions as observed in the magnetotail boundary layer and northern plasma lobe. J. Geophys. Res.: Space Phys. 87 (A11), 9097–9106. http://dx.doi.org/10.1029/JA087iA11p09097, arXiv:https://agupubs.onlinelibrary.wiley.com/doi/pdf/10.1029/JA087iA11p09097. https://agupubs.onlinelibrary.wiley.com/doi/abs/10.1029/JA087iA11p09097.

Carpenter, D.L., 1962. Electron-density variations in the magnetosphere deduced from whistler data. J. Geophys. Res. 67 (9), 3345–3360. http://dx.doi.org/10.1029/JZ067i009p03345, arXiv:https://agupubs.onlinelibrary.wiley.com/doi/pdf/10.1029/JZ067i009p03345. https://agupubs.onlinelibrary.wiley.com/doi/abs/10.1029/JZ067i009p03345.

Carpenter, D.L., 1968. Ducted whistler-mode propagation in the magnetosphere; A half-gyrofrequency upper intensity cutoff and some associated wave growth phenomena. J. Geophys. Res. 73 (9), 2919–2928. http://dx.doi.org/10.1029/JA073i009p02919, arXiv:https://agupubs.onlinelibrary.wiley.com/doi/pdf/10.1029/JA073i009p02919. https://agupubs.onlinelibrary.wiley.com/doi/abs/10.1029/JA073i009p02919.

Cassak, P.A., Shay, M.A., 2007. Scaling of asymmetric magnetic reconnection: General theory and collisional simulations. Phys. Plasmas 14 (10), 102114. http://dx.doi.org/10.1063/1.2795630, https://doi.org/10.1063/1.2795630.

Chan, K.-W., Holzer, R.E., 1976. ELF hiss associated with plasma density enhancements in the outer magnetosphere. J. Geophys. Res. 81 (13), 2267–2274. http://dx.doi.org/10.1029/JA081i013p02267, arXiv:https://agupubs.onlinelibrary.wiley.com/doi/pdf/10.1029/JA081i013p02267. https://agupubs.onlinelibrary.wiley.com/doi/abs/10.1029/JA081i013p02267.

Chan, K.-W., Holzer, R.E., Smith, E.J., 1974. A relation between ELF hiss amplitude and plasma density in the outer plasmasphere. J. Geophys. Res. 79 (13), 1989–1993. http://dx.doi.org/10.1029/JA079i013p01989, arXiv:https://agupubs.onlinelibrary.wiley.com/doi/pdf/10.1029/JA079i013p01989. https://agupubs.onlinelibrary.wiley.com/doi/abs/10.1029/JA079i013p01989.

Chandler, M.O., Waite Jr., J.H., Moore, T.E., 1991. Observations of polar ion outflows. J. Geophys. Res.: Space Phys. 96 (A2), 1421–1428. http://dx.doi.org/10.1029/90JA02180, arXiv:https://agupubs.onlinelibrary.wiley.com/doi/pdf/10.1029/90JA02180. https://agupubs.onlinelibrary.wiley.com/doi/abs/10.1029/90JA02180.

Chappell, C.R., 1974. Detached plasma regions in the magnetosphere. J. Geophys. Res. 79 (13), 1861–1870. http://dx.doi.org/10.1029/JA079i013p01861, arXiv:https://agupubs.onlinelibrary.wiley.com/doi/pdf/10.1029/JA079i013p01861. https://agupubs.onlinelibrary.wiley.com/doi/abs/10.1029/JA079i013p01861.

Chappell, R.C., 1982a. Initial observations of thermal plasma composition and energetics from Dynamics Explorer-1. Geophys. Res. Lett. 9 (9), 929–932. http://dx.doi.org/10.1029/GL009i009p00929, arXiv:https://agupubs.onlinelibrary.wiley.com/doi/pdf/10.1029/GL009i009p00929. URL: https://agupubs.onlinelibrary.wiley.com/doi/abs/10.1029/GL009i009p00929.

Chappell, C.R., Fields, S.A., Baugher, C.R., Hoffman, J.H., Hanson, W.B., Wright, W.W., Hammack, H.D., Carignan, G.R., Nagy, A.F., 1981. The Retarding Ion Mass Spectrometer on Dynamics Explorer-A. Space Sci. Instrum. 5, 477–491.

Chappell, C.R., Harris, K.K., Sharp, G.W., 1970. The morphology of the bulge region of the plasmasphere. J. Geophys. Res. 75 (19), 3848–3861. http://dx.doi.org/10.1029/JA075i019p03848, arXiv:https://agupubs.onlinelibrary.wiley.com/doi/pdf/10.1029/JA075i019p03848. URL: https://agupubs.onlinelibrary.wiley.com/doi/abs/10.1029/JA075i019p03848.

Chappell, C.R., Huddleston, M.M., Moore, T.E., Giles, B.L., Delcourt, D.C., 2008. Observations of the warm plasma cloak and an explanation of its formation in the magnetosphere. J. Geophys. Res.: Space Phys. 113 (A9), A09206. http://dx.doi.org/10.1029/2007JA012945, arXiv:https://agupubs.onlinelibrary.wiley.com/doi/pdf/10.1029/2007JA012945. URL: https://agupubs.onlinelibrary.wiley.com/doi/abs/10.1029/2007JA012945.

Chappell, C.R., Moore, T.E., Waite Jr., J.H., 1987. The ionosphere as a fully adequate source of plasma for the Earth's magnetosphere. J. Geophys. Res.: Space Phys. 92 (A6), 5896–5910. http://dx.doi.org/10.1029/JA092iA06p05896, arXiv:https://agupubs.onlinelibrary.wiley.com/doi/pdf/10.1029/JA092iA06p05896. URL: https://agupubs.onlinelibrary.wiley.com/doi/abs/10.1029/JA092iA06p05896.

Chappell, C., Olsen, R.C., Green, J.L., Johnson, J.F.E., Jr., J.H.W., 1982b. The discovery of nitrogen ions in the Earth's magnetosphere. Geophys. Res. Lett. 9 (9), 937–940. http://dx.doi.org/10.1029/GL009i009p00937, arXiv:https://agupubs.onlinelibrary.wiley.com/doi/pdf/10.1029/GL009i009p00937. URL: https://agupubs.onlinelibrary.wiley.com/doi/abs/10.1029/GL009i009p00937.

Chaston, C.C., Bonnell, J.W., Carlson, C.W., McFadden, J.P., Ergun, R.E., Strangeway, R.J., Lund, E.J., 2004. Auroral ion acceleration in dispersive Alfvén waves. J. Geophys. Res.: Space Phys. 109 (A4), A04205. http://dx.doi.org/10.1029/2003JA010053, arXiv:https://agupubs.onlinelibrary.wiley.com/doi/pdf/10.1029/2003JA010053. URL: https://agupubs.onlinelibrary.wiley.com/doi/abs/10.1029/2003JA010053.

Chaston, C.C., Wilber, M., Mozer, F.S., Fujimoto, M., Goldstein, M.L., Acuna, M., Reme, H., Fazakerley, A., 2007. Mode Conversion and Anomalous Transport in Kelvin-Helmholtz Vortices and Kinetic Alfvén Waves at the Earth's Magnetopause. Phys. Rev. Lett. 99 (17), 175004. http://dx.doi.org/10.1103/PhysRevLett.99.175004.

Chen, L., Bortnik, J., Li, W., Thorne, R.M., Horne, R.B., 2012. Modeling the properties of plasmaspheric hiss: 2. Dependence on the plasma density distribution. J. Geophys. Res.: Space Phys. 117 (A5), A05202. http://dx.doi.org/10.1029/2011JA017202, arXiv:https://agupubs.onlinelibrary.wiley.com/doi/pdf/10.1029/2011JA017202. URL: https://agupubs.onlinelibrary.wiley.com/doi/abs/10.1029/2011JA017202.

Chen, L., Thorne, R.M., Bortnik, J., 2011. The controlling effect of ion temperature on EMIC wave excitation and scattering. Geophys. Res. Lett. 38 (16), L16109. http://dx.doi.org/10.1029/2011GL048653, arXiv:https://agupubs.onlinelibrary.wiley.com/doi/pdf/10.1029/2011GL048653. URL: https://agupubs.onlinelibrary.wiley.com/doi/abs/10.1029/2011GL048653.

Chen, L., Thorne, R.M., Horne, R.B., 2009. Simulation of EMIC wave excitation in a model magnetosphere including structured high-density plumes. J. Geophys. Res.: Space Phys. 114 (A7), A07221. http://dx.doi.org/10.1029/2009JA014204, arXiv:https://agupubs.onlinelibrary.wiley.com/doi/pdf/10.1029/2009JA014204. URL: https://agupubs.onlinelibrary.wiley.com/doi/abs/10.1029/2009JA014204.

Chen, L., Thorne, R.M., Li, W., Bortnik, J., 2013. Modeling the wave normal distribution of chorus waves. J. Geophys. Res.: Space Phys. 118 (3), 1074–1088. http://dx.doi.org/10.1029/2012JA018343, arXiv:https://agupubs.onlinelibrary.wiley.com/doi/pdf/10.1029/2012JA018343. URL: https://agupubs.onlinelibrary.wiley.com/doi/abs/10.1029/2012JA018343.

Choi, H., Lee, J., Cho, K., Kwak, Y., Cho, I., Park, Y., Kim, Y., Baker, D., Reeves, G., Lee, D., 2011. Analysis of GEO spacecraft anomalies: Space weather relationships. Space Weather 9, S06001.

Cladis, J.B., 1986. Parallel acceleration and transport of ions from polar ionosphere to plasma sheet. Geophys. Res. Lett. 13 (9), 893–896. http://dx.doi.org/10.1029/GL013i009p00893, arXiv:https://agupubs.onlinelibrary.wiley.com/doi/pdf/10.1029/GL013i009p00893. URL: https://agupubs.onlinelibrary.wiley.com/doi/abs/10.1029/GL013i009p00893.

Claudepierre, S.G., Elkington, S.R., Wiltberger, M., 2008. Solar wind driving of magnetospheric ULF waves: Pulsations driven by velocity shear at the magnetopause. J. Geophys. Res.: Space Phys. 113 (A5), A05218. http://dx.doi.org/10.1029/2007JA012890, arXiv:https://agupubs.onlinelibrary.wiley.com/doi/pdf/10.1029/2007JA012890, URL: https://agupubs.onlinelibrary.wiley.com/doi/abs/10.1029/2007JA012890.

Claudepierre, S.G., Toffoletto, F.R., Wiltberger, M., 2016. Global MHD modeling of resonant ULF waves: Simulations with and without a plasmasphere. J. Geophys. Res.: Space Phys. 121 (1), 227–244. http://dx.doi.org/10.1002/2015JA022048, arXiv:https://agupubs.onlinelibrary.wiley.com/doi/pdf/10.1002/2015JA022048. URL: https://agupubs.onlinelibrary.wiley.com/doi/abs/10.1002/2015JA022048.

Clilverd, M.A., Rodger, C.J., Thomson, N.R., Brundell, J.B., Ulich, T., Lichtenberger, J., Cobbett, N., Collier, A.B., Menk, F.W., Seppälä, A., Verronen, P.T., Turunen, E., 2009. Remote sensing space weather events: Antarctic-Arctic Radiation-belt (Dynamic) Deposition-VLF Atmospheric Research Konsortium network. Space Weather 7 (4), S04001. http://dx.doi.org/10.1029/2008SW000412, arXiv:https://agupubs.onlinelibrary.wiley.com/doi/pdf/10.1029/2008SW000412. URL: https://agupubs.onlinelibrary.wiley.com/doi/abs/10.1029/2008SW000412.

Coates, A., Johnstone, A., Sojka, J., Wrenn, G., 1985. Ionospheric photoelectrons observed in the magnetosphere at distances up to 7 earth radii. Planet. Space Sci. 33 (11), 1267–1275. http://dx.doi.org/10.1016/0032-0633(85)90005-4, http://www.sciencedirect.com/science/article/pii/0032063385900054.

Cohen, I.J., Widholm, M., Lessard, M.R., Riley, P., Heavisides, J., Moen, J.I., Clausen, L.B.N., Bekkeng, T.A., 2016. Rocket-borne measurements of electron temperature and density with the Electron Retarding Potential Analyzer instrument. J. Geophys. Res.: Space Phys. 121 (7), 6774–6782. http://dx.doi.org/10.1002/2016JA022562, arXiv:https://agupubs.onlinelibrary.wiley.com/doi/pdf/10.1002/2016JA022562. URL: https://agupubs.onlinelibrary.wiley.com/doi/abs/10.1002/2016JA022562.

Cole, K., 1971. Formation of field-aligned irregularities in the magnetosphere. J. Atmos. Terrest. Phys. 33 (5), 741–750. http://dx.doi.org/10.1016/0021-9169(71)90027-4, http://www.sciencedirect.com/science/article/pii/0021916971900274.

Colpitts, C., Miyoshi, Y., Kasahara, Y., Delzanno, G.L., Wygant, J.R., Cattell, C.A., Breneman, A., Kletzing, C., Cunningham, G., Hikishima, M., Matsuda, S., Katoh, Y., Ripoll, J.-F., Shinohara, I., Matsuoka, A., 2020. First Direct Observations of Propagation of Discrete Chorus Elements From the Equatorial Source to Higher Latitudes, Using the Van Allen Probes and Arase Satellites. J. Geophys. Res.: Space Phys. 125 (10), e2020JA028315. http://dx.doi.org/10.1029/2020JA028315, arXiv:https://agupubs.onlinelibrary.wiley.com/doi/pdf/10.1029/2020JA028315. URL: https://agupubs.onlinelibrary.wiley.com/doi/abs/10.1029/2020JA028315. e2020JA028315 2020JA028315.

Comfort, R.H., Moore, T.E., Craven, P.D., Pollock, C.J., Mozer, F.S., Williamson, W.S., 1998. Spacecraft Potential Control by the Plasma Source Instrument on the POLAR Satellite. J. Spacecr. Rockets 35 (6), 845–849. http://dx.doi.org/10.2514/2.7586, URL: arXiv:https://doi.org/10.2514/2.7586.

Cornwall, J.M., 1965. Cyclotron instabilities and electromagnetic emission in the ultra low frequency and very low frequency ranges. J. Geophys. Res. 70 (1), 61–69. http://dx.doi.org/10.1029/JZ070i001p00061, arXiv:https://agupubs.onlinelibrary.wiley.com/doi/pdf/10.1029/JZ070i001p00061. URL: https://agupubs.onlinelibrary.wiley.com/doi/abs/10.1029/JZ070i001p00061.

Cornwall, J.M., Coroniti, F.V., Thorne, R.M., 1971. Unified theory of SAR arc formation at the plasmapause. J. Geophys. Res. 76 (19), 4428–4445. http://dx.doi.org/10.1029/JA076i019p04428, arXiv:https://agupubs.onlinelibrary.wiley.com/doi/pdf/10.1029/JA076i019p04428. URL: https://agupubs.onlinelibrary.wiley.com/doi/abs/10.1029/JA076i019p04428.

Cowee, M.M., Winske, D., Gary, S.P., 2010. Hybrid simulations of plasma transport by Kelvin-Helmholtz instability at the magnetopause: Density variations and magnetic shear. J. Geophys. Res.: Space Phys. 115 (A6), A06214. http://dx.doi.org/10.1029/2009JA015011, arXiv:https://agupubs.onlinelibrary.wiley.com/doi/pdf/10.1029/2009JA015011. URL: https://agupubs.onlinelibrary.wiley.com/doi/abs/10.1029/2009JA015011.

Crabtree, C., Rudakov, L., Ganguli, G., Mithaiwala, M., 2012. Collisionless and collisional dissipation of magnetospherically reflecting whistler waves. Geophys. Res. Lett. 39 (16), L16103. http://dx.doi.org/10.1029/2012GL052921, arXiv:https://agupubs.onlinelibrary.wiley.com/doi/pdf/10.1029/2012GL052921. URL: https://agupubs.onlinelibrary.wiley.com/doi/abs/10.1029/2012GL052921.

Craven, P.D., Olsen, R.C., Chappell, C.R., Kakani, L., 1985. Observations of molecular ions in the Earth's magnetosphere. J. Geophys. Res.: Space Phys. 90 (A8), 7599–7605. http://dx.doi.org/10.1029/JA090iA08p07599, arXiv:https://agupubs.onlinelibrary.wiley.com/doi/pdf/10.1029/JA090iA08p07599. URL: https://agupubs.onlinelibrary.wiley.com/doi/abs/10.1029/JA090iA08p07599.

Cresswell, G., 1972. The morphology of displays of pulsating auroras. J. Atmos. Terrest. Phys. 34 (3), 549–554. http://dx.doi.org/10.1016/0021-9169(72)90058-X, http://www.sciencedirect.com/science/article/pii/002191697290058X.

Cully, C.M., Donovan, E.F., Yau, A.W., Arkos, G.G., 2003a. Akebono/Suprathermal Mass Spectrometer observations of low-energy ion outflow: Dependence on magnetic activity and solar wind conditions. J. Geophys. Res.: Space Phys. 108 (A2), 1093. http://dx.doi.org/10.1029/2001JA009200, arXiv:https://agupubs.onlinelibrary.wiley.com/doi/pdf/10.1029/2001JA009200. URL: https://agupubs.onlinelibrary.wiley.com/doi/abs/10.1029/2001JA009200.

Cully, C.M., Donovan, E.F., Yau, A.W., Opgenoorth, H.J., 2003b. Supply of thermal ionospheric ions to the central plasma sheet. J. Geophys. Res.: Space Phys. 108 (A2), 1092. http://dx.doi.org/10.1029/2002JA009457, https://agupubs.onlinelibrary.wiley.com/doi/pdf/10.1029/2002JA009457. URL: https://agupubs.onlinelibrary.wiley.com/doi/abs/10.1029/2002JA009457.

Cuperman, S., Landau, R.W., 1974. On the enhancement of the whistler mode instability in the magnetosphere by cold plasma injection. J. Geophys. Res. 79 (1), 128–134. http://dx.doi.org/10.1029/JA079i001p00128, arXiv:https://agupubs.onlinelibrary.wiley.com/doi/pdf/10.1029/JA079i001p00128. URL: https://agupubs.onlinelibrary.wiley.com/doi/abs/10.1029/JA079i001p00128.

Cuperman, S., Salu, Y., Bernstein, W., Williams, D.J., 1973. A computer simulation of cold plasma effects on the whistler instability for geostationary orbit plasma parameters. J. Geophys. Res. 78 (31), 7372–7387. http://dx.doi.org/10.1029/JA078i031p07372, arXiv:https://agupubs.onlinelibrary.wiley.com/doi/pdf/10.1029/JA078i031p07372. URL: https://agupubs.onlinelibrary.wiley.com/doi/abs/10.1029/JA078i031p07372.

Daglis, I.A., Thorne, R.M., Baumjohann, W., Orsini, S., 1999. The terrestrial ring current: Origin, formation, and decay. Rev. Geophys. 37 (4), 407–438. http://dx.doi.org/10.1029/1999RG900009.

Dandouras, I., Pierrard, V., Goldstein, J., Vallat, C., Parks, G.K., Rème, H., Gouillart, C., Sevestre, F., Mccarthy, M., Kistler, L.M., Klecker, B., Korth, A., Bavassano-Cattaneo, M.B., Escoubet, P., Masson, A., 2013. Multipoint Observations of Ionic Structures in the Plasmasphere by CLUSTER-CIS and Comparisons with IMAGE-EUV Observations and with Model Simulations. In: Inner Magnetosphere Interactions: New Perspectives from Imaging. American Geophysical Union (AGU), pp. 23–53. http://dx.doi.org/10.1029/159GM03, arXiv:https://agupubs.onlinelibrary.wiley.com/doi/pdf/10.1029/159GM03. URL: https://agupubs.onlinelibrary.wiley.com/doi/abs/10.1029/159GM03.

Dargent, J., Aunai, N., Lavraud, B., Toledo-Redondo, S., Califano, F., 2020. Simulation of Plasmaspheric Plume Impact on Dayside Magnetic Reconnection. Geophys. Res. Lett. 47 (4), e2019GL086546. http://dx.doi.org/10.1029/2019GL086546, arXiv:https://agupubs.onlinelibrary.wiley.com/doi/pdf/10.1029/2019GL086546. URL: https://agupubs.onlinelibrary.wiley.com/doi/abs/10.1029/2019GL086546 e2019GL086546 10.1029/2019GL086546.

Dargent, J., Aunai, N., Lavraud, B., Toledo-Redondo, S., Shay, M.A., Cassak, P.A., Malakit, K., 2017. Kinetic simulation of asymmetric magnetic reconnection with cold ions. J. Geophys. Res.: Space Phys. 122 (5), 5290–5306. http://dx.doi.org/10.1002/2016JA023831, arXiv:https://agupubs.onlinelibrary.wiley.com/doi/pdf/10.1002/2016JA023831. URL: https://agupubs.onlinelibrary.wiley.com/doi/abs/10.1002/2016JA023831.

Darrouzet, F., Décréau, P.M.E., De Keyser, J., Masson, A., Gallagher, D.L., Santolík, O., Sandel, B.R., Trotignon, J.G., Rauch, J.L., Le Guirriec, E., Canu, P., Sedgemore, F., André, M., Lemaire, J.F., 2004. Density structures inside the plasmasphere: Cluster observations. Ann. Geophys. 22 (7), 2577–2585. http://dx.doi.org/10.5194/angeo-22-2577-2004, https://www.ann-geophys.net/22/2577/2004/.

Darrouzet, F., Gallagher, D.L., André, N., Carpenter, D.L., Dandouras, I., Décréau, P.M.E., De Keyser, J., Denton, R.E., Foster, J.C., Goldstein, J., Moldwin, M.B., Reinisch, B.W., Sandel, B.R., Tu, J., 2009. Plasmaspheric Density Structures and Dynamics: Properties Observed by the CLUSTER and IMAGE Missions. In: Darrouzet, F., De Keyser, J., Pierrard, V. (Eds.), The Earth's Plasmasphere: A CLUSTER and IMAGE Perspective. Springer New York, New York, NY, pp. 55–106. http://dx.doi.org/10.1007/978-1-4419-1323-4_4.

Davidson, G.T., 1990. Pitch-angle diffusion and the origin of temporal and spatial structures in morningside aurorae. Space Sci. Rev. 53 (1), 45–82. http://dx.doi.org/10.1007/BF00217428.

Décréau, P.M.E., Beghin, C., Parrot, M., 1979. Electron Density and Temperature, as Measured by the Mutual Impedance Experiment on Board GEOS-1. In: Knott, K., Durney, A., Ogilvie, K. (Eds.), Advances in Magnetosperic Physics with GEOS-1 and ISEE. Springer Netherlands, Dordrecht, pp. 261–275. http://dx.doi.org/10.1007/978-94-009-9527-7_18.

Décréau, P.M.E., Béghin, C., Parrot, M., 1982. Global characteristics of the cold plasma in the equatorial plasmapause region as deduced from the Geos 1 Mutual Impedance Probe. J. Geophys. Res.: Space Phys. 87 (A2), 695–712. http://dx.doi.org/10.1029/JA087iA02p00695, arXiv:https://agupubs.onlinelibrary.wiley.com/doi/pdf/10.1029/JA087iA02p00695. URL: https://agupubs.onlinelibrary.wiley.com/doi/abs/10.1029/JA087iA02p00695.

Degeling, A.W., Rankin, R., Elkington, S.R., 2011. Convective and diffusive ULF wave driven radiation belt electron transport. J. Geophys. Res.: Space Phys. 116 (A12), A12217. http://dx.doi.org/10.1029/2011JA016896.

Degeling, A.W., Rankin, R., Murphy, K., Rae, I.J., 2013. Magnetospheric convection and magnetopause shadowing effects in ULF wave-driven energetic electron transport. J. Geophys. Res.: Space Phys. 118 (6), 2919–2927. http://dx.doi.org/10.1002/jgra.50219, arXiv:https://agupubs.onlinelibrary.wiley.com/doi/pdf/10.1002/jgra.50219. URL: https://agupubs.onlinelibrary.wiley.com/doi/abs/10.1002/jgra.50219.

Delcourt, D.C., Moore, T.E., Sauvaud, J.A., Chappell, C.R., 1992. Nonadiabatic transport features in the outer cusp region. J. Geophys. Res.: Space Phys. 97 (A11), 16833–16842. http://dx.doi.org/10.1029/92JA00834, arXiv:https://agupubs.onlinelibrary.wiley.com/doi/pdf/10.1029/92JA00834. URL: https://agupubs.onlinelibrary.wiley.com/doi/abs/10.1029/92JA00834.

Delzanno, G.L., Borovsky, J.E., Thomsen, M.F., Moulton, J.D., 2015. Future beam experiments in the magnetosphere with plasma contactors: The electron collection and ion emission routes. J. Geophys. Res.: Space Phys. 120 (5), 3588–3602. http://dx.doi.org/10.1002/2014JA020683, arXiv:https://agupubs.onlinelibrary.wiley.com/doi/pdf/10.1002/2014JA020683. URL: https://agupubs.onlinelibrary.wiley.com/doi/abs/10.1002/2014JA020683.

Demekhov, A.G., Trakhtengerts, V.Y., 1994. A mechanism of formation of pulsating aurorae. J. Geophys. Res.: Space Phys. 99 (A4), 5831–5842. http://dx.doi.org/10.1029/93JA01804.

Denton, R.E., Takahashi, K., Thomsen, M.F., Borovsky, J.E., Singer, H.J., Wang, Y., Goldstein, J., Brandt, P.C., Reinisch, B.W., 2014. Evolution of mass density and O+ concentration at geostationary orbit during storm and quiet events. J. Geophys. Res.: Space Phys. 119 (8), 6417–6431. http://dx.doi.org/10.1002/2014JA019888, arXiv:https://agupubs.onlinelibrary.wiley.com/doi/pdf/10.1002/2014JA019888. URL: https://agupubs.onlinelibrary.wiley.com/doi/abs/10.1002/2014JA019888.

Denton, R.E., Thomsen, M.F., Takahashi, K., Anderson, R.R., Singer, H.J., 2011. Solar cycle dependence of bulk ion composition at geosynchronous orbit. J. Geophys. Res.: Space Phys. 116 (A3), A03212. http://dx.doi.org/10.1029/2010JA016027, arXiv:https://agupubs.onlinelibrary.wiley.com/doi/pdf/10.1029/2010JA016027. URL: https://agupubs.onlinelibrary.wiley.com/doi/abs/10.1029/2010JA016027.

Diego, P., Coco, I., Bertello, I., Candidi, M., Ubertini, P., 2019. Ionospheric Plasma Density Measurements by Swarm Langmuir Probes: Limitations and possible Corrections. Annal. Geophys. Discuss. 1–15.

Dimmock, A.P., Nykyri, K., 2013. The statistical mapping of magnetosheath plasma properties based on THEMIS measurements in the magnetosheath interplanetary medium reference frame. J. Geophys. Res.: Space Phys. 118 (8), 4963–4976. http://dx.doi.org/10.1002/jgra.50465, arXiv:https://agupubs.onlinelibrary.wiley.com/doi/pdf/10.1002/jgra.50465. URL: https://agupubs.onlinelibrary.wiley.com/doi/abs/10.1002/jgra.50465.

Dunckel, N., Helliwell, R.A., 1969. Whistler-mode emissions on the OGO 1 satellite. J. Geophys. Res. 74 (26), 6371–6385. http://dx.doi.org/10.1029/JA074i026p06371, arXiv:https://agupubs.onlinelibrary.wiley.com/doi/pdf/10.1029/JA074i026p06371. URL: https://agupubs.onlinelibrary.wiley.com/doi/abs/10.1029/JA074i026p06371.

Dungey, J.W., 1961. The steady state of the Chapman-Ferraro problem in two dimensions. J. Geophys. Res. 66 (4), 1043–1047. http://dx.doi.org/10.1029/JZ066i004p01043, arXiv:https://agupubs.onlinelibrary.wiley.com/doi/pdf/10.1029/JZ066i004p01043. URL: https://agupubs.onlinelibrary.wiley.com/doi/abs/10.1029/JZ066i004p01043.

Eastwood, J.P., Schwartz, S.J., Horbury, T.S., Carr, C.M., Glassmeier, K.-H., Richter, I., Koenders, C., Plaschke, F., Wild, J.A., 2011. Transient Pc3 wave activity generated by a hot flow anomaly: Cluster, Rosetta, and ground-based observations. J. Geophys. Res.: Space Phys. 116 (A8), A08224. http://dx.doi.org/10.1029/2011JA016467, arXiv:https://agupubs.onlinelibrary.wiley.com/doi/pdf/10.1029/2011JA016467. URL: https://agupubs.onlinelibrary.wiley.com/doi/abs/10.1029/2011JA016467.

Ebihara, Y., Tanaka, Y.-M., Takasaki, S., Weatherwax, A.T., Taguchi, M., 2007. Quasi-stationary auroral patches observed at the South Pole Station. J. Geophys. Res.: Space Phys. 112 (A1), A01201. http://dx.doi.org/10.1029/2006JA012087, arXiv:https://agupubs.onlinelibrary.wiley.com/doi/pdf/10.1029/2006JA012087. URL: https://agupubs.onlinelibrary.wiley.com/doi/abs/10.1029/2006JA012087.

Elkington, S.R., Hudson, M.K., Chan, A.A., 1999. Acceleration of relativistic electrons via drift-resonant interaction with toroidal-mode Pc-5 ULF oscillations. Geophys. Res. Lett. 26 (21), 3273–3276. http://dx.doi.org/10.1029/1999GL003659, arXiv:https://agupubs.onlinelibrary.wiley.com/doi/pdf/10.1029/1999GL003659. URL: https://agupubs.onlinelibrary.wiley.com/doi/abs/10.1029/1999GL003659.

Elkington, S.R., Hudson, M.K., Chan, A.A., 2003. Resonant acceleration and diffusion of outer zone electrons in an asymmetric geomagnetic field. J. Geophys. Res.: Space Phys. 108 (A3), 1116. http://dx.doi.org/10.1029/2001JA009202, arXiv:https://agupubs.onlinelibrary.wiley.com/doi/pdf/10.1029/2001JA009202. URL: https://agupubs.onlinelibrary.wiley.com/doi/abs/10.1029/2001JA009202.

Elphic, R.C., Thomsen, M.F., Borovsky, J.E., McComas, D.J., 1999. Inner edge of the electron plasma sheet: Empirical models of boundary location. J. Geophys. Res.: Space Phys. 104 (A10), 22679–22693. http://dx.doi.org/10.1029/1999JA900213, arXiv:https://agupubs.onlinelibrary.wiley.com/doi/pdf/10.1029/1999JA900213. URL: https://agupubs.onlinelibrary.wiley.com/doi/abs/10.1029/1999JA900213.

Engwall, E., Eriksson, A.I., André, M., Dandouras, I., Paschmann, G., Quinn, J., Torkar, K., 2006. Low-energy (order 10 eV) ion flow in the magneto-tail lobes inferred from spacecraft wake observations. Geophys. Res. Lett. 33 (6), L06110. http://dx.doi.org/10.1029/2005GL025179, arXiv:https://agupubs.onlinelibrary.wiley.com/doi/pdf/10.1029/2005GL025179. URL: https://agupubs.onlinelibrary.wiley.com/doi/abs/10.1029/2005GL025179.

Engwall, E., Eriksson, A.I., Cully, C.M., André, M., Puhl-Quinn, P.A., Vaith, H., Torbert, R., 2009b. Survey of cold ionospheric outflows in the magnetotail. Ann. Geophys. 27 (8), 3185–3201. http://dx.doi.org/10.5194/angeo-27-3185-2009, https://angeo.copernicus.org/articles/27/3185/2009/.

Engwall, E., Eriksson, A.I., Cully, C.M., André, M., Torbert, R., Vaith, H., 2009a. Earth's ionospheric outflow dominated by hidden cold plasma. Nat. Geosci. 2 (1), 24–27. http://dx.doi.org/10.1038/ngeo387.

Eriksson, P., Walker, A., Stephenson, J., 2006. A statistical correlation of Pc5 pulsations and solar wind pressure oscillations. Adv. Space Res. 38 (8), 1763–1771. http://dx.doi.org/10.1016/j.asr.2005.08.023, http://www.sciencedirect.com/science/article/pii/S0273117705010550. Magnetospheric dynamics and the international living with a star program.

Fairfield, D.H., Vinãs, A.F., 1984. The inner edge of the plasma sheet and the diffuse aurora. J. Geophys. Res.: Space Phys. 89 (A2), 841–854. http://dx.doi.org/10.1029/JA089iA02p00841, arXiv:https://agupubs.onlinelibrary.wiley.com/doi/pdf/10.1029/JA089iA02p00841. URL: https://agupubs.onlinelibrary.wiley.com/doi/abs/10.1029/JA089iA02p00841.

Fälthammar, C.-G., 1965. Effects of time-dependent electric fields on geomagnetically trapped radiation. J. Geophys. Res. 70 (11), 2503–2516. http://dx.doi.org/10.1029/JZ070i011p02503, arXiv:https://agupubs.onlinelibrary.wiley.com/doi/pdf/10.1029/JZ070i011p02503. URL: https://agupubs.onlinelibrary.wiley.com/doi/abs/10.1029/JZ070i011p02503.

Farrugia, C., Gratton, F.T., Contin, J., Cocheci, C.C., Arnoldy, R.L., Ogilvie, K.W., Lepping, R.P., Zastenker, G.N., Nozdrachev, M.N., Fedorov, A., Sauvaud, J.-A., Steinberg, J.T., Rostoker, G., 2000. Coordinated Wind, Interball/tail, and ground observations of Kelvin-Helmholtz waves at the near-tail, equatorial magnetopause at dusk: January 11, 1997. J. Geophys. Res.: Space Phys. 105 (A4), 7639–7667. http://dx.doi.org/10.1029/1999JA000267, arXiv:https://agupubs.onlinelibrary.wiley.com/doi/pdf/10.1029/1999JA000267. URL: https://agupubs.onlinelibrary.wiley.com/doi/abs/10.1029/1999JA000267.

Feldstein, Y.I., Galperin, Y.I., 1985. The auroral luminosity structure in the high-latitude upper atmosphere: Its dynamics and relationship to the large-scale structure of the Earth's magnetosphere. Rev. Geophys. 23 (3), 217–275. http://dx.doi.org/10.1029/RG023i003p00217, arXiv:https://agupubs.onlinelibrary.wiley.com/doi/pdf/10.1029/RG023i003p00217. URL: https://agupubs.onlinelibrary.wiley.com/doi/abs/10.1029/RG023i003p00217.

Ferguson, D., Worden, S., Hastings, D., 2015. The Space Weather Threat to Situational Awareness, Communications, and Positioning Systems. IEEE Trans. Plasma Sci. 43, 3086–3098.

Fernandes, P.A., Lynch, K.A., 2016. Electrostatic analyzer measurements of ionospheric thermal ion populations. J. Geophys. Res.: Space Phys. 121 (7), 7316–7325. http://dx.doi.org/10.1002/2016JA022582, arXiv:https://agupubs.onlinelibrary.wiley.com/doi/pdf/10.1002/2016JA022582. URL: https://agupubs.onlinelibrary.wiley.com/doi/abs/10.1002/2016JA022582.

Fields, S.A., Baugher, C.R., Chappell, C.R., Reasoner, D.L., Hammack, H.D., Wright, W.W., Hoffman, J.H., 1982. Instrument manual for the retarding ion mass spectrometer on Dynamics Explorer-1. NASA STI/Recon Technical Report N 30527.

Fitzpatrick, R., 2014. Plasma Physics: An Introduction. Taylor & Francis, https://books.google.com/books?id=0RwbBAAAQBAJ.

Foster, J.C., Burke, W.J., 2002. SAPS: A new categorization for sub-auroral electric fields. EOS Trans. Am. Geophys. Union 83 (36), 393–394. http://dx.doi.org/10.1029/2002EO000289, arXiv:https://agupubs.onlinelibrary.wiley.com/doi/pdf/10.1029/2002EO000289. URL: https://agupubs.onlinelibrary.wiley.com/doi/abs/10.1029/2002EO000289.

Fraser, B.J., Horwitz, J.L., Slavin, J.A., Dent, Z.C., Mann, I.R., 2005. Heavy ion mass loading of the geomagnetic field near the plasmapause and ULF wave implications. Geophys. Res. Lett. 32 (4), L04102. http://dx.doi.org/10.1029/2004GL021315, arXiv:https://agupubs.onlinelibrary.wiley.com/doi/pdf/10.1029/2004GL021315. URL: https://agupubs.onlinelibrary.wiley.com/doi/abs/10.1029/2004GL021315.

Fraser, B.J., Loto'aniu, T.M., Singer, H.J., 2013. Electromagnetic Ion Cyclotron Waves in the Magnetosphere. In: Magnetospheric ULF Waves: Synthesis and New Directions. American Geophysical Union (AGU), pp. 195–212. http://dx.doi.org/10.1029/169GM13, arXiv:https://agupubs.onlinelibrary.wiley.com/doi/pdf/10.1029/169GM13. URL: https://agupubs.onlinelibrary.wiley.com/doi/abs/10.1029/169GM13.

Fraser, B.J., Samson, J.C., Hu, Y.D., McPherron, R.L., Russell, C.T., 1992. Electromagnetic ion cyclotron waves observed near the oxygen cyclotron frequency by ISEE 1 and 2. J. Geophys. Res.: Space Phys. 97 (A3), 3063–3074. http://dx.doi.org/10.1029/91JA02447, arXiv:https://agupubs.onlinelibrary.wiley.com/doi/pdf/10.1029/91JA02447. URL: https://agupubs.onlinelibrary.wiley.com/doi/abs/10.1029/91JA02447.

Frey, H.U., 2004. Substorm onset observations by IMAGE-FUV. J. Geophys. Res. 109 (A10), A10304. http://dx.doi.org/10.1029/2004JA010607, http://doi.wiley.com/10.1029/2004JA010607.

Frey, H.U., Han, D., Kataoka, R., Lessard, M.R., Milan, S.E., Nishimura, Y., Strangeway, R.J., Zou, Y., 2019. Dayside Aurora. Space Sci. Rev. 215 (8), 51, https://doi.org/10.1007/s11214-019-0617-7.

Fried, B.D., Conte, S.D., 1961. The Plasma Dispersion Function. Academic Press, London-New York.

Fujimoto, M., Terasawa, T., Mukai, T., Saito, Y., Yamamoto, T., Kokubun, S., 1998. Plasma entry from the flanks of the near-Earth magnetotail: Geotail observations. J. Geophys. Res.: Space Phys. 103 (A3), 4391–4408. http://dx.doi.org/10.1029/97JA03340, arXiv:https://agupubs.onlinelibrary.wiley.com/doi/pdf/10.1029/97JA03340. URL: https://agupubs.onlinelibrary.wiley.com/doi/abs/10.1029/97JA03340.

Fukizawa, M., Sakanoi, T., Miyoshi, Y., Hosokawa, K., Shiokawa, K., Katoh, Y., Kazama, Y., Kumamoto, A., Tsuchiya, F., Miyashita, Y., Tanaka, Y.M., Kasahara, Y., Ozaki, M., Matsuoka, A., Matsuda, S., Hikishima, M., Oyama, S., Ogawa, Y., Kurita, S., Fujii, R., 2018. Electrostatic Electron Cyclotron Harmonic Waves as a Candidate to Cause Pulsating Auroras. Geophys. Res. Lett. 45 (23), 12,661–12,668. http://dx.doi.org/10.1029/2018GL080145, arXiv:https://agupubs.onlinelibrary.wiley.com/doi/pdf/10.1029/2018GL080145. URL: https://agupubs.onlinelibrary.wiley.com/doi/abs/10.1029/2018GL080145.

Fuselier, S.A., Burch, J.L., Mukherjee, J., Genestreti, K.J., Vines, S.K., Gomez, R., Goldstein, J., Trattner, K.J., Petrinec, S.M., Lavraud, B., Strangeway, R.J., 2017. Magnetospheric ion influence at the dayside magnetopause. J. Geophys. Res.: Space Phys. 122 (8), 8617–8631. http://dx.doi.org/10.1002/2017JA024515, arXiv:https://agupubs.onlinelibrary.wiley.com/doi/pdf/10.1002/2017JA024515. URL: https://agupubs.onlinelibrary.wiley.com/doi/abs/10.1002/2017JA024515.

Fuselier, S.A., Lewis, W.S., 2011. Properties of Near-Earth Magnetic Reconnection from In-Situ Observations. Space Sci. Rev. 160 (1), 95, https://doi.org/10.1007/s11214-011-9820-x.

Fuselier, S.A., Mukherjee, J., Denton, M.H., Petrinec, S.M., Trattner, K.J., Toledo-Redondo, S., André, M., Aunai, N., Chappell, C.R., Glocer, A., Haaland, S., Hesse, M., Kistler, L.M., Lavraud, B., Li, W.Y., Moore, T.E., Graham, D., Tenfjord, P., Dargent, J., Vines, S.K., Strangeway, R.J., Burch, J.L., 2019. High-density O+ in Earth's outer magnetosphere and its effect on dayside magnetopause magnetic reconnection. J. Geophys. Res.: Space Phys. 124 (12), 10257–10269. http://dx.doi.org/10.1029/2019JA027396, arXiv:https://agupubs.onlinelibrary.wiley.com/doi/pdf/10.1029/2019JA027396. URL: https://agupubs.onlinelibrary.wiley.com/doi/abs/10.1029/2019JA027396.

Gallagher, D.L., Craven, P.D., Comfort, R.H., Moore, T.E., 1995. On the azimuthal variation of core plasma in the equatorial magnetosphere. J. Geophys. Res.: Space Phys. 100 (A12), 23597–23605. http://dx.doi.org/10.1029/95JA02100, arXiv:https://agupubs.onlinelibrary.wiley.com/doi/pdf/10.1029/95JA02100. URL: https://agupubs.onlinelibrary.wiley.com/doi/abs/10.1029/95JA02100.

Gallardo-Lacourt, B., Liang, J., Nishimura, Y., Donovan, E., 2018. On the Origin of STEVE: Particle Precipitation or Ionospheric Skyglow?. Geophys. Res. Lett. 45 (16), 7968–7973. http://dx.doi.org/10.1029/2018GL078509, arXiv:https://agupubs.onlinelibrary.wiley.com/doi/pdf/10.1029/2018GL078509. URL: https://agupubs.onlinelibrary.wiley.com/doi/abs/10.1029/2018GL078509.

Galperin, Y.I., Feldstein, Y.I., 1996. Mapping of the Precipitation Regions to the Plasma Sheet. J. Geomagn. Geoelectr. 48 (5–6), 857–875. http://dx.doi.org/10.5636/jgg.48.857.

Gary, S.P., 2005. Theory Of Space Plasma Microinstabilities. Cambridge University Press.

Gary, S.P., Lavraud, B., Thomsen, M.F., Lefebvre, B., Schwartz, S.J., 2005. Electron anisotropy constraint in the magnetosheath: Cluster observations. Geophys. Res. Lett. 32 (13), L13109. http://dx.doi.org/10.1029/2005GL023234, arXiv:https://agupubs.onlinelibrary.wiley.com/doi/pdf/10.1029/2005GL023234. URL: https://agupubs.onlinelibrary.wiley.com/doi/abs/10.1029/2005GL023234.

Gary, S.P., Liu, K., Chen, L., 2012a. Alfvén-cyclotron instability with singly ionized helium: Linear theory. J. Geophys. Res.: Space Phys. 117 (A8), A08201. http://dx.doi.org/10.1029/2012JA017740, arXiv:https://agupubs.onlinelibrary.wiley.com/doi/pdf/10.1029/2012JA017740. URL: https://agupubs.onlinelibrary.wiley.com/doi/abs/10.1029/2012JA017740.

Gary, S.P., Liu, K., Denton, R.E., Wu, S., 2012b. Whistler anisotropy instability with a cold electron component: Linear theory. J. Geophys. Res.: Space Phys. 117 (A7), A07203. http://dx.doi.org/10.1029/2012JA017631, arXiv:https://agupubs.onlinelibrary.wiley.com/doi/pdf/10.1029/2012JA017631.

Gary, S.P., Moldwin, M.B., Thomsen, M.F., Winske, D., McComas, D.J., 1994. Hot proton anisotropies and cool proton temperatures in the outer magnetosphere. J. Geophys. Res.: Space Phys. 99 (A12), 23603–23615. http://dx.doi.org/10.1029/94JA02069, arXiv:https://agupubs.onlinelibrary.wiley.com/doi/pdf/10.1029/94JA02069. URL: https://agupubs.onlinelibrary.wiley.com/doi/abs/10.1029/94JA02069.

Genestreti, K.J., Goldstein, J., Corley, G.D., Farner, W., Kistler, L.M., Larsen, B.A., Mouikis, C.G., Ramnarace, C., Skoug, R.M., Turner, N.E., 2017. Temperature of the plasmasphere from Van Allen Probes HOPE. J. Geophys. Res.: Space Phys. 122 (1), 310–323. http://dx.doi.org/10.1002/2016JA023047, arXiv:https://agupubs.onlinelibrary.wiley.com/doi/pdf/10.1002/2016JA023047. URL: https://agupubs.onlinelibrary.wiley.com/doi/abs/10.1002/2016JA023047.

Gershman, D.J., Avanov, L.A., Boardsen, S.A., Dorelli, J.C., Gliese, U., Barrie, A.C., Schiff, C., Paterson, W.R., Torbert, R.B., Giles, B.L., Pollock, C.J., 2017. Spacecraft and Instrument Photoelectrons Measured by the Dual Electron Spectrometers on MMS. J. Geophys. Res.: Space Phys. 122 (11), 11,548–11,558. http://dx.doi.org/10.1002/2017JA024518, arXiv:https://agupubs.onlinelibrary.wiley.com/doi/pdf/10.1002/2017JA024518. URL: https://agupubs.onlinelibrary.wiley.com/doi/abs/10.1002/2017JA024518.

Gillies, D.M., Knudsen, D., Rankin, R., Milan, S., Donovan, E., 2018. A Statistical Survey of the 630.0-nm Optical Signature of Periodic Auroral Arcs Resulting From Magnetospheric Field Line Resonances. Geophys. Res. Lett. 45 (10), 4648–4655. http://dx.doi.org/10.1029/2018GL077491, arXiv:https://agupubs.onlinelibrary.wiley.com/doi/pdf/10.1029/2018GL077491. URL: https://agupubs.onlinelibrary.wiley.com/doi/abs/10.1029/2018GL077491.

Gkioulidou, M., Ohtani, S., Ukhorskiy, A.Y., Mitchell, D.G., Takahashi, K., Spence, H.E., Wygant, J.R., Kletzing, C.A., Barnes, R.J., 2019. Low-Energy (<keV) O+ Ion Outflow Directly Into the Inner Magnetosphere: Van Allen Probes Observations. J. Geophys. Res.: Space Phys. 124 (1), 405–419. http://dx.doi.org/10.1029/2018JA025862, arXiv:https://agupubs.onlinelibrary.wiley.com/doi/pdf/10.1029/2018JA025862. URL: https://agupubs.onlinelibrary.wiley.com/doi/abs/10.1029/2018JA025862.

Glauert, S.A., Horne, R.B., 2005. Calculation of pitch angle and energy diffusion coefficients with the PADIE code. J. Geophys. Res.: Space Phys. 110 (A4), A04206. http://dx.doi.org/10.1029/2004JA010851, arXiv:https://agupubs.onlinelibrary.wiley.com/doi/pdf/10.1029/2004JA010851. URL: https://agupubs.onlinelibrary.wiley.com/doi/abs/10.1029/2004JA010851.

Glocer, A., Khazanov, G., Liemohn, M., 2017. Photoelectrons in the quiet polar wind. J. Geophys. Res.: Space Phys. 122 (6), 6708–6726. http://dx.doi.org/10.1002/2017JA024177, arXiv:https://agupubs.onlinelibrary.wiley.com/doi/pdf/10.1002/2017JA024177. URL: https://agupubs.onlinelibrary.wiley.com/doi/abs/10.1002/2017JA024177.

Glocer, A., Tóth, G., Gombosi, T., Welling, D., 2009. Modeling ionospheric outflows and their impact on the magnetosphere, initial results. J. Geophys. Res.: Space Phys. 114 (A5), A05216. http://dx.doi.org/10.1029/2009JA014053, arXiv:https://agupubs.onlinelibrary.wiley.com/doi/pdf/10.1029/2009JA014053. URL: https://agupubs.onlinelibrary.wiley.com/doi/abs/10.1029/2009JA014053.

Goldstein, J., 2007. Plasmasphere Response: Tutorial and Review of Recent Imaging Results. In: Baker, D.N., Klecker, B., Schwartz, S.J., Schwenn, R., Von Steiger, R. (Eds.), Solar Dynamics and Its Effects on the Heliosphere and Earth. Springer New York, New York, NY, pp. 203–216. http://dx.doi.org/10.1007/978-0-387-69532-7_14.

Goldstein, J., Sandel, B.R., 2013. The Global Pattern of Evolution of Plasmaspheric Drainage Plumes. In: Inner Magnetosphere Interactions: New Perspectives from Imaging. American Geophysical Union (AGU), pp. 1–22. http://dx.doi.org/10.1029/159GM02, arXiv:https://agupubs.onlinelibrary.wiley.com/doi/pdf/10.1029/159GM02. URL: https://agupubs.onlinelibrary.wiley.com/doi/abs/10.1029/159GM02.

Goldstein, J., Sandel, B.R., Hairston, M.R., Reiff, P.H., 2003. Control of plasmaspheric dynamics by both convection and sub-auroral polarization stream. Geophys. Res. Lett. 30 (24), 2243. http://dx.doi.org/10.1029/2003GL018390, arXiv:https://agupubs.onlinelibrary.wiley.com/doi/pdf/10.1029/2003GL018390. URL: https://agupubs.onlinelibrary.wiley.com/doi/abs/10.1029/2003GL018390.

Graham, D.B., Khotyaintsev, Y.V., Norgren, C., Vaivads, A., André, M., Toledo-Redondo, S., Lindqvist, P.-A., Marklund, G.T., Ergun, R.E., Paterson, W.R., Gershman, D.J., Giles, B.L., Pollock, C.J., Dorelli, J.C., Avanov, L.A., Lavraud, B., Saito, Y., Magnes, W., Russell, C.T., Strangeway, R.J., Torbert, R.B., Burch, J.L., 2017. Lower hybrid waves in the ion diffusion and magnetospheric inflow regions. J. Geophys. Res.: Space Phys. 122 (1), 517–533. http://dx.doi.org/10.1002/2016JA023572, arXiv:https://agupubs.onlinelibrary.wiley.com/doi/pdf/10.1002/2016JA023572: URL: https://agupubs.onlinelibrary.wiley.com/doi/abs/10.1002/2016JA023572.

Grebowsky, J.M., 1970. Model study of plasmapause motion. J. Geophys. Res. 75 (22), 4329–4333. http://dx.doi.org/10.1029/JA075i022p04329, arXiv:https://agupubs.onlinelibrary.wiley.com/doi/pdf/10.1029/JA075i022p04329. URL: https://agupubs.onlinelibrary.wiley.com/doi/abs/10.1029/JA075i022p04329.

Grew, R.S., Menk, F.W., Clilverd, M.A., Sandel, B.R., 2007. Mass and electron densities in the inner magnetosphere during a prolonged disturbed interval. Geophys. Res. Lett. 34 (2), L02108. http://dx.doi.org/10.1029/2006GL028254, arXiv:https://agupubs.onlinelibrary.wiley.com/doi/pdf/10.1029/2006GL028254. URL: https://agupubs.onlinelibrary.wiley.com/doi/abs/10.1029/2006GL028254.

Grison, B., Hanzelka, M., Breuillard, H., Darrouzet, F., Santolík, O., Cornilleau-Wehrlin, N., Dandouras, I., 2018. Plasmaspheric Plumes and EMIC Rising Tone Emissions. J. Geophys. Res.: Space Phys. 123 (11), 9443–9452. http://dx.doi.org/10.1029/2018JA025796, arXiv:https://agupubs.onlinelibrary.wiley.com/doi/pdf/10.1029/2018JA025796. URL: https://agupubs.onlinelibrary.wiley.com/doi/abs/10.1029/2018JA025796.

Gussenhoven, M.S., Hardy, D.A., Heinemann, N., 1983. Systematics of the equatorward diffuse auroral boundary. J. Geophys. Res.: Space Phys. 88 (A7), 5692–5708. http://dx.doi.org/10.1029/JA088iA07p05692, arXiv:https://agupubs.onlinelibrary.wiley.com/doi/pdf/10.1029/JA088iA07p05692. URL: https://agupubs.onlinelibrary.wiley.com/doi/abs/10.1029/JA088iA07p05692.

Haaland, S., Eriksson, A., André, M., Maes, L., Baddeley, L., Barakat, A., Chappell, R., Eccles, V., Johnsen, C., Lybekk, B., Li, K., Pedersen, A., Schunk, R., Welling, D., 2015. Estimation of cold plasma outflow during geomagnetic storms. J. Geophys. Res.: Space Phys. 120 (12), 10,622–10,639. http://dx.doi.org/10.1002/2015JA021810, arXiv:https://agupubs.onlinelibrary.wiley.com/doi/pdf/10.1002/2015JA021810. URL: https://agupubs.onlinelibrary.wiley.com/doi/abs/10.1002/2015JA021810.

Haerendel, G., 2019. Experiments With Plasmas Artificially Injected Into Near-Earth Space. Front. Astron. Space Sci. 6, 29. http://dx.doi.org/10.3389/fspas.2019.00029, https://www.frontiersin.org/article/10.3389/fspas.2019.00029.

Halford, A.J., Fraser, B.J., Morley, S.K., 2010. EMIC wave activity during geomagnetic storm and nonstorm periods: CRRES results. J. Geophys. Res.: Space Phys. 115 (A12), A12248. http://dx.doi.org/10.1029/2010JA015716, arXiv:https://agupubs.onlinelibrary.wiley.com/doi/pdf/10.1029/2010JA015716. URL: https://agupubs.onlinelibrary.wiley.com/doi/abs/10.1029/2010JA015716.

Halford, A.J., Fraser, B.J., Morley, S.K., 2015. EMIC Waves and plasmaspheric and plume density: CRRES results. J. Geophys. Res.: Space Phys. 120 (3), 1974–1992. http://dx.doi.org/10.1002/2014JA020338, arXiv:https://agupubs.onlinelibrary.wiley.com/doi/pdf/10.1002/2014JA020338. URL: https://agupubs.onlinelibrary.wiley.com/doi/abs/10.1002/2014JA020338.

Han, D.-S., Chen, X.-C., Liu, J.-J., Qiu, Q., Keika, K., Hu, Z.-J., Liu, J.-M., Hu, H.-Q., Yang, H.-G., 2015. An extensive survey of dayside diffuse aurora based on optical observations at Yellow River Station. J. Geophys. Res.: Space Phys. 120 (9), 7447–7465. http://dx.doi.org/10.1002/2015JA021699, arXiv:https://agupubs.onlinelibrary.wiley.com/doi/pdf/10.1002/2015JA021699. URL: https://agupubs.onlinelibrary.wiley.com/doi/abs/10.1002/2015JA021699.

Han, D.-S., Hietala, H., Chen, X.-C., Nishimura, Y., Lyons, L.R., Liu, J.-J., Hu, H.-Q., Yang, H.-G., 2017. Observational properties of dayside throat aurora and implications on the possible generation mechanisms. J. Geophys. Res.: Space Phys. 122 (2), 1853–1870. http://dx.doi.org/10.1002/2016JA023394, arXiv:https://agupubs.onlinelibrary.wiley.com/doi/pdf/10.1002/2016JA023394. URL: https://agupubs.onlinelibrary.wiley.com/doi/abs/10.1002/2016JA023394.

Haque, N., Inan, U.S., Bell, T.F., Pickett, J.S., Trotignon, J.G., Facskó, G., 2011. Cluster observations of whistler mode ducts and banded chorus. Geophys. Res. Lett. 38 (18), L18107. http://dx.doi.org/10.1029/2011GL049112, arXiv:https://agupubs.onlinelibrary.wiley.com/doi/pdf/10.1029/2011GL049112. URL: https://agupubs.onlinelibrary.wiley.com/doi/abs/10.1029/2011GL049112.

Hartinger, M.D., Angelopoulos, V., Moldwin, M.B., Takahashi, K., Clausen, L.B.N., 2013a. Statistical study of global modes outside the plasmasphere. J. Geophys. Res.: Space Phys. 118 (2), 804–822. http://dx.doi.org/10.1002/jgra.50140, arXiv:https://agupubs.onlinelibrary.wiley.com/doi/pdf/10.1002/jgra.50140. URL: https://agupubs.onlinelibrary.wiley.com/doi/abs/10.1002/jgra.50140.

Hartinger, M.D., Moldwin, M.B., Zou, S., Bonnell, J.W., Angelopoulos, V., 2015. ULF wave electromagnetic energy flux into the ionosphere: Joule heating implications. J. Geophys. Res.: Space Phys. 120 (1), 494–510. http://dx.doi.org/10.1002/2014JA020129, arXiv:https://agupubs.onlinelibrary.wiley.com/doi/pdf/10.1002/2014JA020129. URL: https://agupubs.onlinelibrary.wiley.com/doi/abs/10.1002/2014JA020129.

Hartinger, M.D., Turner, D.L., Plaschke, F., Angelopoulos, V., Singer, H., 2013b. The role of transient ion foreshock phenomena in driving Pc5 ULF wave activity. J. Geophys. Res.: Space Phys. 118 (1), 299–312. http://dx.doi.org/10.1029/2012JA018349, arXiv:https://agupubs.onlinelibrary.wiley.com/doi/pdf/10.1029/2012JA018349. URL: https://agupubs.onlinelibrary.wiley.com/doi/abs/10.1029/2012JA018349.

Hartley, D.P., Kletzing, C.A., Santolík, O., Chen, L., Horne, R.B., 2018. Statistical Properties of Plasmaspheric Hiss From Van Allen Probes Observations. J. Geophys. Res.: Space Phys. 123 (4), 2605–2619. http://dx.doi.org/10.1002/2017JA024593, arXiv:https://agupubs.onlinelibrary.wiley.com/doi/pdf/10.1002/2017JA024593. URL: https://agupubs.onlinelibrary.wiley.com/doi/abs/10.1002/2017JA024593.

Hasegawa, A., 1971. Drift-wave instability at the plasmapause. J. Geophys. Res. 76 (22), 5361–5364. http://dx.doi.org/10.1029/JA076i022p05361, arXiv:https://agupubs.onlinelibrary.wiley.com/doi/pdf/10.1029/JA076i022p05361. URL: https://agupubs.onlinelibrary.wiley.com/doi/abs/10.1029/JA076i022p05361.

Hasegawa, H., Fujimoto, M., Phan, T.D., Rème, H., Balogh, A., Dunlop, M.W., Hashimoto, C., TanDokoro, R., 2004. Transport of solar wind into Earth's magnetosphere through rolled-up Kelvin–Helmholtz vortices. Nature 430 (7001), 755–758, https://doi.org/10.1038/nature02799.

Hastings, D., Garrett, H., 2004. Spacecraft-Environment Interactions. Cambridge University Press.

Hayosh, M., Santolík, O., Parrot, M., 2010. Location and size of the global source region of whistler mode chorus. J. Geophys. Res.: Space Phys. 115 (A3), A00F06. http://dx.doi.org/10.1029/2009JA014950, arXiv:https://agupubs.onlinelibrary.wiley.com/doi/pdf/10.1029/2009JA014950. URL: https://agupubs.onlinelibrary.wiley.com/doi/abs/10.1029/2009JA014950.

Henderson, M.G., 2013. Auroral Substorms, Poleward Boundary Activations, Auroral Streamers, Omega Bands, and Onset Precursor Activity. In: Auroral Phenomenology and Magnetospheric Processes: Earth and Other Planets. American Geophysical Union (AGU), pp. 39–54. http://dx.doi.org/10.1029/2011GM001165, arXiv:https://agupubs.onlinelibrary.wiley.com/doi/pdf/10.1029/2011GM001165. URL: https://agupubs.onlinelibrary.wiley.com/doi/abs/10.1029/2011GM001165.

Henderson, M.G., Donovan, E.F., Foster, J.C., Mann, I.R., Immel, T.J., Mende, S.B., Sigwarth, J.B., 2010. Start-to-end global imaging of a sunward propagating, SAPS-associated giant undulation event. J. Geophys. Res.: Space Phys. 115 (A4), A04210. http://dx.doi.org/10.1029/2009JA014106, arXiv:https://agupubs.onlinelibrary.wiley.com/doi/pdf/10.1029/2009JA014106. URL: https://agupubs.onlinelibrary.wiley.com/doi/abs/10.1029/2009JA014106.

Henderson, M.G., Morley, S.K., Kepko, L.E., 2018. SAPS-Associated Explosive Brightening on the Duskside: A New Type of Onset-Like Disturbance. J. Geophys. Res.: Space Phys. 123 (1), 197–210. http://dx.doi.org/10.1002/2017JA024472, arXiv:https://agupubs.onlinelibrary.wiley.com/doi/pdf/10.1002/2017JA024472. URL: https://agupubs.onlinelibrary.wiley.com/doi/abs/10.1002/2017JA024472.

Hesse, M., Birn, J., 2004. On the cessation of magnetic reconnection. Ann. Geophys. 22 (2), 603–612. http://dx.doi.org/10.5194/angeo-22-603-2004, https://www.ann-geophys.net/22/603/2004/.

Hoffman, J.H., 1967. Composition Measurements of the Topside Ionosphere. Science 155 (3760), 322–324. http://dx.doi.org/10.1126/science.155.3760.322, arXiv:https://science.sciencemag.org/content/155/3760/322.full.pdf. URL: https://science.sciencemag.org/content/155/3760/322.

Hoogeveen, G.W., Jacobson, A.R., 1997. Improved analysis of plasmasphere motion using the VLA radio interferometer. Ann. Geophys. 15 (2), 236–245, https://doi.org/10.1007/s00585-997-0236-6.

Horne, R.B., 1989. Path-integrated growth of electrostatic waves: The generation of terrestrial myriametric radiation. J. Geophys. Res.: Space Phys. 94 (A7), 8895–8909. http://dx.doi.org/10.1029/JA094iA07p08895, arXiv:https://agupubs.onlinelibrary.wiley.com/doi/pdf/10.1029/JA094iA07p08895. URL: https://agupubs.onlinelibrary.wiley.com/doi/abs/10.1029/JA094iA07p08895.

Horne, R.B., Thorne, R.M., 1994. Convective instabilities of electromagnetic ion cyclotron waves in the outer magnetosphere. J. Geophys. Res.: Space Phys. 99 (A9), 17259–17273. http://dx.doi.org/10.1029/94JA01259, arXiv:https://agupubs.onlinelibrary.wiley.com/doi/pdf/10.1029/94JA01259. URL: https://agupubs.onlinelibrary.wiley.com/doi/abs/10.1029/94JA01259.

Horwitz, J.L., 1986. The tail lobe ion spectrometer. J. Geophys. Res.: Space Phys. 91 (A5), 5689–5699. http://dx.doi.org/10.1029/JA091iA05p05689, arXiv:https://agupubs.onlinelibrary.wiley.com/doi/pdf/10.1029/JA091iA05p05689. URL: https://agupubs.onlinelibrary.wiley.com/doi/abs/10.1029/JA091iA05p05689.

Horwitz, J.L., Cobb, W.K., Baugher, C.R., Chappell, C.R., Frank, L.A., Eastman, T.E., Anderson, R.R., Shelley, E.G., Young, D.T., 1982. On the relationship of the plasmapause to the equatorward boundary of the auroral oval and to the inner edge of the plasma sheet. J. Geophys. Res.: Space Phys. 87 (A11), 9059–9069. http://dx.doi.org/10.1029/JA087iA11p09059, arXiv:https://agupubs.onlinelibrary.wiley.com/doi/pdf/10.1029/JA087iA11p09059. URL: https://agupubs.onlinelibrary.wiley.com/doi/abs/10.1029/JA087iA11p09059.

Horwitz, J.L., Comfort, R.H., Chappell, C.R., 1984. Thermal ion composition measurements of the formation of the new outer plasmasphere and double plasmapause during storm recovery phase. Geophys. Res. Lett. 11 (8), 701–704. http://dx.doi.org/10.1029/GL011i008p00701, arXiv:https://agupubs.onlinelibrary.wiley.com/doi/pdf/10.1029/GL011i008p00701. URL: https://agupubs.onlinelibrary.wiley.com/doi/abs/10.1029/GL011i008p00701.

Horwitz, J.L., Ho, C.W., Scarbro, H.D., Wilson, G.R., Moore, T.E., 1994. Centrifugal acceleration of the polar wind. J. Geophys. Res.: Space Phys. 99 (A8), 15051–15064. http://dx.doi.org/10.1029/94JA00924, arXiv:https://agupubs.onlinelibrary.wiley.com/doi/pdf/10.1029/94JA00924. URL: https://agupubs.onlinelibrary.wiley.com/doi/abs/10.1029/94JA00924.

Huang, C.-S., Foster, J.C., Song, P., Sofko, G.J., Frank, L.A., Paterson, W.R., 2002. Geotail observations of magnetospheric midtail during an extended period of strongly northward interplanetary magnetic field. Geophys. Res. Lett. 29 (4), 15–1–15–4. http://dx.doi.org/10.1029/2001GL014170, arXiv:https://agupubs.onlinelibrary.wiley.com/doi/pdf/10.1029/2001GL014170. URL: https://agupubs.onlinelibrary.wiley.com/doi/abs/10.1029/2001GL014170.

Huddleston, M.M., Chappell, C.R., Delcourt, D.C., Moore, T.E., Giles, B.L., Chandler, M.O., 2005. An examination of the process and magnitude of ionospheric plasma supply to the magnetosphere. J. Geophys. Res.: Space Phys. 110 (A12), A12202. http://dx.doi.org/10.1029/2004JA010401, arXiv:https://agupubs.onlinelibrary.wiley.com/doi/pdf/10.1029/2004JA010401. URL: https://agupubs.onlinelibrary.wiley.com/doi/abs/10.1029/2004JA010401.

Hughes, W.J., Southwood, D.J., Mauk, B., McPherron, R.L., Barfield, J.N., 1978. Alfvén waves generated by an inverted plasma energy distribution. Nature 275 (5675), 43–45, https://doi.org/10.1038/275043a0.

Hultqvist, B., Øieroset, M., Paschmann, G., Treumann, R., 1999. Magnetospheric Plasma Sources and Losses: Final Report of the ISSI Study Project on Source and Loss Processes of Magnetospheric Plasma. In: Space Sciences Series of ISSI, Springer Netherlands, https://books.google.com/books?id=ea559fHgMAsC.

Humberset, B.K., Gjerloev, J.W., Samara, M., Michell, R.G., Mann, I.R., 2016. Temporal characteristics and energy deposition of pulsating auroral patches. J. Geophys. Res.: Space Phys. 121 (7), 7087–7107. http://dx.doi.org/10.1002/2016JA022921, arXiv:https://agupubs.onlinelibrary.wiley.com/doi/pdf/10.1002/2016JA022921. URL: https://agupubs.onlinelibrary.wiley.com/doi/abs/10.1002/2016JA022921.

Ilie, R., Liemohn, M.W., 2016. The outflow of ionospheric nitrogen ions: A possible tracer for the altitude-dependent transport and energization processes of ionospheric plasma. J. Geophys. Res.: Space Phys. 121 (9), 9250–9255. http://dx.doi.org/10.1002/2015JA022162, arXiv:https://agupubs.onlinelibrary.wiley.com/doi/pdf/10.1002/2015JA022162. URL: https://agupubs.onlinelibrary.wiley.com/doi/abs/10.1002/2015JA022162.

Jacobson, A.R., Carlos, R.C., Massey, R.S., Wu, G., Hoogeveen, G., 1995. Total-electron-content signatures of plasmaspheric motions. Geophys. Res. Lett. 22 (18), 2461–2464. http://dx.doi.org/10.1029/95GL02550, arXiv:https://agupubs.onlinelibrary.wiley.com/doi/pdf/10.1029/95GL02550. URL: https://agupubs.onlinelibrary.wiley.com/doi/abs/10.1029/95GL02550.

Jacobson, A.R., Hoogeveen, G., Carlos, R.C., Wu, G., Fejer, B.G., Kelley, M.C., 1996. Observations of inner plasmasphere irregularities with a satellite-beacon radio-interferometer array. J. Geophys. Res.: Space Phys. 101 (A9), 19665–19682. http://dx.doi.org/10.1029/96JA01253, arXiv:https://agupubs.onlinelibrary.wiley.com/doi/pdf/10.1029/96JA01253. URL: https://agupubs.onlinelibrary.wiley.com/doi/abs/10.1029/96JA01253.

Jahn, J.-M., Goldstein, J., Reeves, G.D., Fernandes, P.A., Skoug, R.M., Larsen, B.A., Spence, H.E., 2017. The Warm Plasma Composition in the Inner Magnetosphere During 2012-2015. J. Geophys. Res.: Space Phys. 122 (11), 11,018–11,043. http://dx.doi.org/10.1002/2017JA024183, arXiv:https://agupubs.onlinelibrary.wiley.com/doi/pdf/10.1002/2017JA024183: https://agupubs.onlinelibrary.wiley.com/doi/abs/10.1002/2017JA024183.

Jaynes, A.N., Lessard, M.R., Takahashi, K., Ali, A.F., Malaspina, D.M., Michell, R.G., Spanswick, E.L., Baker, D.N., Blake, J.B., Cully, C., Donovan, E.F., Kletzing, C.A., Reeves, G.D., Samara, M., Spence, H.E., Wygant, J.R., 2015. Correlated Pc4-5 ULF waves, whistler-mode chorus, and pulsating aurora observed by the Van Allen Probes and ground-based systems. J. Geophys. Res.: Space Phys. 120 (10), 8749–8761. http://dx.doi.org/10.1002/2015JA021380, arXiv:https://agupubs.onlinelibrary.wiley.com/doi/pdf/10.1002/2015JA021380. URL: https://agupubs.onlinelibrary.wiley.com/doi/abs/10.1002/2015JA021380.

Johnstone, A.D., 1978. Pulsating aurora. Nature 274 (5667), 119–126, https://doi.org/10.1038/274119a0.

Jones, S.L., Lessard, M.R., Rychert, K., Spanswick, E., Donovan, E., 2011. Large-scale aspects and temporal evolution of pulsating aurora. J. Geophys. Res.: Space Phys. 116 (A3), A03214. http://dx.doi.org/10.1029/2010JA015840, arXiv:https://agupubs.onlinelibrary.wiley.com/doi/pdf/10.1029/2010JA015840. URL: https://agupubs.onlinelibrary.wiley.com/doi/abs/10.1029/2010JA015840.

Jordanova, V.K., Spasojevic, M., Thomsen, M.F., 2007. Modeling the electromagnetic ion cyclotron wave-induced formation of detached subauroral proton arcs. J. Geophys. Res.: Space Phys. 112 (A8), A08209. http://dx.doi.org/10.1029/2006JA012215, arXiv:https://agupubs.onlinelibrary.wiley.com/doi/pdf/10.1029/2006JA012215. URL: https://agupubs.onlinelibrary.wiley.com/doi/abs/10.1029/2006JA012215.

Jordanova, V.K., Tu, W., Chen, Y., Morley, S.K., Panaitescu, A.-D., Reeves, G.D., Kletzing, C.A., 2016. RAM-SCB Simulations of electron transport and plasma wave scattering during the October 2012 'double-dip' storm. J. Geophys. Res.: Space Phys. 121 (9), 8712–8727. http://dx.doi.org/10.1002/2016JA022470, arXiv:https://agupubs.onlinelibrary.wiley.com/doi/pdf/10.1002/2016JA022470. URL: https://agupubs.onlinelibrary.wiley.com/doi/abs/10.1002/2016JA022470.

Karimabadi, H., Roytershteyn, V., Mouikis, C.G., Kistler, L.M., Daughton, W., 2011. Flushing effect in reconnection: Effects of minority species of oxygen ions. Planet. Space Sci. 59 (7), 526–536. http://dx.doi.org/10.1016/j.pss.2010.07.014, http://www.sciencedirect.com/science/article/pii/S0032063310002163.

Karpman, V.I., Kaufman, R.N., 1987. Whistler wave propagation in plasma ducts. Radio Science 22 (6), 1023–1025. http://dx.doi.org/10.1029/RS022i006p01023, arXiv:https://agupubs.onlinelibrary.wiley.com/doi/pdf/10.1029/RS022i006p01023. URL: https://agupubs.onlinelibrary.wiley.com/doi/abs/10.1029/RS022i006p01023.

Kasahara, S., Miyoshi, Y., Yokota, S., Mitani, T., Kasahara, Y., Matsuda, S., Kumamoto, A., Matsuoka, A., Kazama, Y., Frey, H.U., Angelopoulos, V., Kurita, S., Keika, K., Seki, K., Shinohara, I., 2018. Pulsating aurora from electron scattering by chorus waves. Nature 554, 337.

Kataoka, R., Miyoshi, Y., Hampton, D., Ishii, T., Kozako, H., 2012. Pulsating aurora beyond the ultra-low-frequency range. J. Geophys. Res.: Space Phys. 117 (A8), A08336. http://dx.doi.org/10.1029/2012JA017987, arXiv:https://agupubs.onlinelibrary.wiley.com/doi/pdf/10.1029/2012JA017987. URL: https://www.agupubs.onlinelibrary.wiley.com/doi/abs/10.1029/2012JA017987.

Kavosi, S., Raeder, J., 2015. Ubiquity of Kelvin–Helmholtz waves at Earth's magnetopause. Nature Commun. 6 (1), 7019, https://doi.org/10.1038/ncomms8019.

Kazue, T., McPherron, R.L., 1984. Standing hydromagnetic oscillations in the magnetosphere. Planet. Space Sci. 32 (11), 1343–1359. http://dx.doi.org/10.1016/0032-0633(84)90078-3, http://www.sciencedirect.com/science/article/pii/0032063384900783.

Keika, K., Takahashi, K., Ukhorskiy, A.Y., Miyoshi, Y., 2013. Global characteristics of electromagnetic ion cyclotron waves: Occurrence rate and its storm dependence. J. Geophys. Res.: Space Phys. 118 (7), 4135–4150. http://dx.doi.org/10.1002/jgra.50385, arXiv:https://agupubs.onlinelibrary.wiley.com/doi/pdf/10.1002/jgra.50385. URL: https://agupubs.onlinelibrary.wiley.com/doi/abs/10.1002/jgra.50385.

Kelley, M.C., 1986. Intense sheared flow as the origin of large-scale undulations of the edge of the diffuse aurora. J. Geophys. Res.: Space Phys. 91 (A3), 3225–3230. http://dx.doi.org/10.1029/JA091iA03p03225, arXiv:https://agupubs.onlinelibrary.wiley.com/doi/pdf/10.1029/JA091iA03p03225. URL: https://agupubs.onlinelibrary.wiley.com/doi/abs/10.1029/JA091iA03p03225.

Kennel, C.F., Petschek, H.E., 1966. Limit on stably trapped particle fluxes. J. Geophys. Res. 71 (1), 1–28. http://dx.doi.org/10.1029/JZ071i001p00001, arXiv:https://agupubs.onlinelibrary.wiley.com/doi/pdf/10.1029/JZ071i001p00001. URL: https://agupubs.onlinelibrary.wiley.com/doi/abs/10.1029/JZ071i001p00001.

Kepko, L., Viall, N.M., 2019. The Source, Significance, and Magnetospheric Impact of Periodic Density Structures Within Stream Interaction Regions. J. Geophys. Res.: Space Phys. 124 (10), 7722–7743. http://dx.doi.org/10.1029/2019JA026962, arXiv:https://agupubs.onlinelibrary.wiley.com/doi/pdf/10.1029/2019JA026962. URL: https://agupubs.onlinelibrary.wiley.com/doi/abs/10.1029/2019JA026962.

Kessel, R.L., 2008. Solar wind excitation of Pc5 fluctuations in the magnetosphere and on the ground. J. Geophys. Res.: Space Phys. 113 (A4), A04202. http://dx.doi.org/10.1029/2007JA012255, arXiv:https://agupubs.onlinelibrary.wiley.com/doi/pdf/10.1029/2007JA012255. URL: https://agupubs.onlinelibrary.wiley.com/doi/abs/10.1029/2007JA012255.

Khazanov, G.V., Liemohn, M.W., Moore, T.E., 1997. Photoelectron effects on the self-consistent potential in the collisionless polar wind. J. Geophys. Res.: Space Phys. 102 (A4), 7509–7521. http://dx.doi.org/10.1029/96JA03343, arXiv:https://agupubs.onlinelibrary.wiley.com/doi/pdf/10.1029/96JA03343. URL: https://agupubs.onlinelibrary.wiley.com/doi/abs/10.1029/96JA03343.

Kistler, L.M., Mouikis, C.G., 2016. The inner magnetosphere ion composition and local time distribution over a solar cycle. J. Geophys. Res.: Space Phys. 121 (3), 2009–2032. http://dx.doi.org/10.1002/2015JA021883, arXiv:https://agupubs.onlinelibrary.wiley.com/doi/pdf/10.1002/2015JA021883. URL: https://agupubs.onlinelibrary.wiley.com/doi/abs/10.1002/2015JA021883.

Kistler, L.M., Mouikis, C.G., Cao, X., Frey, H., Klecker, B., Dandouras, I., Korth, A., Marcucci, M.F., Lundin, R., McCarthy, M., Friedel, R., Lucek, E., 2006. Ion composition and pressure changes in storm time and nonstorm substorms in the vicinity of the near-Earth neutral line. J. Geophys. Res.: Space Phys. 111 (11), 1–12. http://dx.doi.org/10.1029/2006JA011939.

Kistler, L.M., Mouikis, C.G., Klecker, B., Dandouras, I., 2010. Cusp as a source for oxygen in the plasma sheet during geomagnetic storms. J. Geophys. Res.: Space Phys. 115 (A3), A03209. http://dx.doi.org/10.1029/2009JA014838, arXiv:https://agupubs.onlinelibrary.wiley.com/doi/pdf/10.1029/2009JA014838. URL: https://agupubs.onlinelibrary.wiley.com/doi/abs/10.1029/2009JA014838.

Kistler, L.M., Mouikis, C., Möbius, E., Klecker, B., Sauvaud, J.A., Réme, H., Korth, A., Marcucci, M.F., Lundin, R., Parks, G.K., Balogh, A., 2005. Contribution of nonadiabatic ions to the cross-tail current in an O+ dominated thin current sheet. J. Geophys. Res.: Space Phys. 110 (A6), A06213. http://dx.doi.org/10.1029/2004JA010653.

Kitamura, N., Ogawa, Y., Nishimura, Y., Terada, N., Ono, T., Shinbori, A., Kumamoto, A., Truhlik, V., Smilauer, J., 2011. Solar zenith angle dependence of plasma density and temperature in the polar cap ionosphere and low-altitude magnetosphere during geomagnetically quiet periods at solar maximum. J. Geophys. Res.: Space Phys. 116 (A8), A08227. http://dx.doi.org/10.1029/2011JA016631, arXiv:https://agupubs.onlinelibrary.wiley.com/doi/pdf/10.1029/2011JA016631. URL: https://agupubs.onlinelibrary.wiley.com/doi/abs/10.1029/2011JA016631.

Kitamura, N., Seki, K., Nishimura, Y., Terada, N., Ono, T., Hori, T., Strangeway, R.J., 2012. Photoelectron flows in the polar wind during geomagnetically quiet periods. J. Geophys. Res.: Space Phys. 117 (A7), A07214. http://dx.doi.org/10.1029/2011JA017459, arXiv:https://agupubs.onlinelibrary.wiley.com/doi/pdf/10.1029/2011JA017459. URL: https://agupubs.onlinelibrary.wiley.com/doi/abs/10.1029/2011JA017459.

Knudsen, D., Burchill, J., Buchert, S., Eriksson, A., Gill, R., Wahlund, J.-E., Åhlen, L., Smith, M., Moffat, B., 2017. Thermal ion imagers and Langmuir probes in the Swarm electric field instruments. J. Geophys. Res.: Space Phys. 122 (2), 2655–2673.

Kolstø, H.M., Hesse, M., Norgren, C., Tenfjord, P., Spinnangr, S.F., Kwagala, N., 2020. Collisionless Magnetic Reconnection in an Asymmetric Oxygen Density Configuration. Geophys. Res. Lett. 47 (1), e2019GL085359. http://dx.doi.org/10.1029/2019GL085359, arXiv:https://agupubs.onlinelibrary.wiley.com/doi/pdf/10.1029/2019GL085359. URL: https://agupubs.onlinelibrary.wiley.com/doi/abs/10.1029/2019GL085359.

Koons, H.C., 1989. Observations of large-amplitude, whistler mode wave ducts in the outer plasmasphere. J. Geophys. Res.: Space Phys. 94 (A11), 15393–15397. http://dx.doi.org/10.1029/JA094iA11p15393, arXiv:https://agupubs.onlinelibrary.wiley.com/doi/pdf/10.1029/JA094iA11p15393. URL: https://agupubs.onlinelibrary.wiley.com/doi/abs/10.1029/JA094iA11p15393.

Kotova, G.A., 2007. The Earth's plasmasphere: State of studies (a Review). Geomagn. Aeronomy 47 (4), 409–422, https://doi.org/10.1134/S0016793207040019.

Kozyra, J.U., Liemohn, M.W., Clauer, C.R., Ridley, A.J., Thomsen, M.F., Borovsky, J.E., Roeder, J.L., Jordanova, V.K., Gonzalez, W.D., 2002. Multistep Dst development and ring current composition changes during the 4-6 June 1991 magnetic storm. J. Geophys. Res.: Space Phys. 107 (A8), 1224. http://dx.doi.org/10.1029/2001JA000023, arXiv:https://agupubs.onlinelibrary.wiley.com/doi/pdf/10.1029/2001JA000023. URL: https://agupubs.onlinelibrary.wiley.com/doi/abs/10.1029/2001JA000023.

Kozyra, J.U., Rasmussen, C.E., Miller, R.H., Lyons, L.R., 1994. Interaction of ring current and radiation belt protons with ducted plasmaspheric hiss: 1. Diffusion coefficients and timescales. J. Geophys. Res.: Space Phys. 99 (A3), 4069–4084. http://dx.doi.org/10.1029/93JA01532, arXiv:https://agupubs.onlinelibrary.wiley.com/doi/pdf/10.1029/93JA01532. URL: https://agupubs.onlinelibrary.wiley.com/doi/abs/10.1029/93JA01532.

Kozyreva, O.V., Kleimenova, N.G., 2009. Variations in the ULF index of geomagnetic pulsations during strong magnetic storms. Geomagn. Aeronomy 49 (4), 425–437, https://doi.org/10.1134/S0016793209040021.

Kozyreva, O.V., Kleimenova, N.G., 2010. Variations in the ULF index of daytime geomagnetic pulsations during recurrent magnetic storms. Geomagn. Aeronomy 50 (6), 770–780, https://doi.org/10.1134/S0016793210060083.

Kozyreva, O., Pilipenko, V., Engebretson, M., Yumoto, K., Watermann, J., Romanova, N., 2007. In search of a new ULF wave index: Comparison of Pc5 power with dynamics of geostationary relativistic electrons. Planet. Space Sci. 55 (6), 755–769. http://dx.doi.org/10.1016/j.pss.2006.03.013, http://www.sciencedirect.com/science/article/pii/S0032063306002911. Ultra-Low Frequency Waves in the Magnetosphere.

Krimigis, S.M., Haerendel, G., McEntire, R.W., Paschmann, G., Bryant, D.A., 1982. The active magnetospheric particle tracer explorers (AMPTE) program. EOS Trans. Am. Geophys. Union 63 (45), 843–850. http://dx.doi.org/10.1029/EO063i045p00843, arXiv:https://agupubs.onlinelibrary.wiley.com/doi/pdf/10.1029/EO063i045p00843. URL: https://agupubs.onlinelibrary.wiley.com/doi/abs/10.1029/EO063i045p00843.

Kronberg, E.A., Ashour-Abdalla, M., Dandouras, I., Delcourt, D.C., Grigorenko, E.E., Kistler, L.M., Kuzichev, I.V., Liao, J., Maggiolo, R., Malova, H.V., Orlova, K.G., Peroomian, V., Shklyar, D.R., Shprits, Y.Y., Welling, D.T., Zelenyi, L.M., 2014. Circulation of Heavy Ions and Their Dynamical Effects in the Magnetosphere: Recent Observations and Models. Space Sci. Rev. 184 (1), 173–235, https://doi.org/10.1007/s11214-014-0104-0.

Kronberg, E.A., Haaland, S.E., Daly, P.W., Grigorenko, E.E., Kistler, L.M., Fränz, M., Dandouras, I., 2012. Oxygen and hydrogen ion abundance in the near-Earth magnetosphere: Statistical results on the response to the geomagnetic and solar wind activity conditions. J. Geophys. Res.: Space Phys. 117 (A12), A12208. http://dx.doi.org/10.1029/2012JA018071, arXiv:https://agupubs.onlinelibrary.wiley.com/doi/pdf/10.1029/2012JA018071. URL: https://agupubs.onlinelibrary.wiley.com/doi/abs/10.1029/2012JA018071.

Kulkarni, P., Inan, U.S., Bell, T.F., 2008. Energetic electron precipitation induced by space based VLF transmitters. J. Geophys. Res.: Space Phys. 113 (A9), A09203. http://dx.doi.org/10.1029/2008JA013120, arXiv:https://agupubs.onlinelibrary.wiley.com/doi/pdf/10.1029/2008JA013120. URL: https://agupubs.onlinelibrary.wiley.com/doi/abs/10.1029/2008JA013120.

Kurth, W.S., De Pascuale, S., Faden, J.B., Kletzing, C.A., Hospodarsky, G.B., Thaller, S., Wygant, J.R., 2015. Electron densities inferred from plasma wave spectra obtained by the Waves instrument on Van Allen Probes. J. Geophys. Res.: Space Phys. 120 (2), 904–914. http://dx.doi.org/10.1002/2014JA020857, arXiv:https://agupubs.onlinelibrary.wiley.com/doi/pdf/10.1002/2014JA020857. URL: https://agupubs.onlinelibrary.wiley.com/doi/abs/10.1002/2014JA020857.

Laakso, H., Santolík, O., Horne, R., Kolmasová, I., Escoubet, P., Masson, A., Taylor, M., 2015. Identifying the source region of plasmaspheric hiss. Geophys. Res. Lett. 42 (9), 3141–3149. http://dx.doi.org/10.1002/2015GL063755, arXiv:https://agupubs.onlinelibrary.wiley.com/doi/pdf/10.1002/2015GL063755. URL: https://agupubs.onlinelibrary.wiley.com/doi/abs/10.1002/2015GL063755.

Lai, S., 2003. A critical overview on spacecraft charging mitigation methods. IEEE Trans. Plasma Sci. 31 (6), 1118–1124.

Lai, S., 2011. Fundamentals of Spacecraft Charging. Princeton University Press.

Lakhina, G., Mond, M., Hameiri, E., 1990. Ballooning mode instability at the plasmapause. J. Geophys. Res.: Space Phys. 95 (A4), 4007–4016. http://dx.doi.org/10.1029/JA095iA04p04007, arXiv:https://agupubs.onlinelibrary.wiley.com/doi/pdf/10.1029/JA095iA04p04007. URL: https://agupubs.onlinelibrary.wiley.com/doi/abs/10.1029/JA095iA04p04007.

Lanzerotti, L.J., Surkan, A.J., 1974. ULF geomagnetic power near L=4, 4. Relationship to the Fredericksburg K index. J. Geophys. Res. 79 (16), 2413–2419. http://dx.doi.org/10.1029/JA079i016p02413, arXiv:https://agupubs.onlinelibrary.wiley.com/doi/pdf/10.1029/JA079i016p02413. URL: https://agupubs.onlinelibrary.wiley.com/doi/abs/10.1029/JA079i016p02413.

Lassen, K., 1974. Relation of the plasma sheet to the nighttime auroral oval. J. Geophys. Res. 79 (25), 3857–3858. http://dx.doi.org/10.1029/JA079i025p03857, arXiv:https://agupubs.onlinelibrary.wiley.com/doi/pdf/10.1029/JA079i025p03857. URL: https://agupubs.onlinelibrary.wiley.com/doi/abs/10.1029/JA079i025p03857.

Lavraud, B., Thomsen, M.F., Borovsky, J.E., Denton, M.H., Pulkkinen, T.I., 2006. Magnetosphere preconditioning under northward IMF: Evidence from the study of coronal mass ejection and corotating interaction region geoeffectiveness. J. Geophys. Res.: Space Phys. 111 (A9), A09208. http://dx.doi.org/10.1029/2005JA011566, arXiv:https://agupubs.onlinelibrary.wiley.com/doi/pdf/10.1029/2005JA011566. URL: https://agupubs.onlinelibrary.wiley.com/doi/abs/10.1029/2005JA011566.

Lee, J.H., Angelopoulos, V., 2014a. Observations and modeling of EMIC wave properties in the presence of multiple ion species as function of magnetic local time. J. Geophys. Res.: Space Phys. 119 (11), 8942–8970. http://dx.doi.org/10.1002/2014JA020469, arXiv:https://agupubs.onlinelibrary.wiley.com/doi/pdf/10.1002/2014JA020469. URL: https://agupubs.onlinelibrary.wiley.com/doi/abs/10.1002/2014JA020469.

Lee, J.H., Angelopoulos, V., 2014b. On the presence and properties of cold ions near Earth's equatorial magnetosphere. J. Geophys. Res.: Space Phys. 119 (3), 1749–1770. http://dx.doi.org/10.1002/2013JA019305, arXiv:https://agupubs.onlinelibrary.wiley.com/doi/pdf/10.1002/2013JA019305. URL: https://agupubs.onlinelibrary.wiley.com/doi/abs/10.1002/2013JA019305.

Lemaire, J.F., Gringauz, K.I., Carpenter, D.L., Bassolo, V., 1998. The Earth's Plasmasphere. In: Cambridge Atmospheric and Space Science Series, Cambridge University Press, http://dx.doi.org/10.1017/CBO9780511600098.

Lemaire, J., Schunk, R., 1992. Plasmaspheric wind. J. Atmos. Terrest. Phys. 54 (3), 467–477. http://dx.doi.org/10.1016/0021-9169(92)90026-H, http://www.sciencedirect.com/science/article/pii/002191699290026H.

Lennartsson, W., 1989. Energetic (0.1- to 16-keV/e) magnetospheric ion composition at different levels of solar F10.7. J. Geophys. Res.: Space Phys. 94 (A4), 3600–3610. http://dx.doi.org/10.1029/JA094iA04p03600, arXiv:https://agupubs.onlinelibrary.wiley.com/doi/pdf/10.1029/JA094iA04p03600. URL: https://agupubs.onlinelibrary.wiley.com/doi/abs/10.1029/JA094iA04p03600.

Lennartsson, W., 1992. A scenario for solar wind penetration of Earth's magnetic tail based on ion composition data from the ISEE 1 spacecraft. J. Geophys. Res.: Space Phys. 97 (A12), 19221–19238. http://dx.doi.org/10.1029/92JA01604, arXiv:https://agupubs.onlinelibrary.wiley.com/doi/pdf/10.1029/92JA01604. URL: https://agupubs.onlinelibrary.wiley.com/doi/abs/10.1029/92JA01604.

Lennartsson, W., Shelley, E.G., 1986. Survey of 0.1- to 16-keV/e plasma sheet ion composition. J. Geophys. Res.: Space Phys. 91 (A3), 3061–3076. http://dx.doi.org/10.1029/JA091iA03p03061, arXiv:https://agupubs.onlinelibrary.wiley.com/doi/pdf/10.1029/JA091iA03p03061. URL: https://agupubs.onlinelibrary.wiley.com/doi/abs/10.1029/JA091iA03p03061.

Lessard, M.R., 2013. A Review of Pulsating Aurora. In: Auroral Phenomenology and Magnetospheric Processes: Earth and Other Planets. American Geophysical Union (AGU), pp. 55–68. http://dx.doi.org/10.1029/2011GM001187, arXiv:https://agupubs.onlinelibrary.wiley.com/doi/pdf/10.1029/2011GM001187. URL: https://agupubs.onlinelibrary.wiley.com/doi/abs/10.1029/2011GM001187.

Li, W., Bortnik, J., Thorne, R.M., Cully, C.M., Chen, L., Angelopoulos, V., Nishimura, Y., Tao, J.B., Bonnell, J.W., LeContel, O., 2013b. Characteristics of the Poynting flux and wave normal vectors of whistler-mode waves observed on THEMIS. J. Geophys. Res.: Space Phys. 118 (4), 1461–1471. http://dx.doi.org/10.1002/jgra.50176, https://agupubs.onlinelibrary.wiley.com/doi/pdf/10.1002/jgra.50176. URL: https://agupubs.onlinelibrary.wiley.com/doi/abs/10.1002/jgra.50176.

Li, W., Bortnik, J., Thorne, R.M., Nishimura, Y., Angelopoulos, V., Chen, L., 2011a. Modulation of whistler mode chorus waves: 2. Role of density variations. J. Geophys. Res.: Space Phys. 116 (A6), A06206. http://dx.doi.org/10.1029/2010JA016313, arXiv:https://agupubs.onlinelibrary.wiley.com/doi/pdf/10.1029/2010JA016313. URL: https://agupubs.onlinelibrary.wiley.com/doi/abs/10.1029/2010JA016313.

Li, K., Haaland, S., Eriksson, A., André, M., Engwall, E., Wei, Y., Kronberg, E.A., Fränz, M., Daly, P.W., Zhao, H., Ren, Q.Y., 2013a. Transport of cold ions from the polar ionosphere to the plasma sheet. J. Geophys. Res.: Space Phys. 118 (9), 5467–5477. http://dx.doi.org/10.1002/jgra.50518, arXiv:https://agupubs.onlinelibrary.wiley.com/doi/pdf/10.1002/jgra.50518. URL: https://agupubs.onlinelibrary.wiley.com/doi/abs/10.1002/jgra.50518.

Li, W., Thorne, R.M., Bortnik, J., Nishimura, Y., Angelopoulos, V., 2011b. Modulation of whistler mode chorus waves: 1. Role of compressional Pc4-5 pulsations. J. Geophys. Res.: Space Phys. 116 (A6), A06205. http://dx.doi.org/10.1029/2010JA016312, arXiv:https://agupubs.onlinelibrary.wiley.com/doi/pdf/10.1029/2010JA016312. URL: https://agupubs.onlinelibrary.wiley.com/doi/abs/10.1029/2010JA016312.

Li, W.-W., Whipple, E.C., 1988. A study of SCATHA eclipse charging. J. Geophys. Res.: Space Phys. 93 (A9), 10041–10046. http://dx.doi.org/10.1029/JA093iA09p10041, arXiv:https://agupubs.onlinelibrary.wiley.com/doi/pdf/10.1029/JA093iA09p10041. URL: https://agupubs.onlinelibrary.wiley.com/doi/abs/10.1029/JA093iA09p10041.

Liang, J., Donovan, E., Jackel, B., Spanswick, E., Gillies, M., 2016. On the 630 nm red-line pulsating aurora: Red-line Emission Geospace Observatory observations and model simulations. J. Geophys. Res.: Space Phys. 121 (8), 7988–8012. http://dx.doi.org/10.1002/2016JA022901, arXiv:https://agupubs.onlinelibrary.wiley.com/doi/pdf/10.1002/2016JA022901. URL: https://agupubs.onlinelibrary.wiley.com/doi/abs/10.1002/2016JA022901.

Liang, J., Donovan, E., Nishimura, Y., Yang, B., Spanswick, E., Asamura, K., Sakanoi, T., Evans, D., Redmon, R., 2015. Low-energy ion precipitation structures associated with pulsating auroral patches. J. Geophys. Res.: Space Phys. 120 (7), 5408–5431. http://dx.doi.org/10.1002/2015JA021094, arXiv:https://agupubs.onlinelibrary.wiley.com/doi/pdf/10.1002/2015JA021094. URL: https://agupubs.onlinelibrary.wiley.com/doi/abs/10.1002/2015JA021094.

Liang, J., Donovan, E., Reimer, A., Hampton, D., Zou, S., Varney, R., 2018. Ionospheric Electron Heating Associated With Pulsating Auroras: Joint Optical and PFISR Observations. J. Geophys. Res.: Space Phys. 123 (5), 4430–4456. http://dx.doi.org/10.1029/2017JA025138, arXiv:https://agupubs.onlinelibrary.wiley.com/doi/pdf/10.1029/2017JA025138. URL: https://agupubs.onlinelibrary.wiley.com/doi/abs/10.1029/2017JA025138.

Liang, J., Uritsky, V., Donovan, E., Ni, B., Spanswick, E., Trondsen, T., Bonnell, J., Roux, A., Auster, U., Larson, D., 2010. THEMIS observations of electron cyclotron harmonic emissions, ULF waves, and pulsating auroras. J. Geophys. Res.: Space Phys. 115 (A10), A10235. http://dx.doi.org/10.1029/2009JA015148, arXiv:https://agupubs.onlinelibrary.wiley.com/doi/pdf/10.1029/2009JA015148. URL: https://agupubs.onlinelibrary.wiley.com/doi/abs/10.1029/2009JA015148.

Liang, J., Yang, B., Donovan, E., Burchill, J., Knudsen, D., 2017. Ionospheric electron heating associated with pulsating auroras: A Swarm survey and model simulation. J. Geophys. Res.: Space Phys. 122 (8), 8781–8807. http://dx.doi.org/10.1002/2017JA024127, arXiv:https://agupubs.onlinelibrary.wiley.com/doi/pdf/10.1002/2017JA024127. URL: https://agupubs.onlinelibrary.wiley.com/doi/abs/10.1002/2017JA024127.

Liao, J., Kistler, L.M., Mouikis, C.G., Klecker, B., Dandouras, I., 2015. Acceleration of O+ from the cusp to the plasma sheet. J. Geophys. Res.: Space Phys. 120 (2), 1022–1034. http://dx.doi.org/10.1002/2014JA020341, arXiv:https://agupubs.onlinelibrary.wiley.com/doi/pdf/10.1002/2014JA020341. URL: https://agupubs.onlinelibrary.wiley.com/doi/abs/10.1002/2014JA020341.

Liao, J., Kistler, L.M., Mouikis, C.G., Klecker, B., Dandouras, I., Zhang, J.-C., 2010. Statistical study of O+ transport from the cusp to the lobes with Cluster CODIF data. J. Geophys. Res.: Space Phys. 115 (A12), A00J15. http://dx.doi.org/10.1029/2010JA015613, arXiv:https://agupubs.onlinelibrary.wiley.com/doi/pdf/10.1029/2010JA015613. URL: https://agupubs.onlinelibrary.wiley.com/doi/abs/10.1029/2010JA015613.

Liu, W., Cao, J.B., Li, X., Sarris, T.E., Zong, Q.-G., Hartinger, M., Takahashi, K., Zhang, H., Shi, Q.Q., Angelopoulos, V., 2013a. Poloidal ULF wave observed in the plasmasphere boundary layer. J. Geophys. Res.: Space Phys. 118 (7), 4298–4307. http://dx.doi.org/10.1002/jgra.50427, arXiv:https://agupubs.onlinelibrary.wiley.com/doi/pdf/10.1002/jgra.50427. URL: https://agupubs.onlinelibrary.wiley.com/doi/abs/10.1002/jgra.50427.

Liu, Y., Kistler, L.M., Mouikis, C.G., Klecker, B., Dandouras, I., 2013b. Heavy ion effects on substorm loading and unloading in the Earth's magnetotail. J. Geophys. Res.: Space Phys. 118 (5), 2101–2112, http://doi.wiley.com/10.1002/jgra.50240.

Liu, W., Sarris, T.E., Li, X., Ergun, R., Angelopoulos, V., Bonnell, J., Glassmeier, K.H., 2010. Solar wind influence on Pc4 and Pc5 ULF wave activity in the inner magnetosphere. J. Geophys. Res.: Space Phys. 115 (A12), A12201. http://dx.doi.org/10.1029/2010JA015299, arXiv:https://agupubs.onlinelibrary.wiley.com/doi/pdf/10.1029/2010JA015299.

Loi, S.T., Cairns, I.H., Murphy, T., Erickson, P.J., Bell, M.E., Rowlinson, A., Arora, B.S., Morgan, J., Ekers, R.D., Hurley-Walker, N., Kaplan, D.L., 2016. Density duct formation in the wake of a travelling ionospheric disturbance: Murchison Widefield Array observations. J. Geophys. Res.: Space Phys. 121 (2), 1569–1586. http://dx.doi.org/10.1002/2015JA022052, arXiv:https://agupubs.onlinelibrary.wiley.com/doi/pdf/10.1002/2015JA022052. URL: https://agupubs.onlinelibrary.wiley.com/doi/abs/10.1002/2015JA022052.

Loi, S.T., Murphy, T., Cairns, I.H., Menk, F.W., Waters, C.L., Erickson, P.J., Trott, C.M., Hurley-Walker, N., Morgan, J., Lenc, E., Offringa, A.R., Bell, M.E., Ekers, R.D., Gaensler, B.M., Lonsdale, C.J., Feng, L., Hancock, P.J., Kaplan, D.L., Bernardi, G., Bowman, J.D., Briggs, F., Cappallo, R.J., Deshpande, A.A., Greenhill, L.J., Hazelton, B.J., Johnston-Hollitt, M., McWhirter, S.R., Mitchell, D.A., Morales, M.F., Morgan, E., Oberoi, D., Ord, S.M., Prabu, T., Shankar, N.U., Srivani, K.S., Subrahmanyan, R., Tingay, S.J., Wayth, R.B., Webster, R.L., Williams, A., Williams, C.L., 2015. Real-time imaging of density ducts between the plasmasphere and ionosphere. Geophys. Res. Lett. 42 (10), 3707–3714. http://dx.doi.org/10.1002/2015GL063699, arXiv:https://agupubs.onlinelibrary.wiley.com/doi/pdf/10.1002/2015GL063699. URL: https://agupubs.onlinelibrary.wiley.com/doi/abs/10.1002/2015GL063699.

Lopez, R.E., 2016. The integrated dayside merging rate is controlled primarily by the solar wind. J. Geophys. Res.: Space Phys. 121 (5), 4435–4445. http://dx.doi.org/10.1002/2016JA022556, arXiv:https://agupubs.onlinelibrary.wiley.com/doi/pdf/10.1002/2016JA022556. URL: https://agupubs.onlinelibrary.wiley.com/doi/abs/10.1002/2016JA022556.

Loto'aniu, T.M., Singer, H.J., Waters, C.L., Angelopoulos, V., Mann, I.R., Elkington, S.R., Bonnell, J.W., 2010. Relativistic electron loss due to ultralow frequency waves and enhanced outward radial diffusion. J. Geophys. Res.: Space Phys. 115 (A12), A12245. http://dx.doi.org/10.1029/2010JA015755, arXiv:https://agupubs.onlinelibrary.wiley.com/doi/pdf/10.1029/2010JA015755. URL: https://agupubs.onlinelibrary.wiley.com/doi/abs/10.1029/2010JA015755.

Lui, A.T.Y., Meng, C.-I., Ismail, S., 1982. Large amplitude undulations on the equatorward boundary of the diffuse aurora. J. Geophys. Res.: Space Phys. 87 (A4), 2385–2400. http://dx.doi.org/10.1029/JA087iA04p02385, arXiv:https://agupubs.onlinelibrary.wiley.com/doi/pdf/10.1029/JA087iA04p02385. URL: https://agupubs.onlinelibrary.wiley.com/doi/abs/10.1029/JA087iA04p02385.

Lyons, L.R., Thorne, R.M., Kennel, C.F., 1972. Pitch-angle diffusion of radiation belt electrons within the plasmasphere. J. Geophys. Res. 77 (19), 3455–3474. http://dx.doi.org/10.1029/JA077i019p03455, arXiv:https://agupubs.onlinelibrary.wiley.com/doi/pdf/10.1029/JA077i019p03455. URL: https://agupubs.onlinelibrary.wiley.com/doi/abs/10.1029/JA077i019p03455.

MacDonald, E., Denton, M., Thomsen, M., Gary, S., 2008. Superposed epoch analysis of a whistler instability criterion at geosynchronous orbit during geomagnetic storms. J. Atmos. Sol.-Terr. Phys. 70 (14), 1789–1796. http://dx.doi.org/10.1016/j.jastp.2008.03.021, http://www.sciencedirect.com/science/article/pii/S1364682608000898. Dynamic Variability of Earth's Radiation Belts.

MacDonald, E.A., Donovan, E., Nishimura, Y., Case, N.A., Gillies, D.M., Gallardo-Lacourt, B., Archer, W.E., Spanswick, E.L., Bourassa, N., Connors, M., Heavner, M., Jackel, B., Kosar, B., Knudsen, D.J., Ratzlaff, C., Schofield, I., 2018. New science in plain sight: Citizen scientists lead to the discovery of optical structure in the upper atmosphere. Sci. Adv. 4 (3), eaaq0030. http://dx.doi.org/10.1126/sciadv.aaq0030, arXiv:https://advances.sciencemag.org/content/4/3/eaaq0030.full.pdf. URL: https://advances.sciencemag.org/content/4/3/eaaq0030.

Macúšová, E., Santolík, O., Décréau, P., Demekhov, A.G., Nunn, D., Gurnett, D.A., Pickett, J.S., Titova, E.E., Kozelov, B.V., Rauch, J.-L., Trotignon, J.-G., 2010. Observations of the relationship between frequency sweep rates of chorus wave packets and plasma density. J. Geophys. Res.: Space Phys. 115 (A12), A12257. http://dx.doi.org/10.1029/2010JA015468, arXiv:https://agupubs.onlinelibrary.wiley.com/doi/pdf/10.1029/2010JA015468. URL: https://agupubs.onlinelibrary.wiley.com/doi/abs/10.1029/2010JA015468.

Mager, P.N., Klimushkin, D.Y., Kostarev, D.V., 2013. Drift-compressional modes generated by inverted plasma distributions in the magnetosphere. J. Geophys. Res.: Space Phys. 118 (8), 4915–4923. http://dx.doi.org/10.1002/jgra.50471, arXiv:https://agupubs.onlinelibrary.wiley.com/doi/pdf/10.1002/jgra.50471. URL: https://agupubs.onlinelibrary.wiley.com/doi/abs/10.1002/jgra.50471.

Maggiolo, R., Kistler, L.M., 2014. Spatial variation in the plasma sheet composition: Dependence on geomagnetic and solar activity. J. Geophys. Res.: Space Phys. 119 (4), 2836–2857. http://dx.doi.org/10.1002/2013JA019517.

Mann, I.R., Usanova, M.E., Murphy, K., Robertson, M.T., Milling, D.K., Kale, A., Kletzing, C., Wygant, J., Thaller, S., Raita, T., 2014. Spatial localization and ducting of EMIC waves: Van Allen Probes and ground-based observations. Geophys. Res. Lett. 41 (3), 785–792. http://dx.doi.org/10.1002/2013GL058581, arXiv:https://agupubs.onlinelibrary.wiley.com/doi/pdf/10.1002/2013GL058581. URL: https://agupubs.onlinelibrary.wiley.com/doi/abs/10.1002/2013GL058581.

Mann, I.R., Wright, A.N., Mills, K.J., Nakariakov, V.M., 1999. Excitation of magnetospheric waveguide modes by magnetosheath flows. J. Geophys. Res.: Space Phys. 104 (A1), 333–353. http://dx.doi.org/10.1029/1998JA900026, arXiv:https://agupubs.onlinelibrary.wiley.com/doi/pdf/10.1029/1998JA900026. URL: https://agupubs.onlinelibrary.wiley.com/doi/abs/10.1029/1998JA900026.

Mantas, G.P., Carlson, H.C., Wickwar, V.B., 1978. Photoelectron flux buildup in the plasmasphere. J. Geophys. Res.: Space Phys. 83 (A1), 1–15. http://dx.doi.org/10.1029/JA083iA01p00001, arXiv:https://agupubs.onlinelibrary.wiley.com/doi/pdf/10.1029/JA083iA01p00001. URL: https://agupubs.onlinelibrary.wiley.com/doi/abs/10.1029/JA083iA01p00001.

Markidis, S., Lapenta, G., Bettarini, L., Goldman, M., Newman, D., Andersson, L., 2011. Kinetic simulations of magnetic reconnection in presence of a background O+ population. J. Geophys. Res.: Space Phys. 116 (9), 1–13. http://dx.doi.org/10.1029/2011JA016429.

Masson, A., Nykyri, K., 2018. Kelvin–Helmholtz Instability: Lessons Learned and Ways Forward. Space Sci. Rev. 214 (4), 71, https://doi.org/10.1007/s11214-018-0505-6.

Mathie, R.A., Mann, I.R., 2000. A correlation between extended intervals of ULF wave power and storm-time geosynchronous relativistic electron flux enhancements. Geophys. Res. Lett. 27 (20), 3261–3264. http://dx.doi.org/10.1029/2000GL003822, arXiv:https://agupubs.onlinelibrary.wiley.com/doi/pdf/10.1029/2000GL003822. URL: https://agupubs.onlinelibrary.wiley.com/doi/abs/10.1029/2000GL003822.

Mathie, R.A., Mann, I.R., 2001. On the solar wind control of Pc5 ULF pulsation power at mid-latitudes: Implications for MeV electron acceleration in the outer radiation belt. J. Geophys. Res.: Space Phys. 106 (A12), 29783–29796. http://dx.doi.org/10.1029/2001JA000002.

Matsui, H., Darrouzet, F., Goldstein, J., Puhl-Quinn, P.A., Khotyaintsev, Y.V., Lindqvist, P.-A., Georgescu, E., Mouikis, C.G., Torbert, R.B., 2012. Multi-spacecraft observations of small-scale fluctuations in density and fields in plasmaspheric plumes. Ann. Geophys. 30 (3), 623–637. http://dx.doi.org/10.5194/angeo-30-623-2012, https://www.ann-geophys.net/30/623/2012/.

Maxworth, A.S., Golkowski, M., 2017. Magnetospheric whistler mode ray tracing in a warm background plasma with finite electron and ion temperature. J. Geophys. Res.: Space Phys. 122 (7), 7323–7335. http://dx.doi.org/10.1002/2016JA023546, arXiv:https://agupubs.onlinelibrary.wiley.com/doi/pdf/10.1002/2016JA023546. URL: https://agupubs.onlinelibrary.wiley.com/doi/abs/10.1002/2016JA023546.

McEwen, D.J., Yee, E., Whalen, B.A., Yau, A.W., 1981. Electron energy measurements in pulsating auroras.. Can. J. Phys. 59, 1106–1115. http://dx.doi.org/10.1139/p81-146.

McPherron, R.L., 2005. Magnetic Pulsations: Their Sources and Relation to Solar Wind and Geomagnetic Activity. Surv. Geophys. 26 (5), 545–592. http://dx.doi.org/10.1007/s10712-005-1758-7.

Mendillo, M., Baumgardner, J., Providakes, J., 1989. Ground-based imaging of detached arcs, ripples in the diffuse aurora, and patches of 6300-Å emission. J. Geophys. Res.: Space Phys. 94 (A5), 5367–5381. http://dx.doi.org/10.1029/JA094iA05p05367.

Meredith, N.P., Cain, M., Horne, R.B., Thorne, R.M., Summers, D., Anderson, R.R., 2003a. Evidence for chorus-driven electron acceleration to relativistic energies from a survey of geomagnetically disturbed periods. J. Geophys. Res.: Space Phys. 108 (A6), 1248. http://dx.doi.org/10.1029/2002JA009764, arXiv:https://agupubs.onlinelibrary.wiley.com/doi/pdf/10.1029/2002JA009764. URL: https://agupubs.onlinelibrary.wiley.com/doi/abs/10.1029/2002JA009764.

Meredith, N.P., Horne, R.B., Iles, R.H.A., Thorne, R.M., Heynderickx, D., Anderson, R.R., 2002. Outer zone relativistic electron acceleration associated with substorm-enhanced whistler mode chorus. J. Geophys. Res.: Space Phys. 107 (A7), 1144. http://dx.doi.org/10.1029/2001JA900146, arXiv:https://agupubs.onlinelibrary.wiley.com/doi/pdf/10.1029/2001JA900146. URL: https://agupubs.onlinelibrary.wiley.com/doi/abs/10.1029/2001JA900146.

Meredith, N.P., Horne, R.B., Thorne, R.M., Anderson, R.R., 2003b. Favored regions for chorus-driven electron acceleration to relativistic energies in the Earth's outer radiation belt. Geophys. Res. Lett. 30 (16), 1871. http://dx.doi.org/10.1029/2003GL017698, arXiv:https://agupubs.onlinelibrary.wiley.com/doi/pdf/10.1029/2003GL017698. URL: https://agupubs.onlinelibrary.wiley.com/doi/abs/10.1029/2003GL017698.

Meredith, N.P., Thorne, R.M., Horne, R.B., Summers, D., Fraser, B.J., Anderson, R.R., 2003c. Statistical analysis of relativistic electron energies for cyclotron resonance with EMIC waves observed on CRRES. J. Geophys. Res.: Space Phys. 108 (A6), 1250. http://dx.doi.org/10.1029/2002JA009700, arXiv:https://agupubs.onlinelibrary.wiley.com/doi/pdf/10.1029/2002JA009700. URL: https://agupubs.onlinelibrary.wiley.com/doi/abs/10.1029/2002JA009700.

Min, K., Lee, J., Keika, K., Li, W., 2012. Global distribution of EMIC waves derived from THEMIS observations. J. Geophys. Res.: Space Phys. 117 (A5), A05219. http://dx.doi.org/10.1029/2012JA017515, arXiv:https://agupubs.onlinelibrary.wiley.com/doi/pdf/10.1029/2012JA017515. URL: https://agupubs.onlinelibrary.wiley.com/doi/abs/10.1029/2012JA017515.

Miura, A., Pritchett, P.L., 1982. Nonlocal stability analysis of the MHD Kelvin-Helmholtz instability in a compressible plasma. J. Geophys. Res. 87 (A9), 7431, http://doi.wiley.com/10.1029/JA087iA09p07431.

Miyoshi, Y., Oyama, S., Saito, S., Kurita, S., Fujiwara, H., Kataoka, R., Ebihara, Y., Kletzing, C., Reeves, G., Santolík, O., Clilverd, M., Rodger, C.J., Turunen, E., Tsuchiya, F., 2015. Energetic electron precipitation associated with pulsating aurora: EISCAT and Van Allen Probe observations. J. Geophys. Res.: Space Phys. 120 (4), 2754–2766. http://dx.doi.org/10.1002/2014JA020690, arXiv:https://agupubs.onlinelibrary.wiley.com/doi/pdf/10.1002/2014JA020690. URL: https://agupubs.onlinelibrary.wiley.com/doi/abs/10.1002/2014JA020690.

Moore, T.E., Chappell, C.R., Chandler, M.O., Fields, S.A., Pollock, C.J., Reasoner, D.L., Young, D.T., Burch, J.L., Eaker, N., Waite, J.H., McComas, D.J., Nordholdt, J.E., Thomsen, M.F., Berthelier, J.J., Robson, R., 1995. The Thermal Ion Dynamics Experiment and Plasma Source Instrument. Space Sci. Rev. 71 (1), 409–458, https://doi.org/10.1007/BF00751337.

Moore, T., Fok, M.-C., Garcia-Sage, K., 2014. The ionospheric outflow feedback loop. J. Atmos. Sol.-Terr. Phys. 115–116, 59–66. http://dx.doi.org/10.1016/j.jastp.2014.02.002, http://www.sciencedirect.com/science/article/pii/S1364682614000431. Sun-Earth System Exploration: Moderate and Extreme Disturbances.

Moore, T.E., Khazanov, G.V., 2010. Mechanisms of ionospheric mass escape. J. Geophys. Res.: Space Phys. 115 (A12), A00J13. http://dx.doi.org/10.1029/2009JA014905, arXiv:https://agupubs.onlinelibrary.wiley.com/doi/pdf/10.1029/2009JA014905. URL: https://agupubs.onlinelibrary.wiley.com/doi/abs/10.1029/2009JA014905.

Moore, T.E., Lundin, R., Alcayde, D., André, M., Ganguli, S.B., Temerin, M., Yau, A., 1999a. Source processes in the high-latitude ionosphere. Space Sci. Rev. 88 (1), 7–84, https://doi.org/10.1023/A:1005299616446.

Moore, T.E., Peterson, W.K., Russell, C.T., Chandler, M.O., Collier, M.R., Collin, H.L., Craven, P.D., Fitzenreiter, R., Giles, B.L., Pollock, C.J., 1999b. Ionospheric mass ejection in response to a CME. Geophys. Res. Lett. 26 (15), 2339–2342. http://dx.doi.org/10.1029/1999GL900456, arXiv:https://agupubs.onlinelibrary.wiley.com/doi/pdf/10.1029/1999GL900456. URL: https://agupubs.onlinelibrary.wiley.com/doi/abs/10.1029/1999GL900456.

Moore, T., Spann, J., 2017. Introduction: Particles and fields. J. Geophys. Res.: Space Phys. 122 (2), 1435–1436. http://dx.doi.org/10.1002/2017JA023887, arXiv:https://agupubs.onlinelibrary.wiley.com/doi/pdf/10.1002/2017JA023887. URL: https://agupubs.onlinelibrary.wiley.com/doi/abs/10.1002/2017JA023887.

Mott-Smith, H.M., Langmuir, I., 1926. The Theory of Collectors in Gaseous Discharges. Phys. Rev. 28, 727–763. http://dx.doi.org/10.1103/PhysRev.28.727, https://link.aps.org/doi/10.1103/PhysRev.28.727.

Mouikis, C.G., Kistler, L.M., Liu, Y.H., Klecker, B., Korth, A., Dandouras, I., 2010. H+ and O+ content of the plasma sheet at 15-19 Re as a function of geomagnetic and solar activity. J. Geophys. Res.: Space Phys. 115 (A12), A00J16, http://doi.wiley.com/10.1029/2010JA015978.

Mozer, F.S., Agapitov, O.A., Angelopoulos, V., Hull, A., Larson, D., Lejosne, S., McFadden, J.P., 2017b. Extremely field-aligned cool electrons in the dayside outer magnetosphere. Geophys. Res. Lett. 44 (1), 44–51. http://dx.doi.org/10.1002/2016GL072054.

Mozer, F.S., Agapitov, O.V., Hull, A., Lejosne, S., Vasko, I.Y., 2017a. Pulsating auroras produced by interactions of electrons and time domain structures. J. Geophys. Res. Space Phys. 122 (8), 8604–8616. http://dx.doi.org/10.1002/2017JA024223.

Murphree, J., Johnson, M., 1996. Clues to plasma processes based on Freja UV observations. Adv. Space Res. 18 (8), 95–105. http://dx.doi.org/10.1016/0273-1177(95)00973-6, http://www.sciencedirect.com/science/article/pii/0273117795009736 The Three-dimensional Magnetosphere.

Murphy, K.R., Mann, I.R., Ozeke, L.G., 2014. A ULF wave driver of ring current energization. Geophys. Res. Lett. 41 (19), 6595–6602. http://dx.doi.org/10.1002/2014GL061253, arXiv:https://agupubs.onlinelibrary.wiley.com/doi/pdf/10.1002/2014GL061253. URL: https://agupubs.onlinelibrary.wiley.com/doi/abs/10.1002/2014GL061253.

Nakamura, T.K.M., Hasegawa, H., Daughton, W., Eriksson, S., Li, W.Y., Nakamura, R., 2017. Turbulent mass transfer caused by vortex induced reconnection in collisionless magnetospheric plasmas. Nature Commun. 8 (1), 1582, https://doi.org/10.1038/s41467-017-01579-0.

Nemzek, R.J., Nakamura, R., Baker, D.N., Belian, R.D., McComas, D.J., Thomsen, M.F., Yamamoto, T., 1995. The relationship between pulsating auroras observed from the ground and energetic electrons and plasma density measured at geosynchronous orbit. J. Geophys. Res.: Space Phys. 100 (A12), 23935–23944. http://dx.doi.org/10.1029/95JA01756, arXiv:https://agupubs.onlinelibrary.wiley.com/doi/pdf/10.1029/95JA01756. URL: https://agupubs.onlinelibrary.wiley.com/doi/abs/10.1029/95JA01756.

Ni, B., Bortnik, J., Nishimura, Y., Thorne, R.M., Li, W., Angelopoulos, V., Ebihara, Y., Weatherwax, A.T., 2014. Chorus wave scattering responsible for the Earth's dayside diffuse auroral precipitation: A detailed case study. J. Geophys. Res.: Space Phys. 119 (2), 897–908. http://dx.doi.org/10.1002/2013JA019507, arXiv:https://agupubs.onlinelibrary.wiley.com/doi/pdf/10.1002/2013JA019507. URL: https://agupubs.onlinelibrary.wiley.com/doi/abs/10.1002/2013JA019507.

Nishimura, Y., Bortnik, J., Li, W., Liang, J., Thorne, R.M., Angelopoulos, V., Le Contel, O., Auster, U., Bonnell, J.W., 2015. Chorus intensity modulation driven by time-varying field-aligned low-energy plasma. J. Geophys. Res.: Space Phys. 120 (9), 7433–7446. http://dx.doi.org/10.1002/2015JA021330, arXiv:https://agupubs.onlinelibrary.wiley.com/doi/pdf/10.1002/2015JA021330. URL: https://agupubs.onlinelibrary.wiley.com/doi/abs/10.1002/2015JA021330.

Nishimura, Y., Bortnik, J., Li, W., Thorne, R.M., Lyons, L.R., Angelopoulos, V., Mende, S.B., Bonnell, J.W., Le Contel, O., Cully, C., Ergun, R., Auster, U., 2010. Identifying the Driver of Pulsating Aurora. Science 330 (6000), 81–84. http://dx.doi.org/10.1126/science.1193186, arXiv:https://science.sciencemag.org/content/330/6000/81.full.pdf. URL: https://science.sciencemag.org/content/330/6000/81.

Nishimura, Y., Bortnik, J., Li, W., Thorne, R.M., Ni, B., Lyons, L.R., Angelopoulos, V., Ebihara, Y., Bonnell, J.W., Le Contel, O., Auster, U., 2013. Structures of dayside whistler-mode waves deduced from conjugate diffuse aurora. J. Geophys. Res.: Space Phys. 118 (2), 664–673. http://dx.doi.org/10.1029/2012JA018242, arXiv:https://agupubs.onlinelibrary.wiley.com/doi/pdf/10.1029/2012JA018242. URL: https://agupubs.onlinelibrary.wiley.com/doi/abs/10.1029/2012JA018242.

Nishimura, Y., Gallardo-Lacourt, B., Zou, Y., Mishin, E., Knudsen, D.J., Donovan, E.F., Angelopoulos, V., Raybell, R., 2019. Magnetospheric Signatures of STEVE: Implications for the Magnetospheric Energy Source and Interhemispheric Conjugacy. Geophys. Res. Lett. 46 (11), 5637–5644. http://dx.doi.org/10.1029/2019GL082460, arXiv:https://agupubs.onlinelibrary.wiley.com/doi/pdf/10.1029/2019GL082460. URL: https://agupubs.onlinelibrary.wiley.com/doi/abs/10.1029/2019GL082460.

Nishimura, Y., Lessard, M.R., Katoh, Y., Miyoshi, Y., Grono, E., Partamies, N., Sivadas, N., Hosokawa, K., Fukizawa, M., Samara, M., Michell, R.G., Kataoka, R., Sakanoi, T., Whiter, D.K., Oyama, S.-i., Ogawa, Y., Kurita, S., 2020. Diffuse and Pulsating Aurora. Space Sci. Rev. 216 (1), 4, https://doi.org/10.1007/s11214-019-0629-3.

Nishitani, N., Hough, G., Scourfield, M.W.J., 1994. Spatial and temporal characteristics of giant undulations. Geophys. Res. Lett. 21 (24), 2673–2676. http://dx.doi.org/10.1029/94GL02240, arXiv:https://agupubs.onlinelibrary.wiley.com/doi/pdf/10.1029/94GL02240. URL: https://agupubs.onlinelibrary.wiley.com/doi/abs/10.1029/94GL02240.

Nishiyama, T., Sakanoi, T., Miyoshi, Y., Kataoka, R., Hampton, D., Katoh, Y., Asamura, K., Okano, S., 2012. Fine scale structures of pulsating auroras in the early recovery phase of substorm using ground-based EMCCD camera. J. Geophys. Res.: Space Phys. 117 (A10), A10229. http://dx.doi.org/10.1029/2012JA017921, arXiv:https://agupubs.onlinelibrary.wiley.com/doi/pdf/10.1029/2012JA017921.

Nosé, M., Ieda, A., Christon, S.P., 2009. Geotail observations of plasma sheet ion composition over 16 years: On variations of average plasma ion mass and O+ triggering substorm model. J. Geophys. Res.: Space Phys. 114 (A7), A07223. http://dx.doi.org/10.1029/2009JA014203, n/a–n/a. http://doi.wiley.com/10.1029/2009JA014203.

Nosé, M., Matsuoka, A., Kumamoto, A., Kasahara, Y., Teramoto, M., Kurita, S., Goldstein, J., Kistler, L.M., Singh, S., Gololobov, A., Shiokawa, K., Imajo, S., Oimatsu, S., Yamamoto, K., Obana, Y., Shoji, M., Tsuchiya, F., Shinohara, I., Miyoshi, Y., Kurth, W.S., Kletzing, C.A., Smith, C.W., MacDowall, R.J., Spence, H., Reeves, G.D., 2020. Oxygen torus and its coincidence with EMIC wave in the deep inner magnetosphere: Van Allen Probe B and Arase observations. Earth, Planets Space 72 (1), 111, https://doi.org/10.1186/s40623-020-01235-w.

Nosé, M., Oimatsu, S., Keika, K., Kletzing, C.A., Kurth, W.S., Pascuale, S.D., Smith, C.W., MacDowall, R.J., Nakano, S., Reeves, G.D., Spence, H.E., Larsen, B.A., 2015. Formation of the oxygen torus in the inner magnetosphere: Van Allen Probes observations. J. Geophys. Res.: Space Phys. 120 (2), 1182–1196. http://dx.doi.org/10.1002/2014JA020593, arXiv:https://agupubs.onlinelibrary.wiley.com/doi/pdf/10.1002/2014JA020593. URL: https://agupubs.onlinelibrary.wiley.com/doi/abs/10.1002/2014JA020593.

Nykyri, K., Otto, A., 2001. Plasma transport at the magnetospheric boundary due to reconnection in Kelvin-Helmholtz vortices. Geophys. Res. Lett. 28 (18), 3565–3568. http://dx.doi.org/10.1029/2001GL013239, arXiv:https://agupubs.onlinelibrary.wiley.com/doi/pdf/10.1029/2001GL013239. URL: https://agupubs.onlinelibrary.wiley.com/doi/abs/10.1029/2001GL013239.

Obana, Y., Menk, F.W., Yoshikawa, I., 2010. Plasma refilling rates for L = 2.3-3.8 flux tubes. J. Geophys. Res.: Space Phys. 115 (A3), A03204. http://dx.doi.org/10.1029/2009JA014191, arXiv:https://agupubs.onlinelibrary.wiley.com/doi/pdf/10.1029/2009JA014191. URL: https://agupubs.onlinelibrary.wiley.com/doi/abs/10.1029/2009JA014191.

Oguti, T., 1976. Recurrent Auroral Patterns. J. Geophys. Res. 81 (10), 1782–1786. http://dx.doi.org/10.1029/JA081i010p01782, arXiv:https://agupubs.onlinelibrary.wiley.com/doi/pdf/10.1029/JA081i010p01782. URL: https://agupubs.onlinelibrary.wiley.com/doi/abs/10.1029/JA081i010p01782.

Øieroset, M., Raeder, J., Phan, T.D., Wing, S., McFadden, J.P., Li, W., Fujimoto, M., Rème, H., Balogh, A., 2005. Global cooling and densification of the plasma sheet during an extended period of purely northward IMF on October 22-24, 2003. Geophys. Res. Lett. 32 (12), L12S07. http://dx.doi.org/10.1029/2004GL021523, arXiv:https://agupubs.onlinelibrary.wiley.com/doi/pdf/10.1029/2004GL021523. URL: https://agupubs.onlinelibrary.wiley.com/doi/abs/10.1029/2004GL021523.

Oliven, M.N., Gurnett, D.A., 1968. Microburst phenomena: 3. An association between microbursts and VLF chorus. J. Geophys. Res. 73 (7), 2355–2362. http://dx.doi.org/10.1029/JA073i007p02355, arXiv:https://agupubs.onlinelibrary.wiley.com/doi/pdf/10.1029/JA073i007p02355. URL: https://agupubs.onlinelibrary.wiley.com/doi/abs/10.1029/JA073i007p02355.

Omidi, N., Bortnik, J., Thorne, R., Chen, L., 2013. Impact of cold O+ ions on the generation and evolution of EMIC waves. J. Geophys. Res.: Space Phys. 118 (1), 434–445. http://dx.doi.org/10.1029/2012JA018319, arXiv:https://agupubs.onlinelibrary.wiley.com/doi/pdf/10.1029/2012JA018319. URL: https://agupubs.onlinelibrary.wiley.com/doi/abs/10.1029/2012JA018319.

Omidi, N., Thorne, R.M., Bortnik, J., 2010. Nonlinear evolution of EMIC waves in a uniform magnetic field: 1. Hybrid simulations. J. Geophys. Res.: Space Phys. 115 (A12), A12241. http://dx.doi.org/10.1029/2010JA015607, arXiv:https://agupubs.onlinelibrary.wiley.com/doi/pdf/10.1029/2010JA015607. URL: https://agupubs.onlinelibrary.wiley.com/doi/abs/10.1029/2010JA015607.

Østgaard, N., Stadsnes, J., Aarsnes, K., Søraas, F., Måseide, K., Smith, M., Sharber, J., 1998. Simultaneous measurements of X-rays and electrons during a pulsating aurora. Ann. Geophys. 16 (2), 148–160, https://doi.org/10.1007/s00585-998-0148-0.

Otto, A., Fairfield, D.H., 2000. Kelvin-Helmholtz instability at the magnetotail boundary: MHD simulation and comparison with Geotail observations. J. Geophys. Res.: Space Phys. 105 (A9), 21175–21190. http://dx.doi.org/10.1029/1999JA000312, arXiv:https://agupubs.onlinelibrary.wiley.com/doi/pdf/10.1029/1999JA000312. URL: https://agupubs.onlinelibrary.wiley.com/doi/abs/10.1029/1999JA000312.

Ouellette, J.E., Brambles, O.J., Lyon, J.G., Lotko, W., Rogers, B.N., 2013. Properties of outflow-driven sawtooth substorms. J. Geophys. Res.: Space Phys. 118 (6), 3223–3232. http://dx.doi.org/10.1002/jgra.50309, arXiv:https://agupubs.onlinelibrary.wiley.com/doi/pdf/10.1002/jgra.50309. URL: https://agupubs.onlinelibrary.wiley.com/doi/abs/10.1002/jgra.50309.

Ouellette, J.E., Lyon, J.G., Brambles, O.J., Zhang, B., Lotko, W., 2016. The effects of plasmaspheric plumes on dayside reconnection. J. Geophys. Res.: Space Phys. 121 (5), 4111–4118. http://dx.doi.org/10.1002/2016JA022597, arXiv:https://agupubs.onlinelibrary.wiley.com/doi/pdf/10.1002/2016JA022597. URL: https://agupubs.onlinelibrary.wiley.com/doi/abs/10.1002/2016JA022597.

Ozaki, M., Yagitani, S., Sawai, K., Shiokawa, K., Miyoshi, Y., Kataoka, R., Ieda, A., Ebihara, Y., Connors, M., Schofield, I., Katoh, Y., Otsuka, Y., Sunagawa, N., Jordanova, V.K., 2015. A direct link between chorus emissions and pulsating aurora on timescales from milliseconds to minutes: A case study at subauroral latitudes. J. Geophys. Res.: Space Phys. 120 (11), 9617–9631. http://dx.doi.org/10.1002/2015JA021381, arXiv:https://agupubs.onlinelibrary.wiley.com/doi/pdf/10.1002/2015JA021381. URL: https://agupubs.onlinelibrary.wiley.com/doi/abs/10.1002/2015JA021381.

Ozeke, L.G., Mann, I.R., 2008. Energization of radiation belt electrons by ring current ion driven ULF waves. J. Geophys. Res.: Space Phys. 113 (A2), A02201. http://dx.doi.org/10.1029/2007JA012468, arXiv:https://agupubs.onlinelibrary.wiley.com/doi/pdf/10.1029/2007JA012468. URL: https://agupubs.onlinelibrary.wiley.com/doi/abs/10.1029/2007JA012468.

Ozeke, L.G., Mann, I.R., Murphy, K.R., Rae, I.J., Milling, D.K., Elkington, S.R., Chan, A.A., Singer, H.J., 2012. ULF wave derived radiation belt radial diffusion coefficients. J. Geophys. Res.: Space Phys. 117 (A4), A04222. http://dx.doi.org/10.1029/2011JA017463, arXiv:https://agupubs.onlinelibrary.wiley.com/doi/pdf/10.1029/2011JA017463. URL: https://agupubs.onlinelibrary.wiley.com/doi/abs/10.1029/2011JA017463.

Ozhogin, P., Song, P., Tu, J., Reinisch, B.W., 2014. Evaluating the diffusive equilibrium models: Comparison with the IMAGE RPI field-aligned electron density measurements. J. Geophys. Res.: Space Phys. 119 (6), 4400–4411. http://dx.doi.org/10.1002/2014JA019982, arXiv:https://agupubs.onlinelibrary.wiley.com/doi/pdf/10.1002/2014JA019982. URL: https://agupubs.onlinelibrary.wiley.com/doi/abs/10.1002/2014JA019982.

Pahud, D., Rae, I., Mann, I., Murphy, K., Amalraj, V., 2009. Ground-based Pc5 ULF wave power: Solar wind speed and MLT dependence. J. Atmos. Sol.-Terr. Phys. 71 (10), 1082–1092. http://dx.doi.org/10.1016/j.jastp.2008.12.004, http://www.sciencedirect.com/science/article/pii/S1364682608003957 High Speed Solar Wind Streams and Geospace Interactions.

Park, C.G., 1970. Whistler observations of the interchange of ionization between the ionosphere and the protonosphere. J. Geophys. Res. 75 (22), 4249–4260. http://dx.doi.org/10.1029/JA075i022p04249, arXiv:https://agupubs.onlinelibrary.wiley.com/doi/pdf/10.1029/JA075i022p04249. URLL https://agupubs.onlinelibrary.wiley.com/doi/abs/10.1029/JA075i022p04249.

Park, C.G., Banks, P.M., 1974. Influence of thermal plasma flow on the mid-latitude nighttime F2 layer: Effects of electric fields and neutral winds inside the plasmasphere. J. Geophys. Res. 79 (31), 4661–4668. http://dx.doi.org/10.1029/JA079i031p04661, arXiv:https://agupubs.onlinelibrary.wiley.com/doi/pdf/10.1029/JA079i031p04661. URL: https://agupubs.onlinelibrary.wiley.com/doi/abs/10.1029/JA079i031p04661.

Park, C., Helliwell, R.A., 1971. The formation by electric fields of field-aligned irregularities in the magnetosphere. Radio Sci. 6 (2), 299–304.

Parker, E.N., 1973. The Reconnection Rate of Magnetic Fields. Astrophysical Journal 180, 247–252. http://dx.doi.org/10.1086/151959.

Partamies, N., Bolmgren, K., Heino, E., Ivchenko, N., Borovsky, J.E., Sundberg, H., 2019. Patch Size Evolution During Pulsating Aurora. J. Geophys. Res.: Space Phys. 124 (6), 4725–4738. http://dx.doi.org/10.1029/2018JA026423, arXiv:https://agupubs.onlinelibrary.wiley.com/doi/pdf/10.1029/2018JA026423. URL: https://agupubs.onlinelibrary.wiley.com/doi/abs/10.1029/2018JA026423.

Partamies, N., Weygand, J.M., Juusola, L., 2017a. Statistical study of auroral omega bands. Ann. Geophys. 35 (5), 1069–1083. http://dx.doi.org/10.5194/angeo-35-1069-2017, arXiv:1710.06688.

Partamies, N., Whiter, D., Kadokura, A., Kauristie, K., Nesse Tyssøy, H., Massetti, S., Stauning, P., Raita, T., 2017b. Occurrence and average behavior of pulsating aurora. J. Geophys. Res.: Space Phys. 122 (5), 5606–5618. http://dx.doi.org/10.1002/2017JA024039, arXiv:https://agupubs.onlinelibrary.wiley.com/doi/pdf/10.1002/2017JA024039. URL: https://agupubs.onlinelibrary.wiley.com/doi/abs/10.1002/2017JA024039.

Paschmann, G., Øieroset, M., Phan, T., 2013. In-Situ Observations of Reconnection in Space. Space Sci. Rev. 178 (2), 385–417, https://doi.org/10.1007/s11214-012-9957-2.

Peterson, W.K., Brain, D.A., Mitchell, D.L., Bailey, S.M., Chamberlin, P.C., 2013. Correlations between variations in solar EUV and soft X-ray irradiance and photoelectron energy spectra observed on Mars and Earth. J. Geophys. Res.: Space Phys. 118 (11), 7338–7347. http://dx.doi.org/10.1002/2013JA019251, arXiv:https://agupubs.onlinelibrary.wiley.com/doi/pdf/10.1002/2013JA019251. URL: https://agupubs.onlinelibrary.wiley.com/doi/abs/10.1002/2013JA019251.

Peterson, W.K., Stavros, E.N., Richards, P.G., Chamberlin, P.C., Woods, T.N., Bailey, S.M., Solomon, S.C., 2009. Photoelectrons as a tool to evaluate spectral variations in solar EUV irradiance over solar cycle timescales. J. Geophys. Res.: Space Phys. 114 (A10), A10304. http://dx.doi.org/10.1029/2009JA014362, arXiv:https://agupubs.onlinelibrary.wiley.com/doi/pdf/10.1029/2009JA014362. URL: https://agupubs.onlinelibrary.wiley.com/doi/abs/10.1029/2009JA014362.

Petschek, H.E., 1964. Magnetic Field Annihilation. In: NASA Special Publication, vol. 50. p. 425.

Phan, T.D., Lin, R.P., Fuselier, S.A., Fujimoto, M., 2000. Wind observations of mixed magnetosheath-plasma sheet ions deep inside the magnetosphere. J. Geophys. Res.: Space Phys. 105 (A3), 5497–5505. http://dx.doi.org/10.1029/1999JA900455, arXiv:https://agupubs.onlinelibrary.wiley.com/doi/pdf/10.1029/1999JA900455. URL: https://agupubs.onlinelibrary.wiley.com/doi/abs/10.1029/1999JA900455.

Pierrard, V., Goldstein, J., André, N., Jordanova, V.K., Kotova, G.A., Lemaire, J.F., Liemohn, M.W., Matsui, H., 2009. Recent Progress in Physics-Based Models of the Plasmasphere. Space Sci. Rev. 145 (1), 193–229, https://doi.org/10.1007/s11214-008-9480-7.

Pierrard, V., Lemaire, J.F., 2004. Development of shoulders and plumes in the frame of the interchange instability mechanism for plasmapause formation. Geophys. Res. Lett. 31 (5), L05809. http://dx.doi.org/10.1029/2003GL018919, arXiv:https://agupubs.onlinelibrary.wiley.com/doi/pdf/10.1029/2003GL018919. URL: https://agupubs.onlinelibrary.wiley.com/doi/abs/10.1029/2003GL018919.

Pilipenko, V., Belakhovsky, V., Murr, D., Fedorov, E., Engebretson, M., 2014. Modulation of total electron content by ULF Pc5 waves. J. Geophys. Res.: Space Phys. 119 (6), 4358–4369. http://dx.doi.org/10.1002/2013JA019594.

Pollock, C.J., Coffey, V.N., England, J.D., Martinez, N.G., Moore, T.E., Adrian, M.L., 2013. Thermal Electron Capped Hemisphere Spectrometer (TECHS) for Ionospheric Studies. In: Measurement Techniques in Space Plasmas: Particles. American Geophysical Union (AGU), pp. 201–207. http://dx.doi.org/10.1029/GM102p0201, arXiv:https://agupubs.onlinelibrary.wiley.com/doi/pdf/10.1029/GM102p0201. https://agupubs.onlinelibrary.wiley.com/doi/abs/10.1029/GM102p0201.

Poppe, A.R., Fillingim, M.O., Halekas, J.S., Raeder, J., Angelopoulos, V., 2016. ARTEMIS Observations of terrestrial ionospheric molecular ion outflow at the Moon. Geophys. Res. Lett. 43 (13), 6749–6758. http://dx.doi.org/10.1002/2016GL069715, arXiv:https://agupubs.onlinelibrary.wiley.com/doi/pdf/10.1002/2016GL069715. URL: https://agupubs.onlinelibrary.wiley.com/doi/abs/10.1002/2016GL069715.

Poulter, E., Allan, W., Bailey, G., 1988. ULF pulsation eigenperiods within the plasmasphere. Planet. Space Sci. 36 (2), 185–196. http://dx.doi.org/10.1016/0032-0633(88)90054-2, http://www.sciencedirect.com/science/article/pii/0032063388900542.

Providakes, J.F., Kelley, M.C., Swartz, W.E., Mendillo, M., Holt, J.M., 1989. Radar and optical measurements of ionospheric processes associated with intense subauroral electric fields. J. Geophys. Res.: Space Phys. 94 (A5), 5350–5366. http://dx.doi.org/10.1029/JA094iA05p05350, arXiv:https://agupubs.onlinelibrary.wiley.com/doi/pdf/10.1029/JA094iA05p05350. URL: https://agupubs.onlinelibrary.wiley.com/doi/abs/10.1029/JA094iA05p05350.

Rae, I.J., Watt, C.E.J., Fenrich, F.R., Mann, I.R., Ozeke, L.G., Kale, A., 2007. Energy deposition in the ionosphere through a global field line resonance. Ann. Geophys. 25 (12), 2529–2539.

Reinisch, B.W., Moldwin, M.B., Denton, R.E., Gallagher, D.L., Matsui, H., Pierrard, V., Tu, J., 2009. Augmented Empirical Models of Plasmaspheric Density and Electric Field Using IMAGE and CLUSTER Data. In: Darrouzet, F., De Keyser, J., Pierrard, V. (Eds.), The Earth's Plasmasphere: A CLUSTER and IMAGE Perspective. Springer New York, New York, NY, pp. 231–261. http://dx.doi.org/10.1007/978-1-4419-1323-4_8.

Richmond, A., 1973. Self-induced motions of thermal plasma in the magnetosphere and the stability of the plasmapause. Radio Sci. 8 (11), 1019–1027.

Ripoll, J.-F., Claudepierre, S.G., Ukhorskiy, A.Y., Colpitts, C., Li, X., Fennell, J.F., Crabtree, C., 2020. Particle Dynamics in the Earth's Radiation Belts: Review of Current Research and Open Questions. J. Geophys. Res.: Space Phys. 125 (5), e2019JA026735. http://dx.doi.org/10.1029/2019JA026735, arXiv:https://agupubs.onlinelibrary.wiley.com/doi/pdf/10.1029/2019JA026735. URL: https://agupubs.onlinelibrary.wiley.com/doi/abs/10.1029/2019JA026735.

Rodger, C.J., Carson, B.R., Cummer, S.A., Gamble, R.J., Clilverd, M.A., Green, J.C., Sauvaud, J.-A., Parrot, M., Berthelier, J.-J., 2010. Contrasting the efficiency of radiation belt losses caused by ducted and nonducted whistler-mode waves from ground-based transmitters. J. Geophys. Res.: Space Phys. 115 (A12), A12208. http://dx.doi.org/10.1029/2010JA015880, arXiv:https://agupubs.onlinelibrary.wiley.com/doi/pdf/10.1029/2010JA015880. URL: https://agupubs.onlinelibrary.wiley.com/doi/abs/10.1029/2010JA015880.

Rodger, C.J., Enell, C.-F., Turunen, E., Clilverd, M.A., Thomson, N.R., Verronen, P.T., 2007. Lightning-driven inner radiation belt energy deposition into the atmosphere: implications for ionisation-levels and neutral chemistry. Ann. Geophys. 25 (8), 1745–1757. http://dx.doi.org/10.5194/angeo-25-1745-2007, https://www.ann-geophys.net/25/1745/2007/.

Rodger, C.J., Thomson, N.R., Dowden, R.L., 1998. Are whistler ducts created by thunderstorm electrostatic fields?. J. Geophys. Res.: Space Phys. 103 (A2), 2163–2169. http://dx.doi.org/10.1029/97JA02927, arXiv:https://agupubs.onlinelibrary.wiley.com/doi/pdf/10.1029/97JA02927. URL: https://agupubs.onlinelibrary.wiley.com/doi/abs/10.1029/97JA02927.

Romanova, N., Pilipenko, V., Crosby, N.B., Khabarova, O.V., 2007. ULF Wave Index and Its Possible Applications in Space Physics. Bulgarian J. Phys. (34), 136.

Rosenbauer, H., Grünwaldt, H., Montgomery, M.D., Paschmann, G., Sckopke, N., 1975. Heos 2 plasma observations in the distant polar magnetosphere: The plasma mantle. J. Geophys. Res. 80 (19), 2723–2737. http://dx.doi.org/10.1029/JA080i019p02723, arXiv:https://agupubs.onlinelibrary.wiley.com/doi/pdf/10.1029/JA080i019p02723. URL: https://agupubs.onlinelibrary.wiley.com/doi/abs/10.1029/JA080i019p02723.

Rostoker, G., Skone, S., Baker, D.N., 1998. On the origin of relativistic electrons in the magnetosphere associated with some geomagnetic storms. Geophys. Res. Lett. 25 (19), 3701–3704. http://dx.doi.org/10.1029/98GL02801, arXiv:https://agupubs.onlinelibrary.wiley.com/doi/pdf/10.1029/98GL02801. URL: https://agupubs.onlinelibrary.wiley.com/doi/abs/10.1029/98GL02801.

Roux, A., Perraut, S., Rauch, J.L., de Villedary, C., Kremser, G., Korth, A., Young, D.T., 1982. Wave-particle interactions near Ω_{He^+} observed on board GEOS 1 and 2: 2. Generation of ion cyclotron waves and heating of He+ ions. J. Geophys. Res.: Space Phys. 87 (A10), 8174–8190. http://dx.doi.org/10.1029/JA087iA10p08174, arXiv:https://agupubs.onlinelibrary.wiley.com/doi/pdf/10.1029/JA087iA10p08174. URL: https://agupubs.onlinelibrary.wiley.com/doi/abs/10.1029/JA087iA10p08174.

Royrvik, O., Davis, T.N., 1977. Pulsating aurora: Local and global morphology. J. Geophys. Res. 82 (29), 4720–4740. http://dx.doi.org/10.1029/JA082i029p04720, arXiv:https://agupubs.onlinelibrary.wiley.com/doi/pdf/10.1029/JA082i029p04720. URL: https://agupubs.onlinelibrary.wiley.com/doi/abs/10.1029/JA082i029p04720.

Roytershteyn, V., Delzanno, G.L., 2021. Nonlinear coupling of whistler waves to oblique electrostatic turbulence enabled by cold plasma. Physics of Plasmas 28 (4), 042903, https://doi.org/10.1063/5.0041838.

Russell, C.T., Holzer, R.E., Smith, E.J., 1969. OGO 3 observations of ELF noise in the magnetosphere: 1. Spatial extent and frequency of occurrence. J. Geophys. Res. 74 (3), 755–777. http://dx.doi.org/10.1029/JA074i003p00755, arXiv:https://agupubs.onlinelibrary.wiley.com/doi/pdf/10.1029/JA074i003p00755. URL: https://agupubs.onlinelibrary.wiley.com/doi/abs/10.1029/JA074i003p00755.

Saikin, A.A., Zhang, J.-C., Allen, R.C., Smith, C.W., Kistler, L.M., Spence, H.E., Torbert, R.B., Kletzing, C.A., Jordanova, V.K., 2015. The occurrence and wave properties of H+-, He+-, and O+-band EMIC waves observed by the Van Allen Probes. J. Geophys. Res.: Space Phys. 120 (9), 7477–7492. http://dx.doi.org/10.1002/2015JA021358, arXiv:https://agupubs.onlinelibrary.wiley.com/doi/pdf/10.1002/2015JA021358. URL: https://agupubs.onlinelibrary.wiley.com/doi/abs/10.1002/2015JA021358.

Saito, S., Miyoshi, Y., Seki, K., 2012. Relativistic electron microbursts associated with whistler chorus rising tone elements: GEMSIS-RBW simulations. J. Geophys. Res.: Space Phys. 117 (A10), A10206. http://dx.doi.org/10.1029/2012JA018020, arXiv:https://agupubs.onlinelibrary.wiley.com/doi/pdf/10.1029/2012JA018020. URL: https://agupubs.onlinelibrary.wiley.com/doi/abs/10.1029/2012JA018020.

Samara, M., Michell, R.G., Khazanov, G.V., 2017. First optical observations of interhemispheric electron reflections within pulsating aurora. Geophys. Res. Lett. 44 (6), 2618–2623. http://dx.doi.org/10.1002/2017GL072794, arXiv:https://agupubs.onlinelibrary.wiley.com/doi/pdf/10.1002/2017GL072794. URL: https://agupubs.onlinelibrary.wiley.com/doi/abs/10.1002/2017GL072794.

Samir, U., Willmore, A., 1966. The equilibrium potential of a spacecraft in the ionosphere. Planet. Space Sci. 14 (11), 1131–1137.

Sandel, B.R., Goldstein, J., Gallagher, D.L., Spasojević, M., 2003. Extreme Ultraviolet Imager Observations of the Structure and Dynamics of the Plasmasphere. Space Sci. Rev. 109 (1), 25–46, https://doi.org/10.1023/B:SPAC.0000007511.47727.5b.

Santolík, O., Chum, J., 2009. The Origin of Plasmaspheric Hiss. Science 324 (5928), 729–730. http://dx.doi.org/10.1126/science.1172878, arXiv:https://science.sciencemag.org/content/324/5928/729.full.pdf. URL: https://science.sciencemag.org/content/324/5928/729.

Santolík, O., Gurnett, D.A., Pickett, J.S., Chum, J., Cornilleau-Wehrlin, N., 2009. Oblique propagation of whistler mode waves in the chorus source region. J. Geophys. Res.: Space Phys. 114 (A12), A00F03. http://dx.doi.org/10.1029/2009JA014586, arXiv:https://agupubs.onlinelibrary.wiley.com/doi/pdf/10.1029/2009JA014586. URL: https://agupubs.onlinelibrary.wiley.com/doi/abs/10.1029/2009JA014586.

Santolík, O., Gurnett, D.A., Pickett, J.S., Parrot, M., Cornilleau-Wehrlin, N., 2004. A microscopic and nanoscopic view of storm-time chorus on 31 March 2001. Geophys. Res. Lett. 31 (2), L02801. http://dx.doi.org/10.1029/2003GL018757, arXiv:https://agupubs.onlinelibrary.wiley.com/doi/pdf/10.1029/2003GL018757. URL: https://agupubs.onlinelibrary.wiley.com/doi/abs/10.1029/2003GL018757.

Sato, N., Wright, D.M., Carlson, C.W., Ebihara, Y., Sato, M., Saemundsson, T., Milan, S.E., Lester, M., 2004. Generation region of pulsating aurora obtained simultaneously by the FAST satellite and a Syowa-Iceland conjugate pair of observatories. J. Geophys. Res.: Space Phys. 109 (A10), A10201. http://dx.doi.org/10.1029/2004JA010419, arXiv:https://agupubs.onlinelibrary.wiley.com/doi/pdf/10.1029/2004JA010419. URL: https://agupubs.onlinelibrary.wiley.com/doi/abs/10.1029/2004JA010419.

Satyanarayana, P., Lee, Y.C., Huba, J.D., 1987. The stability of a stratified shear layer. Phys. Fluids 30 (1), 81–83. http://dx.doi.org/10.1063/1.866063.

Sauvaud, J.-A., Louarn, P., Fruit, G., Stenuit, H., Vallat, C., Dandouras, J., Rème, H., André, M., Balogh, A., Dunlop, M., Kistler, L., Möbius, E., Mouikis, C., Klecker, B., Parks, G.K., McFadden, J., Carlson, C., Marcucci, F., Pallocchia, G., Lundin, R., Korth, A., McCarthy, M., 2004. Case studies of the dynamics of ionospheric ions in the Earth's magnetotail. J. Geophys. Res.: Space Phys. 109 (A1), A01212. http://dx.doi.org/10.1029/2003JA009996, arXiv:https://agupubs.onlinelibrary.wiley.com/doi/pdf/10.1029/2003JA009996. URL: https://agupubs.onlinelibrary.wiley.com/doi/abs/10.1029/2003JA009996.

Sauvaud, J.-A., Walt, M., Delcourt, D., Benoist, C., Penou, E., Chen, Y., Russell, C.T., 2013. Inner radiation belt particle acceleration and energy structuring by drift resonance with ULF waves during geomagnetic storms. J. Geophys. Res.: Space Phys. 118 (4), 1723–1736. http://dx.doi.org/10.1002/jgra.50125, arXiv:https://agupubs.onlinelibrary.wiley.com/doi/pdf/10.1002/jgra.50125. URL: https://agupubs.onlinelibrary.wiley.com/doi/abs/10.1002/jgra.50125.

Schindler, K., 1974. A theory of the substorm mechanism. J. Geophys. Res. 79 (19), 2803–2810, http://doi.wiley.com/10.1029/JA079i019p02803.

Schmidt, R., Arends, H., Pedersen, A., Rüdenauer, F., Fehringer, M., Narheim, B.T., Svenes, R., Kvernsveen, K., Tsuruda, K., Mukai, T., Hayakawa, H., Nakamura, M., 1995. Results from active spacecraft potential control on the Geotail spacecraft. J. Geophys. Res.: Space Phys. 100 (A9), 17253–17259. http://dx.doi.org/10.1029/95JA01552, arXiv:https://agupubs.onlinelibrary.wiley.com/doi/pdf/10.1029/95JA01552. URL: https://agupubs.onlinelibrary.wiley.com/doi/abs/10.1029/95JA01552.

Schunk, R.W., Sojka, J.J., 1997. Global ionosphere-polar wind system during changing magnetic activity. J. Geophys. Res.: Space Phys. 102 (A6), 11625–11651. http://dx.doi.org/10.1029/97JA00292, arXiv:https://agupubs.onlinelibrary.wiley.com/doi/pdf/10.1029/97JA00292. URL: https://agupubs.onlinelibrary.wiley.com/doi/abs/10.1029/97JA00292.

Scourfield, M., Innes, W., Parsons, N., 1972. Spatial coherency in pulsating aurora. Planet. Space Sci. 20 (11), 1843–1848. http://dx.doi.org/10.1016/0032-0633(72)90117-1, http://www.sciencedirect.com/science/article/pii/0032063372901171.

Scourfield, M.W.J., Keys, J.G., Nielsen, E., Goertz, C.K., Collin, H., 1983. Evidence for the ExB drift of pulsating auroras. J. Geophys. Res.: Space Phys. 88 (A10), 7983–7988. http://dx.doi.org/10.1029/JA088iA10p07983, arXiv:https://agupubs.onlinelibrary.wiley.com/doi/pdf/10.1029/JA088iA10p07983. URL: https://agupubs.onlinelibrary.wiley.com/doi/abs/10.1029/JA088iA10p07983.

Seki, K., Elphic, R.C., Thomsen, M.F., Bonnell, J., Lund, E.J., Hirahara, M., Terasawa, T., Mukai, T., 2000. Cold flowing O+ beams in the lobe/mantle at Geotail: Does FAST observe the source?. J. Geophys. Res.: Space Phys. 105 (A7), 15931–15944. http://dx.doi.org/10.1029/1999JA900470, arXiv:https://agupubs.onlinelibrary.wiley.com/doi/pdf/10.1029/1999JA900470. URL: https://agupubs.onlinelibrary.wiley.com/doi/abs/10.1029/1999JA900470.

Seki, K., Hirahara, M., Hoshino, M., Terasawa, T., Elphic, R.C., Saito, Y., Mukai, T., Hayakawa, H., Kojima, H., Matsumoto, H., 2003. Cold ions in the hot plasma sheet of Earth's magnetotail. Nature 422 (6932), 589–592, https://doi.org/10.1038/nature01502.

Seki, K., Hirahara, M., Terasawa, T., Mukai, T., Saito, Y., Machida, S., Yamamoto, T., Kokubun, S., 1998. Statistical properties and possible supply mechanisms of tailward cold O+ beams in the lobe/mantle regions. J. Geophys. Res.: Space Phys. 103 (A3), 4477–4489. http://dx.doi.org/10.1029/97JA02137, arXiv:https://agupubs.onlinelibrary.wiley.com/doi/pdf/10.1029/97JA02137. URL: https://agupubs.onlinelibrary.wiley.com/doi/abs/10.1029/97JA02137.

Sharp, R., Lennartsson, W., Strangeway, R.J., 1985. The ionospheric contribution to the plasma environment in near-earth space. Radio Sci. 20 (3), 456–462.

Shay, M.A., Swisdak, M., 2004. Three-Species Collisionless Reconnection: Effect of O+ on Magnetotail Reconnection. Phys. Rev. Lett. 93 (17), 175001. http://dx.doi.org/10.1103/PhysRevLett.93.175001, https://link.aps.org/doi/10.1103/PhysRevLett.93.175001.

Shelley, E.G., Johnson, R.G., Sharp, R.D., 1972. Satellite observations of energetic heavy ions during a geomagnetic storm. J. Geophys. Res. 77 (31), 6104–6110. http://dx.doi.org/10.1029/JA077i031p06104, arXiv:https://agupubs.onlinelibrary.wiley.com/doi/pdf/10.1029/JA077i031p06104. URL: https://agupubs.onlinelibrary.wiley.com/doi/abs/10.1029/JA077i031p06104.

Shen, X.C., Zong, Q.-G., Shi, Q.Q., Tian, A.M., Sun, W.J., Wang, Y.F., Zhou, X.Z., Fu, S.Y., Hartinger, M.D., Angelopoulos, V., 2015. Magnetospheric ULF waves with increasing amplitude related to solar wind dynamic pressure changes: The Time History of Events and Macroscale Interactions during Substorms (THEMIS) observations. J. Geophys. Res.: Space Phys. 120 (9), 7179–7190. http://dx.doi.org/10.1002/2014JA020913, arXiv:https://agupubs.onlinelibrary.wiley.com/doi/pdf/10.1002/2014JA020913. URL: https://agupubs.onlinelibrary.wiley.com/doi/abs/10.1002/2014JA020913.

Shprits, Y.Y., Elkington, S.R., Meredith, N.P., Subbotin, D.A., 2008. Review of modeling of losses and sources of relativistic electrons in the outer radiation belt I: Radial transport. J. Atmos. Sol.-Terr. Phys. 70 (14), 1679–1693. http://dx.doi.org/10.1016/j.jastp.2008.06.008, http://www.sciencedirect.com/science/article/pii/S1364682608001648 Dynamic Variability of Earth's Radiation Belts.

Singer, H.J., Russell, C.T., Kivelson, M.G., Greenstadt, E.W., Olson, J.V., 1977. Evidence for the control of Pc 3,4 magnetic pulsations by the solar wind velocity. Geophys. Res. Lett. 4 (9), 377–379. http://dx.doi.org/10.1029/GL004i009p00377, arXiv:https://agupubs.onlinelibrary.wiley.com/doi/pdf/10.1029/GL004i009p00377. URL: https://agupubs.onlinelibrary.wiley.com/doi/abs/10.1029/GL004i009p00377.

Singh, K.K., Sheikh, S.A., Singh, A.K., Ahmad, F., Lalmani, 2013. Estimation of duct-lifetimes for storm-time low latitude whistlers observed at Srinagar, India. Indian J. Phys. 87 (6), 499–505, https://doi.org/10.1007/s12648-013-0274-8.

Sojka, J.J., Wrenn, G.L., 1985. Refilling of geosynchronous flux tubes as observed at the equator by GEOS 2. J. Geophys. Res.: Space Phys. 90 (A7), 6379–6385. http://dx.doi.org/10.1029/JA090iA07p06379, arXiv:https://agupubs.onlinelibrary.wiley.com/doi/pdf/10.1029/JA090iA07p06379. URL: https://agupubs.onlinelibrary.wiley.com/doi/abs/10.1029/JA090iA07p06379.

Sonwalkar, V.S., Inan, U.S., 1989. Lightning as an embryonic source of VLF hiss. J. Geophys. Res.: Space Phys. 94 (A6), 6986–6994. http://dx.doi.org/10.1029/JA094iA06p06986, arXiv:https://agupubs.onlinelibrary.wiley.com/doi/pdf/10.1029/JA094iA06p06986. URL: https://agupubs.onlinelibrary.wiley.com/doi/abs/10.1029/JA094iA06p06986.

Spasojević, M., Frey, H.U., Thomsen, M.F., Fuselier, S.A., Gary, S.P., Sandel, B.R., Inan, U.S., 2004. The link between a detached subauroral proton arc and a plasmaspheric plume. Geophys. Res. Lett. 31 (4), L04803. http://dx.doi.org/10.1029/2003GL018389, arXiv:https://agupubs.onlinelibrary.wiley.com/doi/pdf/10.1029/2003GL018389. URL: https://agupubs.onlinelibrary.wiley.com/doi/abs/10.1029/2003GL018389.

Spasojević, M., Goldstein, J., Carpenter, D.L., Inan, U.S., Sandel, B.R., Moldwin, M.B., Reinisch, B.W., 2003. Global response of the plasmasphere to a geomagnetic disturbance. J. Geophys. Res.: Space Phys. 108 (A9), 1340. http://dx.doi.org/10.1029/2003JA009987, arXiv:https://agupubs.onlinelibrary.wiley.com/doi/pdf/10.1029/2003JA009987. URL: https://agupubs.onlinelibrary.wiley.com/doi/abs/10.1029/2003JA009987.

Starks, M.J., Albert, J.M., Ling, A.G., O'Malley, S., Quinn, R.A., 2020. VLF Transmitters and Lightning-Generated Whistlers: 1. Modeling Waves From Source to Space. J. Geophys. Res.: Space Phys. 125 (3), e2019JA027029. http://dx.doi.org/10.1029/2019JA027029, arXiv:https://agupubs.onlinelibrary.wiley.com/doi/pdf/10.1029/2019JA027029. URL: https://agupubs.onlinelibrary.wiley.com/doi/abs/10.1029/2019JA027029.

Starks, M.J., Quinn, R.A., Ginet, G.P., Albert, J.M., Sales, G.S., Reinisch, B.W., Song, P., 2008. Illumination of the plasmasphere by terrestrial very low frequency transmitters: Model validation. J. Geophys. Res.: Space Phys. 113 (A9), A09320. http://dx.doi.org/10.1029/2008JA013112, arXiv:https://agupubs.onlinelibrary.wiley.com/doi/pdf/10.1029/2008JA013112. URL: https://agupubs.onlinelibrary.wiley.com/doi/abs/10.1029/2008JA013112.

Strangeway, R.J., Ergun, R.E., Su, Y.-J., Carlson, C.W., Elphic, R.C., 2005. Factors controlling ionospheric outflows as observed at intermediate altitudes. J. Geophys. Res.: Space Phys. 110 (A3), A03221. http://dx.doi.org/10.1029/2004JA010829, arXiv:https://agupubs.onlinelibrary.wiley.com/doi/pdf/10.1029/2004JA010829. URL: https://agupubs.onlinelibrary.wiley.com/doi/abs/10.1029/2004JA010829.

Su, Y.-J., Horwitz, J.L., Wilson, G.R., Richards, P.G., Brown, D.G., Ho, C.W., 1998. Self-consistent simulation of the photoelectron-driven polar wind from 120 km to 9 R_E altitude. J. Geophys. Res.: Space Phys. 103 (A2), 2279–2296. http://dx.doi.org/10.1029/97JA03085.

Su, S.-Y., McPherron, R., Konradi, A., Fritz, T., 1980. Observations of ULF oscillations in the ion fluxes at small pitch angles with ATS 6. J. Geophys. Res.: Space Phys. 85 (A2), 515–522. http://dx.doi.org/10.1029/JA085iA02p00515, arXiv:https://agupubs.onlinelibrary.wiley.com/doi/pdf/10.1029/JA085iA02p00515. URL: https://agupubs.onlinelibrary.wiley.com/doi/abs/10.1029/JA085iA02p00515.

Summers, D., Thorne, R.M., Xiao, F., 1998. Relativistic theory of wave-particle resonant diffusion with application to electron acceleration in the magnetosphere. J. Geophys. Res.: Space Phys. 103 (A9), 20487–20500. http://dx.doi.org/10.1029/98JA01740.

Suszcynsky, D.M., Borovsky, J.E., Thomsen, M.F., McComas, D.J., Belian, R.D., 1997. Coordinated ground-based and geosynchronous satellite-based measurements of auroral pulsations. In: Ivchenko, V.N. (Ed.), 23rd European Meeting on Atmospheric Studies By Optical Methods. 3237, SPIE, pp. 2–7, https://doi.org/10.1117/12.284757.

Swanson, D., 2003. Plasma Waves. In: Series in Plasma Physics, Taylor & Francis, https://books.google.com/books?id=l2X95_N6qk0C.

Takahashi, K., Denton, R.E., Hirahara, M., Min, K., Ohtani, S.-i., Sanchez, E., 2014. Solar cycle variation of plasma mass density in the outer magnetosphere: Magnetoseismic analysis of toroidal standing Alfvén waves detected by Geotail. J. Geophys. Res.: Space Phys. 119 (10), 8338–8356. http://dx.doi.org/10.1002/2014JA020274, arXiv:https://agupubs.onlinelibrary.wiley.com/doi/pdf/10.1002/2014JA020274. URL: https://agupubs.onlinelibrary.wiley.com/doi/abs/10.1002/2014JA020274.

Takahashi, K., Denton, R.E., Singer, H.J., 2010. Solar cycle variation of geosynchronous plasma mass density derived from the frequency of standing Alfvén waves. J. Geophys. Res.: Space Phys. 115 (A7), A07207. http://dx.doi.org/10.1029/2009JA015243, arXiv:https://agupubs.onlinelibrary.wiley.com/doi/pdf/10.1029/2009JA015243. URL: https://agupubs.onlinelibrary.wiley.com/doi/abs/10.1029/2009JA015243.

Tam, S.W.Y., Yasseen, F., Chang, T., 1998. Further development in theory/data closure of the photoelectron-driven polar wind and day-night transition of the outflow. Ann. Geophys. 16 (8), 948–968, https://doi.org/10.1007/s00585-998-0948-2.

Tao, X., Chen, L., Liu, X., Lu, Q., Wang, S., 2017. Quasilinear analysis of saturation properties of broadband whistler mode waves. Geophys. Res. Lett. 44 (16), 8122–8129. http://dx.doi.org/10.1002/2017GL074881, arXiv:https://agupubs.onlinelibrary.wiley.com/doi/pdf/10.1002/2017GL074881. URL: https://agupubs.onlinelibrary.wiley.com/doi/abs/10.1002/2017GL074881.

Terasawa, T., Fujimoto, M., Mukai, T., Shinohara, I., Saito, Y., Yamamoto, T., Machida, S., Kokubun, S., Lazarus, A.J., Steinberg, J.T., Lepping, R.P., 1997. Solar wind control of density and temperature in the near-Earth plasma sheet: WIND/GEOTAIL Collaboration. Geophys. Res. Lett. 24 (8), 935–938. http://dx.doi.org/10.1029/96GL04018, arXiv:https://agupubs.onlinelibrary.wiley.com/doi/pdf/10.1029/96GL04018. URL: https://agupubs.onlinelibrary.wiley.com/doi/abs/10.1029/96GL04018.

Thomsen, M.F., Borovsky, J.E., Skoug, R.M., Smith, C.W., 2003. Delivery of cold, dense plasma sheet material into the near-Earth region. J. Geophys. Res.: Space Phys. 108 (A4), 1151. http://dx.doi.org/10.1029/2002JA009544, arXiv:https://agupubs.onlinelibrary.wiley.com/doi/pdf/10.1029/2002JA009544. URL: https://agupubs.onlinelibrary.wiley.com/doi/abs/10.1029/2002JA009544.

Thomsen, M.F., Henderson, M.G., Jordanova, V.K., 2013. Statistical properties of the surface-charging environment at geosynchronous orbit. Space Weather 11 (5), 237–244. http://dx.doi.org/10.1002/swe.20049, arXiv:https://agupubs.onlinelibrary.wiley.com/doi/pdf/10.1002/swe.20049. URL: https://agupubs.onlinelibrary.wiley.com/doi/abs/10.1002/swe.20049.

Thomson, R., 1978. The formation and lifetime of whistler ducts. Planet. Space Sci. 26 (5), 423–430. http://dx.doi.org/10.1016/0032-0633(78)90064-8, http://www.sciencedirect.com/science/article/pii/0032063378900648.

Thorne, R.M., 2010. Radiation belt dynamics: The importance of wave-particle interactions. Geophys. Res. Lett. 37 (22), L22107. http://dx.doi.org/10.1029/2010GL044990, arXiv:https://agupubs.onlinelibrary.wiley.com/doi/pdf/10.1029/

2010GL044990. URL: https://agupubs.onlinelibrary.wiley.com/doi/abs/10.1029/2010GL044990.

Thorne, R.M., Horne, R.B., 1992. The contribution of ion-cyclotron waves to electron heating and SAR-arc excitation near the storm-time plasmapause. Geophys. Res. Lett. 19 (4), 417–420. http://dx.doi.org/10.1029/92GL00089, arXiv:https://agupubs.onlinelibrary.wiley.com/doi/pdf/10.1029/92GL00089. URL: https://agupubs.onlinelibrary.wiley.com/doi/abs/10.1029/92GL00089.

Thorne, R.M., O'Brien, T.P., Shprits, Y.Y., Summers, D., Horne, R.B., 2005. Timescale for MeV electron microburst loss during geomagnetic storms. J. Geophys. Res.: Space Phys. 110 (A9), A09202. http://dx.doi.org/10.1029/2004JA010882, arXiv:https://agupubs.onlinelibrary.wiley.com/doi/pdf/10.1029/2004JA010882. URL: https://agupubs.onlinelibrary.wiley.com/doi/abs/10.1029/2004JA010882.

Thorne, R.M., Smith, E.J., Burton, R.K., Holzer, R.E., 1973. Plasmaspheric hiss. J. Geophys. Res. 78 (10), 1581–1596. http://dx.doi.org/10.1029/JA078i010p01581, arXiv:https://agupubs.onlinelibrary.wiley.com/doi/pdf/10.1029/JA078i010p01581. URL: https://agupubs.onlinelibrary.wiley.com/doi/abs/10.1029/JA078i010p01581.

Toledo-Redondo, S., André, M., Khotyaintsev, Y.V., Lavraud, B., Vaivads, A., Graham, D.B., Li, W., Perrone, D., Fuselier, S., Gershman, D.J., Aunai, N., Dargent, J., Giles, B., Le Contel, O., Lindqvist, P.-A., Ergun, R.E., Russell, C.T., Burch, J.L., 2017. Energy budget and mechanisms of cold ion heating in asymmetric magnetic reconnection. J. Geophys. Res.: Space Phys. 122 (9), 9396–9413. http://dx.doi.org/10.1002/2017JA024553, arXiv:https://agupubs.onlinelibrary.wiley.com/doi/pdf/10.1002/2017JA024553. URL: https://agupubs.onlinelibrary.wiley.com/doi/abs/10.1002/2017JA024553.

Toledo-Redondo, S., Dargent, J., Aunai, N., Lavraud, B., André, M., Li, W., Giles, B., Lindqvist, P.-A., Ergun, R.E., Russell, C.T., Burch, J.L., 2018. Perpendicular Current Reduction Caused by Cold Ions of Ionospheric Origin in Magnetic Reconnection at the Magnetopause: Particle-in-Cell Simulations and Spacecraft Observations. Geophys. Res. Lett. 45 (19), 10,033–10,042. http://dx.doi.org/10.1029/2018GL079051, arXiv:https://agupubs.onlinelibrary.wiley.com/doi/pdf/10.1029/2018GL079051. URL: https://agupubs.onlinelibrary.wiley.com/doi/abs/10.1029/2018GL079051.

Toledo-Redondo, S., Vaivads, A., André, M., Khotyaintsev, Y.V., 2015. Modification of the Hall physics in magnetic reconnection due to cold ions at the Earth's magnetopause. Geophys. Res. Lett. 42 (15), 6146–6154. http://dx.doi.org/10.1002/2015GL065129, arXiv:https://agupubs.onlinelibrary.wiley.com/doi/pdf/10.1002/2015GL065129. URL: https://agupubs.onlinelibrary.wiley.com/doi/abs/10.1002/2015GL065129.

Torkar, K., Nakamura, R., Tajmar, M., Scharlemann, C., Jeszenszky, H., Laky, G., Fremuth, G., Escoubet, C.P., Svenes, K., 2016. Active Spacecraft Potential Control Investigation. Space Sci. Rev. 199 (1), 515–544, https://doi.org/10.1007/s11214-014-0049-3.

Torkar, K., Riedler, W., Escoubet, C.P., Fehringer, M., Schmidt, R., Grard, R.J.L., Arends, H., Rüdenauer, F., Steiger, W., Narheim, B.T., Svenes, K., Torbert, R., André, M., Fazakerley, A., Goldstein, R., Olsen, R.C., Pedersen, A., Whipple, E., Zhao, H., 2001. Active spacecraft potential control for Cluster – implementation and first results. Ann. Geophys. 19 (10/12), 1289–1302. http://dx.doi.org/10.5194/angeo-19-1289-2001, https://angeo.copernicus.org/articles/19/1289/2001/.

Tracy, E.R., Brizard, A.J., Richardson, A.S., Kaufman, A.N., 2014. Ray Tracing and Beyond: Phase Space Methods in Plasma Wave Theory. Cambridge University Press, http://dx.doi.org/10.1017/CBO9780511667565.

Tsurutani, B.T., Gonzalez, W.D., 1995. The efficiency of "viscous interaction" between the solar wind and the magnetosphere during intense northward IMF events. Geophys. Res. Lett. 22 (6), 663–666. http://dx.doi.org/10.1029/95GL00205, arXiv:https://agupubs.onlinelibrary.wiley.com/doi/pdf/10.1029/95GL00205. URL: https://agupubs.onlinelibrary.wiley.com/doi/abs/10.1029/95GL00205.

Tsurutani, B.T., Smith, E.J., 1974. Postmidnight chorus: A substorm phenomenon. J. Geophys. Res. 79 (1), 118–127. http://dx.doi.org/10.1029/JA079i001p00118, arXiv:https://agupubs.onlinelibrary.wiley.com/doi/pdf/10.1029/JA079i001p00118. URL: https://agupubs.onlinelibrary.wiley.com/doi/abs/10.1029/JA079i001p00118.

Turunen, E., Kero, A., Verronen, P.T., Miyoshi, Y., Oyama, S.-I., Saito, S., 2016. Mesospheric ozone destruction by high-energy electron precipitation associated with pulsating aurora. J. Geophys. Res.: Atmos. 121 (19), 11,852–11,861. http://dx.doi.org/10.1002/2016JD025015, arXiv:https://agupubs.onlinelibrary.wiley.com/doi/pdf/10.1002/2016JD025015. URL: https://agupubs.onlinelibrary.wiley.com/doi/abs/10.1002/2016JD025015.

Usanova, M.E., Darrouzet, F., Mann, I.R., Bortnik, J., 2013. Statistical analysis of EMIC waves in plasmaspheric plumes from Cluster observations. J. Geophys. Res.: Space Phys. 118 (8), 4946–4951. http://dx.doi.org/10.1002/jgra.50464, arXiv:https://agupubs.onlinelibrary.wiley.com/doi/pdf/10.1002/jgra.50464. URL: https://agupubs.onlinelibrary.wiley.com/doi/abs/10.1002/jgra.50464.

Usanova, M.E., Mann, I.R., Bortnik, J., Shao, L., Angelopoulos, V., 2012. THEMIS observations of electromagnetic ion cyclotron wave occurrence: Dependence on AE, SYMH, and solar wind dynamic pressure. J. Geophys. Res.: Space Phys. 117 (A10), A10218. http://dx.doi.org/10.1029/2012JA018049, arXiv:https://agupubs.onlinelibrary.wiley.com/doi/pdf/10.1029/2012JA018049. URL: https://agupubs.onlinelibrary.wiley.com/doi/abs/10.1029/2012JA018049.

Usanova, M.E., Mann, I.R., Darrouzet, F., 2016. EMIC Waves in the Inner Magnetosphere. In: Washington DC American Geophysical Union Geophysical Monograph Series, vol. 216, pp. 65–78. http://dx.doi.org/10.1002/9781119055006.ch5.

Usanova, M.E., Mann, I.R., Kale, Z.C., Rae, I.J., Sydora, R.D., Sandanger, M., Søraas, F., Glassmeier, K.-H., Fornacon, K.-H., Matsui, H., Puhl-Quinn, P.A., Masson, A., Vallières, X., 2010. Conjugate ground and multisatellite observations of compression-related EMIC Pc1 waves and associated proton precipitation. J. Geophys. Res.: Space Phys. 115 (A7), A07208. http://dx.doi.org/10.1029/2009JA014935, arXiv:https://agupubs.onlinelibrary.wiley.com/doi/pdf/10.1029/2009JA014935. URL: https://agupubs.onlinelibrary.wiley.com/doi/abs/10.1029/2009JA014935.

Varney, R.H., Swartz, W.E., Hysell, D.L., Huba, J.D., 2012. SAMI2-PE: A model of the ionosphere including multistream interhemispheric photoelectron transport. J. Geophys. Res.: Space Phys. 117 (A6), A06322. http://dx.doi.org/10.1029/2011JA017280, arXiv:https://agupubs.onlinelibrary.wiley.com/doi/pdf/10.1029/2011JA017280. URL: https://agupubs.onlinelibrary.wiley.com/doi/abs/10.1029/2011JA017280.

Vassiliadis, D., Mann, I., Fung, S., Shao, X., 2007. Ground Pc3-Pc5 wave power distribution and response to solar wind velocity variations. Planet. Space Sci. 55 (6), 743–754. http://dx.doi.org/10.1016/j.pss.2006.03.012, http://www.sciencedirect.com/science/article/pii/S003206330600290X. Ultra-Low Frequency Waves in the Magnetosphere.

Viñas, A.F., Madden, T.R., 1986. Shear flow-ballooning instability as a possible mechanism for hydromagnetic fluctuations. J. Geophys. Res.: Space Phys. 91 (A2), 1519–1528. http://dx.doi.org/10.1029/JA091iA02p01519, arXiv:https://agupubs.onlinelibrary.wiley.com/doi/pdf/10.1029/JA091iA02p01519. URL: https://agupubs.onlinelibrary.wiley.com/doi/abs/10.1029/JA091iA02p01519.

Viall, N.M., Kepko, L., Spence, H.E., 2009. Relative occurrence rates and connection of discrete frequency oscillations in the solar wind density and dayside magnetosphere. J. Geophys. Res.: Space Phys. 114 (A1), A01201. http://dx.doi.org/10.1029/2008JA013334, arXiv:https://agupubs.onlinelibrary.wiley.com/doi/pdf/10.1029/2008JA013334. URL: https://agupubs.onlinelibrary.wiley.com/doi/abs/10.1029/2008JA013334.

Vorontsova, E., Pilipenko, V., Fedorov, E., Sinha, A., Vichare, G., 2016. Modulation of total electron content by global Pc5 waves at low latitudes. Adv. Space Res. 57 (1), 309–319. http://dx.doi.org/10.1016/j.asr.2015.10.041, http://www.sciencedirect.com/science/article/pii/S0273117715007607.

Walker, A., 1998. Excitation of magnetohydrodynamic cavities in the magnetosphere. J. Atmos. Sol.-Terr. Phys. 60 (13), 1279–1293. http://dx.doi.org/10.1016/S1364-6826(98)00077-7, http://www.sciencedirect.com/science/article/pii/S1364682698000777.

Walsh, B.M., Foster, J.C., Erickson, P.J., Sibeck, D.G., 2014. Simultaneous Ground- and Space-Based Observations of the Plasmaspheric Plume and Reconnection. Science 343 (6175), 1122–1125. http://dx.doi.org/10.1126/science.1247212, arXiv:https://science.sciencemag.org/content/343/6175/1122.full.pdf. URL: https://science.sciencemag.org/content/343/6175/1122.

Walsh, B.M., Sibeck, D.G., Nishimura, Y., Angelopoulos, V., 2013. Statistical analysis of the plasmaspheric plume at the magnetopause. J. Geophys. Res.: Space Phys. 118 (8), 4844–4851. http://dx.doi.org/10.1002/jgra.50458, arXiv:https://agupubs.onlinelibrary.wiley.com/doi/pdf/10.1002/jgra.50458. URL: https://agupubs.onlinelibrary.wiley.com/doi/abs/10.1002/jgra.50458.

Walsh, B.M., Thomas, E.G., Hwang, K.-J., Baker, J.B.H., Ruohoniemi, J.M., Bonnell, J.W., 2015. Dense plasma and Kelvin-Helmholtz waves at Earth's dayside magnetopause. J. Geophys. Res.: Space Phys. 120 (7), 5560–5573. http://dx.doi.org/10.1002/2015JA021014, arXiv:https://agupubs.onlinelibrary.wiley.com/doi/pdf/10.1002/2015JA021014. URL: https://agupubs.onlinelibrary.wiley.com/doi/abs/10.1002/2015JA021014.

Walt, M., 1994. Introduction to Geomagnetically Trapped Radiation. In: Cambridge Atmospheric and Space Science Series, Cambridge University Press, http://dx.doi.org/10.1017/CBO9780511524981.

Wang, C.-P., Gkioulidou, M., Lyons, L.R., Angelopoulos, V., 2012. Spatial distributions of the ion to electron temperature ratio in the magnetosheath and plasma sheet. J. Geophys. Res.: Space Phys. 117 (A8), A08215. http://dx.doi.org/10.1029/2012JA017658, arXiv:https://agupubs.onlinelibrary.wiley.com/doi/pdf/10.1029/2012JA017658. URL: https://agupubs.onlinelibrary.wiley.com/doi/abs/10.1029/2012JA017658.

Wang, B., Nishimura, Y., Hartinger, M., Sivadas, N., Lyons, L.L., Varney, R.H., Angelopoulos, V., 2020. Ionospheric Modulation by Storm Time Pc5 ULF Pulsations and the Structure Detected by PFISR-THEMIS Conjunction. Geophys. Res. Lett. 47 (16), e2020GL089060. http://dx.doi.org/10.1029/2020GL089060, arXiv:https://agupubs.onlinelibrary.wiley.com/doi/pdf/10.1029/2020GL089060. URL: https://agupubs.onlinelibrary.wiley.com/doi/abs/10.1029/2020GL089060.

Wang, Z., Pritchett, P.L., 1989. The stability of a compressible stratified shear layer. Phys. Fluids B: Plasma Phys. 1 (9), 1767–1775. http://dx.doi.org/10.1063/1.858906.

Welling, D.T., André, M., Dandouras, I., Delcourt, D., Fazakerley, A., Fontaine, D., Foster, J., Ilie, R., Kistler, L., Lee, J.H., Liemohn, M.W., Slavin, J.A., Wang, C.-P., Wiltberger, M., Yau, A., 2015a. The Earth: Plasma Sources, Losses, and Transport Processes. Space Sci. Rev. 192 (1), 145–208. http://dx.doi.org/10.1007/s11214-015-0187-2, https://doi.org/10.1007/s11214-015-0187-2.

Welling, D.T., Jordanova, V.K., Glocer, A., Toth, G., Liemohn, M.W., Weimer, D.R., 2015b. The two-way relationship between ionospheric outflow and the ring current. J. Geophys. Res.: Space Phys. 120 (6), 4338–4353. http://dx.doi.org/10.1002/2015JA021231, arXiv:https://agupubs.onlinelibrary.wiley.com/doi/pdf/10.1002/2015JA021231. URL: https://agupubs.onlinelibrary.wiley.com/doi/abs/10.1002/2015JA021231.

Welling, D.T., Jordanova, V.K., Zaharia, S.G., Glocer, A., Toth, G., 2011. The effects of dynamic ionospheric outflow on the ring current. J. Geophys. Res.: Space Phys. 116 (A2), A00J19. http://dx.doi.org/10.1029/2010JA015642, arXiv:https://agupubs.onlinelibrary.wiley.com/doi/pdf/10.1029/2010JA015642: URL: https://agupubs.onlinelibrary.wiley.com/doi/abs/10.1029/2010JA015642.

Welling, D.T., Liemohn, M.W., 2016. The ionospheric source of magnetospheric plasma is not a black box input for global models. J. Geophys. Res.: Space Phys. 121 (6), 5559–5565. http://dx.doi.org/10.1002/2016JA022646, arXiv:https://agupubs.onlinelibrary.wiley.com/doi/pdf/10.1002/2016JA022646: URL: https://agupubs.onlinelibrary.wiley.com/doi/abs/10.1002/2016JA022646.

Welling, D.T., Ridley, A.J., 2010. Exploring sources of magnetospheric plasma using multispecies MHD. J. Geophys. Res.: Space Phys. 115 (A4), A04201. http://dx.doi.org/10.1029/2009JA014596, arXiv:https://agupubs.onlinelibrary.wiley.com/doi/pdf/10.1029/2009JA014596. URL: https://agupubs.onlinelibrary.wiley.com/doi/abs/10.1029/2009JA014596.

Whipple, E.C., 1981. Potentials of surfaces in space. Rep. Progr. Phys. 44 (11), 1197–1250. http://dx.doi.org/10.1088/0034-4885/44/11/002.

Wiltberger, M., Lotko, W., Lyon, J.G., Damiano, P., Merkin, V., 2010. Influence of cusp O+ outflow on magnetotail dynamics in a multifluid MHD model of the magnetosphere. J. Geophys. Res.: Space Phys. 115 (A10), A00J05. http://dx.doi.org/10.1029/2010JA015579, arXiv:https://agupubs.onlinelibrary.wiley.com/doi/pdf/10.1029/2010JA015579. URL: https://agupubs.onlinelibrary.wiley.com/doi/abs/10.1029/2010JA015579.

Wing, S., Johnson, J.R., Chaston, C.C., Echim, M., Escoubet, C.P., Lavraud, B., Lemon, C., Nykyri, K., Otto, A., Raeder, J., Wang, C.P., 2014. Review of Solar Wind Entry into and Transport Within the Plasma Sheet. Space Sci. Rev. 184 (1), 33–86, https://doi.org/10.1007/s11214-014-0108-9.

Winglee, R.M., 2000. Mapping of ionospheric outflows into the magnetosphere for varying IMF conditions. J. Atmos. Sol.-Terr. Phys. 62 (6), 527–540. http://dx.doi.org/10.1016/S1364-6826(00)00015-8.

Winglee, R.M., Chua, D., Brittnacher, M., Parks, G.K., Lu, G., 2002. Global impact of ionospheric outflows on the dynamics of the magnetosphere and cross-polar cap potential. J. Geophys. Res.: Space Phys. 107 (A9), 1237. http://dx.doi.org/10.1029/2001JA000214, arXiv:https://agupubs.onlinelibrary.wiley.com/doi/pdf/10.1029/2001JA000214. URL: https://agupubs.onlinelibrary.wiley.com/doi/abs/10.1029/2001JA000214.

Wright, D.M., Yeoman, T.K., 1999. High resolution bistatic HF radar observations of ULF waves in artificially generated backscatter. Geophys. Res. Lett. 26 (18), 2825–2828. http://dx.doi.org/10.1029/1999GL900606, arXiv:https://agupubs.onlinelibrary.wiley.com/doi/pdf/10.1029/1999GL900606. URL: https://agupubs.onlinelibrary.wiley.com/doi/abs/10.1029/1999GL900606.

Wu, S., Denton, R.E., Li, W., 2013. Effects of cold electron density on the whistler anisotropy instability. J. Geophys. Res.: Space Phys. 118 (2), 765–773. http://dx.doi.org/10.1029/2012JA018402, arXiv:https://agupubs.onlinelibrary.wiley.com/doi/pdf/10.1029/2012JA018402: URL: https://agupubs.onlinelibrary.wiley.com/doi/abs/10.1029/2012JA018402.

Yahnin, A., Yahnina, T., 2007. Energetic proton precipitation related to ion-cyclotron waves. J. Atmos. Sol.-Terr. Phys. 69 (14), 1690–1706. http://dx.doi.org/10.1016/j.jastp.2007.02.010, http://www.sciencedirect.com/science/article/pii/S1364682607001885 Pc1 Pearl Waves: Discovery, Morphology and Physics.

Yang, B., Donovan, E., Liang, J., Spanswick, E., 2017. A statistical study of the motion of pulsating aurora patches: using the THEMIS All-Sky Imager. Ann. Geophys. 35 (2), 217–225. http://dx.doi.org/10.5194/angeo-35-217-2017, https://www.ann-geophys.net/35/217/2017/.

Yau, A.W., André, M., 1997. Sources of Ion Outflow in the High Latitude Ionosphere. Space Sci. Rev. 80 (1), 1–25, https://doi.org/10.1023/A:1004947203046.

Yau, A.W., Howarth, A., 2016. Imaging thermal plasma mass and velocity analyzer. J. Geophys. Res.: Space Phys. 121 (7), 7326–7333. http://dx.doi.org/10.1002/2016JA022699, arXiv:https://agupubs.onlinelibrary.wiley.com/doi/pdf/10.1002/2016JA022699. URL: https://agupubs.onlinelibrary.wiley.com/doi/abs/10.1002/2016JA022699.

Yau, A.W., Shelley, E.G., Peterson, W.K., Lenchyshyn, L., 1985. Energetic auroral and polar ion outflow at DE 1 altitudes: Magnitude, composition, magnetic activity dependence, and long-term variations. J. Geophys. Res.: Space Phys. 90 (A9), 8417–8432. http://dx.doi.org/10.1029/JA090iA09p08417, arXiv:https://agupubs.onlinelibrary.wiley.com/doi/pdf/10.1029/JA090iA09p08417. URL: https://agupubs.onlinelibrary.wiley.com/doi/abs/10.1029/JA090iA09p08417.

Yau, A.W., Whalen, B.A., Sagawa, E., 1991. Minor ion composition in the polar ionosphere. Geophys. Res. Lett. 18 (2), 345–348. http://dx.doi.org/10.1029/91GL00034, arXiv:https://agupubs.onlinelibrary.wiley.com/doi/pdf/10.1029/91GL00034. URL: https://agupubs.onlinelibrary.wiley.com/doi/abs/10.1029/91GL00034.

Yeoman, T.K., Klimushkin, D.Y., Mager, P.N., 2010. Intermediate-m ULF waves generated by substorm injection: a case study. Ann. Geophys. 28 (8), 1499–1509. http://dx.doi.org/10.5194/angeo-28-1499-2010, https://www.ann-geophys.net/28/1499/2010/.

Yizengaw, E., Zesta, E., Biouele, C., Moldwin, M., Boudouridis, A., Damtie, B., Mebrahtu, A., Anad, F., Pfaff, R., Hartinger, M., 2013. Observations of ULF wave related equatorial electrojet and density fluctuations. J. Atmos. Sol.-Terr. Phys. 103, 157–168. http://dx.doi.org/10.1016/j.jastp.2013.03.015, http://www.sciencedirect.com/science/article/pii/S1364682613000916. Recent Advances in Equatorial, Low- and Mid-latitude Aeronomy.

Young, D.T., Balsiger, H., Geiss, J., 1982. Correlations of magnetospheric ion composition with geomagnetic and solar activity. J. Geophys. Res.: Space Phys. 87 (A11), 9077–9096. http://dx.doi.org/10.1029/JA087iA11p09077, arXiv:https://agupubs.onlinelibrary.wiley.com/doi/pdf/10.1029/JA087iA11p09077. URL: https://agupubs.onlinelibrary.wiley.com/doi/abs/10.1029/JA087iA11p09077.

Young, D.T., Perraut, S., Roux, A., de Villedary, C., Gendrin, R., Korth, A., Kremser, G., Jones, D., 1981. Wave-particle interactions near Ω_{He^+} observed on GEOS 1 and 2 1. Propagation of ion cyclotron waves in He+-rich plasma. J. Geophys. Res.: Space Phys. 86 (A8), 6755–6772. http://dx.doi.org/10.1029/JA086iA08p06755, arXiv:https://agupubs.onlinelibrary.wiley.com/doi/pdf/10.1029/JA086iA08p06755. URL: https://agupubs.onlinelibrary.wiley.com/doi/abs/10.1029/JA086iA08p06755.

Yuan, Z., Xiong, Y., Huang, S., Deng, X., Pang, Y., Zhou, M., Dandouras, I., Trotignon, J.G., Fazakerley, A.N., Lucek, E., 2014. Cold electron heating by EMIC waves in the plasmaspheric plume with observations of the Cluster satellite. Geophys. Res. Lett. 41 (6), 1830–1837. http://dx.doi.org/10.1002/2014GL059241, arXiv:https://agupubs.onlinelibrary.wiley.com/doi/pdf/10.1002/2014GL059241. URL: https://agupubs.onlinelibrary.wiley.com/doi/abs/10.1002/2014GL059241.

Yuan, Z., Yu, X., Huang, S., Qiao, Z., Yao, F., Funsten, H.O., 2018. Cold Ion Heating by Magnetosonic Waves in a Density Cavity of the Plasmasphere. J. Geophys. Res.: Space Phys. 123 (2), 1242–1250. http://dx.doi.org/10.1002/2017JA024919, arXiv:https://agupubs.onlinelibrary.wiley.com/doi/pdf/10.1002/2017JA024919. URL: https://agupubs.onlinelibrary.wiley.com/doi/abs/10.1002/2017JA024919.

Yuan, Z., Yu, X., Huang, S., Wang, D., Funsten, H.O., 2017. In situ observations of magnetosonic waves modulated by background plasma density. Geophys. Res. Lett. 44 (15), 7628–7633. http://dx.doi.org/10.1002/2017GL074681, arXiv:https://agupubs.onlinelibrary.wiley.com/doi/pdf/10.1002/2017GL074681. URL: https://agupubs.onlinelibrary.wiley.com/doi/abs/10.1002/2017GL074681.

Yue, C., An, X., Bortnik, J., Ma, Q., Li, W., Thorne, R.M., Reeves, G.D., Gkioulidou, M., Mitchell, D.G., Kletzing, C.A., 2016. The relationship between the macroscopic state of electrons and the properties of chorus waves observed by the Van Allen Probes. Geophys. Res. Lett. 43 (15), 7804–7812. http://dx.doi.org/10.1002/2016GL070084, arXiv:https://agupubs.onlinelibrary.wiley.com/doi/pdf/10.1002/2016GL070084. URL: https://agupubs.onlinelibrary.wiley.com/doi/abs/10.1002/2016GL070084.

Zhang, B., Brambles, O.J., Cassak, P.A., Ouellette, J.E., Wiltberger, M., Lotko, W., Lyon, J.G., 2017. Transition from global to local control of dayside reconnection from ionospheric-sourced mass loading. J. Geophys. Res.: Space Phys. 122 (9), 9474–9488. http://dx.doi.org/10.1002/2016JA023646, arXiv:https://agupubs.onlinelibrary.wiley.com/doi/pdf/10.1002/2016JA023646. URL: https://agupubs.onlinelibrary.wiley.com/doi/abs/10.1002/2016JA023646.

Zhang, B., Brambles, O.J., Wiltberger, M., Lotko, W., Ouellette, J.E., Lyon, J.G., 2016. How does mass loading impact local versus global control on dayside reconnection?. Geophys. Res. Lett. 43 (5), 1837–1844. http://dx.doi.org/10.1002/2016GL068005, arXiv:https://agupubs.onlinelibrary.wiley.com/doi/pdf/10.1002/2016GL068005. URL: https://agupubs.onlinelibrary.wiley.com/doi/abs/10.1002/2016GL068005.

Zhou, Q., Xiao, F., Yang, C., He, Y., Tang, L., 2013. Observation and modeling of magnetospheric cold electron heating by electromagnetic ion cyclotron waves. J. Geophys. Res.: Space Phys. 118 (11), 6907–6914. http://dx.doi.org/10.1002/2013JA019263, arXiv:https://agupubs.onlinelibrary.wiley.com/doi/pdf/10.1002/2013JA019263. URL: https://agupubs.onlinelibrary.wiley.com/doi/abs/10.1002/2013JA019263.

Zolotukhina, N.A., Mager, P.N., Klimushkin, D.Y., 2008. Pc5 waves generated by substorm injection: a case study. Ann. Geophys. 26 (7), 2053–2059. http://dx.doi.org/10.5194/angeo-26-2053-2008.